WARSAW UNIVERSITY OF TECHNOLOGY

FACULTY OF PHYSICS

Ph.D. Thesis

Łukasz G. Gajewski, B.Eng., M.Sc.

Reverse engineering multi-layered structures in complex networks

Supervisor

Prof. Janusz A. Hołyst, B.Eng., Ph.D., D.Sc.

Co-Supervisor

Julian Sienkiewicz, B.Eng., Ph.D.

WARSAW 2021

"Nel mezzo del cammin di nostra vita
mi ritrovai per una selva oscura,
ché la diritta via era smarrita."
— Dante Alighieri, *Divina Commedia*

Streszczenie

W pracy tej rozważane, analizowane i rozwijane są metody z dziedziny złożonych sieci wielowarstwowych oraz układów dynamicznych. Głównym celem jest opracowanie metod służących do wykrycia istnienia oraz cech struktur topologicznych, które mogą być niedostępne bezpośredniej obserwacji, oraz pokazanie, że takie ukryte elementy mogą mieć znaczący wpływ na zachowanie całego układu.

Odnajdywanie ukrytych warstw w sieciach złożonych jest istotnym i nietrywialnym problemem współczesnej nauki. Mając do czynienia z procesami propagacji na sieciach, bardzo istotna może okazać się możliwość oceny jakości obserwacji oraz występowania potencjalnych ukrytych ścieżek propagacji. Propagacja ta może oddawać różne procesy (dynamiki), takie jak rozprzestrzenianie się wirusów w epidemiach, czy fałszywych informacji w mediach społecznościowych. Jako że natura takiej dynamiki może przybierać różne formy, w pracy tej pod uwagę brane są dwa oddzielne podejścia – dobrze ugruntowany model epidemiologiczny, tzw. model SI (*Susceptible-Infected*, podatny-zarażony) oraz bardziej egzotyczne i współczesne podejście oddające proces propagacji falowej na grafach metrycznych (tzw. grafy kwantowe).

Modelowanie powyżej wspomnianych układów złożonych, jak również zjawisk interakcji społecznych, wymaga odpowiednich narzędzi wywodzących się z nauk fizycznych. Pomimo tego, że dane eksperymentalne są zwykle trudne do uzyskania, odkrycie logicznych konsekwencji założen i modeli teoretycznych, może być kluczowym elementem w budowaniu opisu procesów zachodzących w naszych społecznościach. Tzw. komory echa (*echo chambers*) i dynamika polaryzacji są ostatnio bardzo istotnym tematem w środowiskach naukowych na całym świecie. Zjawiska te bezpośrednio wpływają na nasze życia, w szczególności teraz, w wyniku ewolucji społeczeństwa i sposobów komunikacji międzyludzkich. Jest zatem kluczowe, abyśmy zrozumieli wszelkie zawiłości współczesnych dynamik opinii.

W pracy tej zwrócono uwagę na powyższe problemy oraz przedstawiono propozycje metod identyfikacji oraz rekonstrukcji ukrytych warstw. Uwzględniono również warunki topologiczne sieci wielowarstwowej, przy których zadanie to staje się trudniejsze. Metody

te opierają się na dokładnym wyrażeniu na prawdopodobieństwo pojawienia się kaskady w modelu SI na dowolnym grafie. Następnie pokazano, że dzięki własnościom rozkładów unimodalnych i prostej heurystyki opisującej prawdopodobieństwo łączne serii kaskad można otrzymać oszacowanie zarówno istnienia, jaki i struktury ukrytych warstw z dokładnością znacznie wykraczającą poza to, co oferuje model zerowy, tj. naiwne zgadywanie. Analizy zostały przeprowadzone zarówno na sieciach syntetycznych jak i rzeczywistych, i wskazały, że przedstawione podejście może mieć praktyczne zastosowanie.

Jak wcześniej wspomniano, rozpatrywano również podejście grafów kwantowych do określenia, czy istnieją ukryte części wielowarstwowego układu oraz oceny ich ilości. Zakładając, że jedyna dostępna informacja o systemie to ewolucja w czasie propagacji fali na jednej warstwie sieci, okazuje się, że w istocie jest możliwe, aby zaobserwować, to co jest ukryte, mając do dyspozycji zaledwie obserwacje dynamiki. Zaprezentowane zostały dowody zarówno na sieciach syntetycznych jak i rzeczywistych na to, że widmo częstotliwości dynamiki fali posiada charakterystyczne cechy, przejawiające się jako dodatkowe maksima częstotliwości. Maksima te wykazują zależność od liczby ukrytych warstw, biorących udział w propagacji i w związku z tym pozwalają na określenie tej liczby. Pokazane zostało również, że dla wystarczająco długich czasów obserwacji można w pełni odtworzyć widmo znormalizowanej macierzy połączeń całego grafu. Podejście to porównano do metod uczenia maszynowego, opierających się na tzw. sygnaturze pakietu falowego, zmodyfikowanej na potrzeby sieci wielowarstwowych.

W ostatnim rozdziale rozprawy, w celu podkreślenia istotności wykrywania ukrytych warstw, zaprezentowany został dwuwarstwowy model dynamiki opinii. Istotność ta wynika z faktu, że ukryte warstwy mogą mieć znaczący wpływ na zachowanie układu, prowadząc do zjawisk, które normalnie, tj. w sytuacji jednowarstwowej, nie zachodziłyby. Rozbudowano istniejący już model komór echa i polaryzacji tak, aby można go było zastosować na topologii dwuwarstwowej. Ten nowy kontekst topologiczny pozwala na wskazanie na możliwe konsekwencje oddziałujących grup w ramach tego modelu. Przeanalizowano cztery różne scenariusze – (i) symetryczne negatywne oraz pozytywne sprzężenia, (ii) asymetryczne i (iii) antysymetryczne sprzężenie oraz (iv) wpływ zewnętrzny. Pokazane zostały zarówno symulacje agentowe jak i rozwiązania analityczne w przybliżeniu średniego pola, nakreślające możliwe konsekwencje takich dynamik w rzeczywistych społecznościach. Predykcje wynikające z tego modelu opisują warunki, dla których układ może osiągnąć stan neutralnego lub spolaryzowanego konsensusu, spolaryzowanej opozycji oraz nawet oscylacji opinii. Przejścia między tymi stanami zostały przeanalizowane za pomocą wyników otrzymanych z modelu średniego pola oraz zidentyfikowane w ujęciu teorii bifurkacji.

Niniejsza rozprawa jest podsumowaniem następujących artykułów naukowych:

- [1] **Gajewski, Ł. G.**, Chołoniewski, J., & Wilinski, M., *Detecting Hidden Layers from Spreading Dynamics on Complex Networks.* Phys. Rev. E 104(2), 2021, 024309. Finansowane z grantu Narodowego Centrum Nauki, nr 2015/19/B/ST6/02612.

- [2] **Gajewski, Ł. G.**, Sienkiewicz, J., & Hołyst, J. A., *Discovering hidden layers in quantum graphs.* Phys. Rev. E 104(3), 2021, 034311. Finansowane z grantu Centrum Badawczego POB Cyberbezpieczeństwo i Analiza Danych.

- [3] **Gajewski, Ł. G.**, Sienkiewicz, J., & Hołyst, J. A. (2021). *Phase transitions and oscillations in a temporal bi-layer echo chambers model.* arXiv preprint arXiv:2101.03430. Finansowane z grantu IDUB przeciwko COVID-19 Politechniki Warszawskiej, w recenzji w Phys. Rev. E.

Słowa kluczowe: *struktura sieci, sieci wielowarstwowe, modele propagacji, grafy kwantowe, dynamika nieliniowa, dynamika opinii, modelowanie agentowe*

Z tematyką rozprawy wiążą się również następujące prace, które nie wchodzą w jej skład:

- [4] Paluch R., **Gajewski Ł.G.**, Suchecki K., Hołyst J.A., *Impact of interactions between layers on source localization in multilayer networks*, Physica A:Statistical Mechanics and its Applications, 582, 126238, 2021

- [5] Paluch R., **Gajewski Ł. G.**, Suchecki K., Szymański B.K., Hołyst J.A., *Enhancing Maximum Likelihood Estimation of Infection Source Localization*, rozdział w Simplicity of Complexity in Economic and Social Systems (ed. D. Grech, J. Miśkiewicz), str. 21-41, 2020

- [6] Paluch R., **Gajewski Ł. G.**, Hołyst J.A., Szymański B.K., *Optimizing sensors placement in complex networks for localization of hidden signal source: A review*, Future Generation Computer Systems 112, 1070-1092, 2020

Abstract

In this work we explore, analyse and develop methods within the field of multi-layered complex networks and dynamical processes. Our focus here is on finding ways of determining the existence and features of topological structures that can be hidden from direct observations and showing that such obscured elements can have a profound impact on the behaviour of the whole system.

Finding hidden layers in complex networks is an important and a non-trivial problem in modern science. When dealing with spreading processes on networks, it can be of the utmost importance to test the reliability of data and identify potential unobserved spreading paths. This spreading can take on many different forms such as viruses in epidemics or fake news in social media. As the nature of the dynamics can be so varied we implore here two different models - a well established epidemiological model of Susceptible-Infected and a more exotic and contemporary framework of wave propagation on metric graphs (quantum graphs).

Physics provides tools that allow for deriving models of such complex systems as mentioned above and even social interactions, and while reproducible experimental data are scarce, seeing where certain assumptions and models lead to can be a crucial element in order to build a solid grasp on what transpires in our society. Echo chambers and polarisation dynamics are as of late a very prominent topic in scientific communities around the world. As these phenomena directly affect our lives. and seemingly more and more as our societies and communication channels evolve, it becomes ever so important for us to understand the intricacies opinion dynamics in modern era.

In this work we address these problems and propose methods for hidden layer identification and reconstruction. We also explore the interplay between difficulty of the task and the structure of the multi-layer network describing the whole system where the spreading process occurs. Our methods stem from an exact expression for the likelihood of a cascade in the Susceptible-Infected model on an arbitrary graph. We then show that by imploring statistical properties of unimodal distributions and simple heuristics describing joint likelihood of a series of cascades one can obtain an estimate of both existence of a

hidden layer and its content with success rates far exceeding those of a null model. We conduct our analyses on both synthetic and real-world networks providing evidence for the viability of the approach presented.

As mentioned before we also explore the framework of quantum graphs to determine whether concealed parts of a multi-layer system exist and if so then what is their extent, i.e., how many unknown layers are there. Assuming that the only information available is the time evolution of a wave propagation on a single layer of a network it is indeed possible to uncover that which is hidden by merely observing the dynamics. We present evidence on both synthetic and real-world networks that the frequency spectrum of the wave dynamics can express distinct features in the form of additional frequency peaks. These peaks exhibit dependence on the number of layers taking part in the propagation and thus allowing for the extraction of the said number. We show that in fact, with sufficient observation time, one can fully reconstruct the row-normalised adjacency matrix spectrum. We compare our propositions to a machine learning approach using a wave packet signature method modified for the purposes of multi-layer systems.

Finally, in order to underline the importance of detecting hidden layers we present a case of a multi(bi)-layer opinion dynamics model. This importance stems from the fact that a hidden layer can profoundly affect the behaviour of the system leading to phenomena that are normally absent in the single layer scenario. We build upon an existing echo chambers and polarisation model and extend it onto a bi-layer topology. This new topological context allows us to indicate possible consequences of interacting groups within this model. Four different cases are presented – (i) symmetric negative and positive couplings, (ii) an asymmetric and (iii) anti-symmetric coupling, and (iv) an external bias. We show both simulation results and mean field solutions for these scenarios outlining the possible consequences of such dynamics in real world societies. Our predictions show that there are conditions in which the system can reach states of neutral consensus, a polarised consensus, polarised opposition and even opinion oscillations. Transitions between these states in terms of bifurcation theory are identified and analysed using a mean field model.

This work is the conclusion of the following three articles:

- [1] **Gajewski, Ł. G.**, Chołoniewski, J., & Wilinski, M., *Detecting Hidden Layers from Spreading Dynamics on Complex Networks.* Phys. Rev. E 104(2), 2021, 024309. Supported by National Science Centre, Poland Grant No. 2015/19/B/ST6/02612.

- [2] **Gajewski, Ł. G.**, Sienkiewicz, J., & Hołyst, J. A., *Discovering hidden layers in quantum graphs.* Phys. Rev. E 104(3), 2021, 034311. Supported by POB Research

Centre Cybersecurity and Data Science of Warsaw University of Technology within the Excellence Initiative Program - Research University (IDUB)

- [3] **Gajewski, Ł. G.**, Sienkiewicz, J., & Hołyst, J. A. (2021). *Phase transitions and oscillations in a temporal bi-layer echo chambers model.* arXiv preprint arXiv:2101.03430. Supported by an IDUB against COVID-19 project granted by Warsaw University of Technology under the program Excellence Initiative: Research University (IDUB), under review in Phys. Rev. E.

Keywords: *network structure, multilayer networks, spreading models, quantum graphs, nonliniear dynamics, opinion dynamics, agent-based modelling*

The following papers are also related to yet not included in this thesis:

- [4] Paluch R., **Gajewski Ł. G.**, Suchecki K., Hołyst J.A., *Impact of interactions between layers on source localization in multilayer networks*, Physica A:Statistical Mechanics and its Applications, 582, 126238, 2021
- [5] Paluch R., **Gajewski Ł. G.**, Suchecki K., Szymański B.K., Hołyst J.A., *Enhancing Maximum Likelihood Estimation of Infection Source Localization*, chapter in Simplicity of Complexity in Economic and Social Systems (ed. D. Grech, J. Miśkiewicz), p. 21-41, 2020
- [6] Paluch R., **Gajewski Ł. G.**, Hołyst J.A., Szymański B.K., *Optimizing sensors placement in complex networks for localization of hidden signal source: A review*, Future Generation Computer Systems 112, 1070-1092, 2020

Contents

Chapter 1

Introduction

The primary aim of this dissertation is to provide novel approaches to detect and reconstruct the topology (or its features) of hidden layers in multi-layer networks. Multiple different dynamics are considered, from two distinct families (epidemiological models and wave propagation), in order to cover a significant range of possible real-world scenarios. These novel methods developed here are of fundamental and theoretical nature and provide grounds for further applied studies. **The secondary goal** is to present the importance of multi-layered models and developing methods for reverse engineering. This is accomplished not only with the use of real-world networks but also with an example of an opinion dynamics model which exhibits new behaviour when extended onto a layered topology.

In this section we shall introduce the basic concepts necessary for later parts of the thesis and also provide some context about the network and dynamical models used. Before we begin, however, I would like to express my gratitude to all the persons and institutions that have made this research possible. Support provided by the grants from Polish National Science Centre, Warsaw University of Technology and European Commission Horizon 2020 was instrumental in this effort. The hospitality of Michał Kosiński (Stanford University) and Prof. Bolesław Szymański (Rensselaer Polytechnic Institute) in the USA, during the RENOIR project, allowed me to grow as a researcher and develop skills that would come to fruition in the later stages of my doctoral programme. I am also very grateful to Mateusz Wiliński (Los Alamos National Laboratory) for sharing his insights and expertise without which this thesis' second chapter would most likely not have existed. I thank as well my colleagues from the Group of Physics in Economy and Social Sciences for the collaborations and fruitful discussions that even if they have not resulted in published articles were always illuminating and most importantly invigorating on this journey. My thanks extend to all my friends and family who are too many to list

here in a reasonable fashion, for all their non-academic support and faith in me. Lastly, I would like to especially express my profound gratitude to both of my supervisors – Prof. Janusz Hołyst and Julian Sienkiewicz whose guidance, investment and most importantly - patience were most vital in me becoming not only the researcher but the person I am today.

Real-world complex systems can often be described by interconnected structures known as multi-layer networks [7–10]. Transportation, social or economic networks, to name just a few general examples, can have various types of connections. Each such type of a connection in a network can be represented as a specific sub-system or sub-network. Whether it is a transportation network (e.g. buses and trams) or a social one (e.g. Twitter and Facebook) various forms of information propagation or state dynamics can be described with multi-layer networks. [7–9, 11–14]

Railway, flights and bus connections can all be described with a network but to have a full description of the transportation system, they need to be joined and described with a multi-layer network. In reality obtaining full information which would allow to create a complete multi-layer network is rarely possible. Moreover, in some cases, even the knowledge about all existing layers is limited. As a result, researchers often have to deal with uncertainty which arise from dealing with partial information about connectivity in analysed system. Therefore, as it is not uncommon for certain parts of a system to remain hidden from observers, it can be crucial to be able to discern what characteristics are unknown and then to try to obtain them. Such inverse problems have been studied in various settings in both topology and dynamics parameters reconstruction in mono- and multi-layer scenarios alike [6, 15–26]. This also posts some specific concerns within the fundamental problems of network science, the spreading processes on networks [11–14, 27–29] but is also of significance for opinion dynamics [3, 30–32].

In a part of this work we focus on the problem of detecting hidden layers based on observations of a dynamical processes of an epidemic spread on graphs. We also propose and explore methods for finding missing connections of different types. By dynamical process we mean a realisation of a spreading process described by a model of the susceptible-infected-recovered (SIR) type. Note that such models can describe not only infections, but also spreading of information, opinions or failures. Furthermore, we assume that the observation of such a process is limited to the states of the nodes, without the knowledge of the actual spreading path. In the rest of the text we will refer to a single spreading realisation as a cascade. Finally, we analyse potential limitations and difficulties as well as beneficial settings, i.e. when solving the problem is easier, for these methods.

The problem of detecting hidden layers has appeared recently in the literature in a non-

markovian setting [33] and is also closely related to the problem of network reconstruction which was extensively analysed in the past [19, 20, 22–24] and also in a partial observation setting [15, 16, 18]. Our initial setting of epidemic spread is a bit simpler in some regards but at the same time still fairly realistic and thus should still be viable for real-world problems. We shall assume a well established epidemic model (Susceptible-Infected) the effects of which we can observe for a *limited* time on a single layer only to try to deduce topology of that which is hidden from us. We feel that our simplifications are justified since solving the general problem was proved to be limited [20] and previous papers often approached only limited cases anyway, such as very short cascades [21]. This is not to say that successful approximations are not possible [22], however, our goal here is to investigate the challenges associated with detecting hidden layers in interconnected networks in the context of spreading processes.

Reader should not confuse the problem of finding hidden layers based on observed spreading with extensively analysed branch of network science called *link prediction*, where the hidden connections are estimated using only the network structure. A seminal paper in this direction is [34]. An extension, including multi-layer networks, can be found in [35].

While epidemiological approaches to propagation modelling in networks are rather ubiquitous, they are not unique. In a later chapter of this work we turn our attention to wave propagation on graphs and the scientific field of the so-called quantum graphs. To our knowledge, there has not been much done specifically for uncovering the multi-layer structures in quantum graphs and thus we address this issue. We present two potentially viable approaches of establishing if hidden layers exist, and in some scenarios to ascertain the exact count of these layers. Traditionally, graphs are discrete, combinatorial abstract mathematical objects. If we supply them with a metric and topology we call such objects *metric graphs*. Those in turn equipped with a second order differential operator acting on its vertices and edges - a Hamiltonian - and appropriate boundary conditions are called *quantum graphs* [36–39]. The (most likely) first use of this framework can be traced back to Pauling's paper in 1936 [40], however, for the most part quantum graphs have not been widely used until more recently. Nowadays they see many various applications in dynamical systems, nanotechnology, photonic crystals and many others [41–46]. A somewhat similar idea to quantum graphs – the topological Dirac equation – has been introduced lately (with possible application to multi-layer networks) [47]. Its essence goes in an opposite direction, however. While quantum graphs describe piece-wise continuous wave functions on each link, the topological Dirac equation describes a completely discretised wave-function taking a given (constant) value on each node and on

each link.

Most recently Aziz *et al.* established a method based on a wave packet propagation on quantum graphs that allows to distinguish between structures in complex networks [48] thanks to many well studied properties of the Laplacian (e.g., a finite speed of propagation [49] as opposed to a discrete Laplacian [28, 29]) and its spectra in quantum graphs [50–56]. The idea of determining the shape of an object based on observable dynamics on it goes back to the work of Kac in 1966 [57] in which he asks whether it is possible to hear the shape of a drum. Giraud and Thas showed that the eigenvalues of different shapes can be identical and therefore answered Kac's question in the negative. Gutkin and Smilansky, on the other hand, showed that in quantum graphs specifically, under certain conditions, one can indeed "hear" the shape as the Hamiltonian uniquely defines the connections and their lengths when the graph is finite (and simple), the bond lengths are rationally independent and the vertex scattering matrices are properly connecting. It is also worth noting that this inverse spectral problem can be extended onto scattering systems as also stated in the same paper (a so called inverse scattering problem [58]). However, in these scattering systems it appears that it is *not* always possible to uniquely find the structure [59, 60], i.e., there is a way to construct iso-scattering pairs of graphs with identical polar structure of their scattering matrices, which was also shown experimentally via microwave networks by Hul *et al.* [61]. Wave packets specifically have also attracted some attention in recent years but not for the purposes of what we aim for in this paper [62, 63]. Some work has been done in the context of sufficient coverage with sensors [64], however, in this case we will not share all the assumptions and thus those methods are not applicable to our problem.

While detecting and inferring the hidden structures can be exciting in itself it is also worth noting the potential impact of these unseen layers on the dynamics of the whole system. It is well established that there is a lot that can be said on how our societies form and function with techniques and approaches familiar to physicists [65–69]. A particular interest lately has been the dynamics of opinion formation, especially in the light of recently better studied phenomena such as echo chambers [70–73] and misinformation [74–79]. One of the major effects that seems to be strongly connected with echo chambers and misinformation is that of polarisation. While not every topic is polarising [80, 81] many certainly can be [71, 82–89]. It seems to have been recognised as dangerous to the state of democracy around the world by the scientific community and the need for research in this very topic is rather clear [90–96] especially in the light of a possible event of democracy backsliding [97, 98].

We recognise that it is of relevance and interest here to study the possible dynamics

between two clearly defined groups as it often can be in politics (e.g. Democrat vs Republican in the USA), topics (pro- or anti-) as well as has precedence in socio-physics [99–105]. In particular we felt inspired by the work of Baumann et al. [70] where the authors introduce an echo chambers and polarisation model on complex networks. In this paper we modify the said model so that it operates on a bi-layer temporal network, as opposed to a mono-layer, where each layer can represent a clearly defined group of individuals (agents). This transformation is directly driven by the fact that many system drastically change their physical properties (e.g., phase transition type change) when considered on a duplex (bi-layer) topology [106, 107]. We show that several complex behaviours can be acquired by simply changing the nature of the coupling between those layers. Let us underline that the question of interacting layers is an extremely vivid topic in the view of COVID-19 epidemic. Recent studies point to a pivotal role played by risk perception layer in the spreading of a disease [108] or explicitly the attitude toward vaccination [109]. In this scope examining the dynamics of two *coupled* opposite groups (e.g., pro- and anti-vaccination) seems to be highly relevant.

This work is organised into five chapters. We have already established the context and motivations of the research presented here and what follows is a description of the major theoretical concepts used. Then, in Chapter 2, we shall inspect whether it is possible to detect hidden layers and maybe even reverse engineer hidden connections when the underlying dynamic in the system is that of an epidemic spread. In Chapter 3, similarly our is to determine whether hidden layers exist and learn something about them, however, this time within the framework of quantum graphs instead of epidemiology. In Chapter 4, we take a detour into the field of opinion dynamics and more concrete socio-physics as to bring the point home that the methods established in chapters two and three are of great significance as adding a layer to a system can have profound consequences on its behaviour. Finally, in the very last chapter we include a brief summary of what has been accomplished on this journey.

1.1 Complex networks

What we mean here by *complex networks* are networks (or graphs) with non-trivial topological structures or dynamical processes. Historically this field has its roots in graph theory yet has certainly grown beyond that [110]. A graph is in essence a collection of points joint together into pairs [111]. These points that can be representative of a wide variety of real world objects are typically called nodes or vertices while the connections between them are referred to as links or edges. A standard example of such a network

would be the Internet. Each computer in the Web is a vertex and all the connections such as optic fibre cables, telephone lines etc., would be the edges. Applications of complex networks are many as it is easy to imagine that any information exchange structure would naturally be modelled with a graph, e.g., social media, author citations or collaborations, transportation, brain, protein interactions and so on and so forth.

There are also many different properties, metrics and possible dynamical processes on complex networks and thus here we would only mention the most relevant ones while for other we refer the Reader to the appropriate literature [14, 66, 110–114].

The usual way of describing the connections within a graph is via a so called adjacency matrix $\mathbf{A}$. Each element $A_{i,j}$ represents whether there is a connection $A_{i,j} > 0$ or not $A_{i,j} = 0$. While the value of the said element can be indicative of some property, e.g., a delay of information propagation often it is simply a 1 to indicate the existence of the link. Adjacency matrix is not the only possible matrix representation of a graph and of note and relevance here is also a structure called the graph Laplacian as it tends to appear in many different problems including random walks on networks, dynamical systems and diffusion. In short the graph Laplacian $\mathbf{L}$ is defined as $\mathbf{L} = \mathbf{D} - \mathbf{A}$ where $\mathbf{D}$ is a diagonal matrix with node degrees k_i on the diagonal.

We shall now briefly describe the structural models that are well established in the literature and are often a convenient way of simulating certain aspects of real world scenarios. One of the simplest models is a square lattice - each vertex is connected to four other vertices (up, down, left, right). This model's advantage is of course its simplicity while still maintaining an intuitive property of relationships between vertices depending on the distance between them. It of course does not reproduce real world characteristics such as being scale-free, having the small world property or high clustering coefficient. One must also decide how to treat the boundary of such a graph and often (as well as in this book) the so called periodic boundary conditions are chosen, i.e. the graph "wraps around". This means that the vertices on the right edge are connected to the vertices on the left edge, and top to bottom. In essence such a graph is in a shape of a torus.

Another relatively simple model is the Erdős–Rényi (ER) graph where each node has a certain probability p of making a connection to another vertex [115]. This results is that the degree (that is the number of connections a node has) distribution is binomial and the model has a *percolation threshold* at $\log N/N$ where N is number the number of vertices (i.e., the size of the graph). If $p > \log N/N$ the graph is most likely connected (or percolated, meaning from any node there is at least one path to any other node), and if $p < \log N/N$ then the size of the graph's largest connected component is smaller than N.

As the ER graph has a fairly small clustering coefficient and is not a "small world" graph we need a different model. A model that addresses both of these issues is a Watts-Strogratz model [116]. In this model we start with constructing a regular lattice, typically a ring (or a circle) such that each vertex is connected to $k/2$ neighbours (where k denotes the desired node degree) to the left and $k/2$ to the right. When $k > 2$ the graph usually looks like a flower. Then we *rewire* each edge with probability p such that if $p = 0$ no edges are rewired and if $p = 1$ all edges are rewired. Rewiring is done randomly only so that we do not double already existing connections. This procedure gives us the small world property which means that from any node in the graph we can reach any other node with only a few steps even if the graph is very large. It also has a high clustering coefficient which can be interpreted as the likelihood that any two neighbours of some node are also connected to each other. Where this model falls short is with its degree distribution as it is not a power-law.

In order to address the issue of the scale-free property we can use the Barabási–Albert model [117]. Its distinct feature that allows for the reproduction of a power-law degree distribution is the preferential attachment rule stating that the probability of making a connection p depends on the current degree of a node we consider connecting to. The procedure to construct such a graph begins with some initial number of nodes m_0 and then in a step-by-step manner we add more nodes. Each time we add a node it makes exactly $m \leq m_0$ connections, at random, however, the probability of connecting to the node i is proportional to its temporary degree, i.e., $p_i \sim k_i$. This results in a power-law degree distribution $P(k) \sim k^{-3}$ and a small world property, unfortunately the clustering coefficient is usually lower than we would expect from real world networks.

The above models were chosen as they are rather ubiquitous in the literature of complex networks and allow for an easy way of testing hypothesis or comparing to past and future work. Quite obviously none of them are a perfect representation of real systems yet that is also what makes them useful as one can sometimes isolate certain phenomena associated with a particular property of the topology. In order to test whether our proposals later could hold merit in the real world we simply use actual real world networks from appropriate data sets.

As mentioned in the very beginning, many real-world systems cannot be accurately described with traditional graphs. As transportation and communication networks become more and more complex, multi-layer extensions become necessary. These layered objects can be described as "networks of networks"[118] or with detailed inter-layer structure [9], or even sophisticated tensor formulations [7]. In this work we shall use two simple variants that here we introduce briefly, and in appropriate amount of detail in the chapters

concerning them.

Let us say that we have N entities (agents) that can exist in multiple network structures at the same time. Each of these structures we shall call a layer. E.g., some person can have an account on Facebook, Twitter and Instagram. On each of these platforms they are active in some, possibly distinct, ways, they interact with their friends or followers, etc. The set of these connections (friends/followers) can but need not be (and most often is not) the same for this person on each of the platforms. For instance they can use Facebook to contact their family, Twitter to talk with strangers about politics and Instagram to share their life with their college friends. In such a case we have three distinct networks, with different dynamics and structures that are *inter-connected* if only by just that one person. Upon receiving some information on one of these platforms the user can now send it further in other layers or it will affect how they interact with their connections, etc. We have just described an example of a multi-layer system and a visual guide is presented in Fig. 1.1.

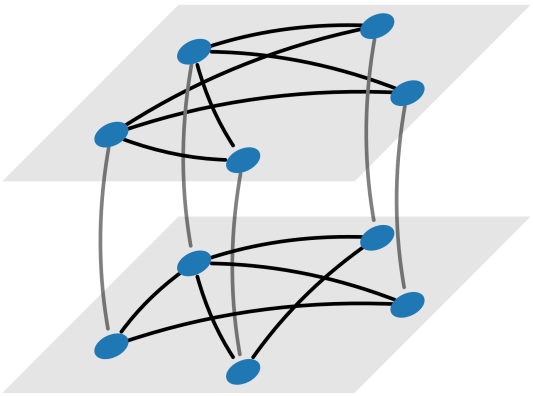

Figure 1.1: Visualisation of a multi(bi)-layer network example. Each layer has its own distinct structure and inter-layer interactions are also possible.

In this work we shall assume that each layer has N vertices, i.e., given entity has its representation in every layer (they may not necessarily have any connections but they exist there) that we can also call a replica r_l where l is an index of a layer. We shall also assume that inter-layer connections (i.e., links between layers) are only of type "replica to replica", meaning that we do not allow for "cross" links. Now, we differentiate between two types of these links: in the first type every replica is connected to every other replica (non-stratified), and in the second we arbitrarily choose an ordering such that r_1 is connected to r_2 which is connected to r_3 and so on, but r_1 and r_3 are *not* connected (stratified). Furthermore, we can either have the state of replicas be always identical (non-delayed) or we can introduce certain physicality to the inter-connection such that the propagation speed is not infinite (delayed). With these labels we can now specify that in the Chapter 2 we use a non-stratified, non-delayed variant and in Chapter 3 we use a stratified, delayed one.

1.2 Epidemiology

Epidemiology in the modern mathematical form has been a vast and constantly developing field for almost a century [14] and has also been expanded recently onto multi-layer systems [11, 12, 119]. Quite naturally it would be of little sense for us to describe here this wide gamut of models and methods and thus we shall focus on one of the simplest models - Susceptible-Infected (SI) [111]. While simple it is definitely not primitive and most surely is very useful. While it does not capture many mechanism typical with epidemics like vaccination, immunisation, death, exposure etc. it is quite apt in capturing the *spreading* phenomenon itself. As such we can use it as a model for not only how a disease would spread but also a rumour, a viral tweet, a meme and so on - in general a piece of information cascading through a network. This notion of information cascade of course also includes things like power failure cascades or viral infections – that is exactly why this simple model can be so useful.

The SI model considers two possible states of agents in the system. An agent here can be a person, a Twitter account, a computer, a protein, etc. – these are our nodes in the graph. Each agent can be either *susceptible* to the disease or already *infected*. When agents are infected they have a certain probability β of sending the information they have to each of their neighbours. A typical phenomenon for this model are the aforementioned cascades where a single node is initially infected and the information rapidly spreads through the system like an avalanche. While this can seem obvious for biological systems or power grids, it has also been recently observed in social media [75, 77–79].

In practice one can either simulate such dynamics with a typical agent-based modelling approach with a use of Monte Carlo methods where we sample agents and draw probabilities of spreading the infection and so on, or use a more general approach where each edge has an attributed weight drawn randomly from an appropriate distribution. This weight corresponds to a *time delay*, i.e., the time it takes for the information to spread from one node to another. Then in order to "spread" the virus one simply utilises a path finding algorithm such as Dijkstra's in order to find the shortest weighted path from a source to a target node [25, 120]. In case of the SI model the appropriate distribution is of course geometric since there we have a series of failed Bernoulli trials followed by a success.

While the SI model is a special case of the more general SIR when the recovery rate $\gamma = 0$, i.e., agents never become "removed" from the dynamics, the other extreme case is the so called Independent Cascade model which is the special case for $\gamma = 1$, i.e., immediately after attempting to pass the infection on to its neighbours, the node becomes removed and no longer takes part in the spreading process [121]. We will consider this

model as well as the SI in order to try to encompass the whole family of SIR-esque models without necessarily conducting an obscene amount of computations.

A useful notion for the purposes of our later considerations in this work is that of likelihood of an SI cascade [15]. Let as assume that we observe C independent cascades where a cascade Σ^c is defined as a collection of activation times of nodes in the network $\forall_{i\in V}\{\tau_i^c\}$. Here V is the set of nodes in the considered graph G. We also assume that we have a limited observation time budget, i.e., we do not necessarily see the whole cascade but only up to time t_{max}. This parameter naturally introduces a certain trade of for any reverse problems, i.e., the smaller t_{max} the more cascades we are going to need to acquire sufficient amount of information and vice versa. If node i in cascade c does not get activated at a certain time prior to t_{max}, we put by definition $\tau_i^c = t$. In other words, $\tau_i^c = t$ means that node i changes its state at time t or later. The full information on all the cascades is $\Sigma = \cup_c \Sigma^c$. We can then write out the likelihood of observed Σ on the graph G:

$$P(\Sigma \mid G) = \prod_{i\in V} \prod_{1\leq c\leq C} P_i(\tau_i^c \mid \Sigma^c, G, \{\beta\}), \tag{1.1}$$

with

$$P_i(\tau_i^c \mid \Sigma^c, G, \{\beta\}) = \left(\prod_{t=0}^{\tau_i^c - 2} \prod_{k\in\partial i} (1 - \beta_{ki}[\tau_k^c \leq t]) \right) \times \\ \times \left(1 - \left(\prod_{k\in\partial i} (1 - \beta_{ki}[\tau_k^c \leq \tau_i^c - 1]) \right) [\tau_i^c < t_{max}] \right), \tag{1.2}$$

where ∂i denotes the set of neighbours of node i in the graph G, and $\{\beta\}$ being the set of transmission probabilities on the links. The expression (1.2) essentially states that the probability that node i has been activated at time τ_i given the activation times of its neighbours is equal to the probability that the activation signal has not been transmitted by any infected neighbour of i until the time $\tau_i - 2$ (first term in the product), and that at least one of the active neighbours actually transmitted the infection at time $\tau_i - 1$ (second term). Note that we use the Iverson bracket notation here [122] meaning that $[\heartsuit]$ is one when $\heartsuit$ is true and zero otherwise. Later on in this work we shall extend this approach onto a multi-layer topology and the Independent Cascade model as well.

1.3 Quantum graphs

In previous section we have discussed what a graph is. A quantum graph is a special type of a structure that is characterised by additional properties applied onto a classical graph. One of these properties is a metric, i.e. each edge e has its length L_e and an appropriate coordinate along it x_e. Another property is a second order differential operator acting on its vertices and edges - a Hamiltonian - with appropriate boundary conditions [36–39]. It is worth underlining here that with this definition we do not specify the exact nature of the Hamiltonian and while it is often a quantum mechanical one, it does not need to be so and thus here we follow the interpretation of taut strings, fused together at the vertices that can be seen as the "limiting case" of a "quantum wire" [123, 124]. While the roots of quantum graphs could probably be traced as far as 1936 [40], only now do they begin to bloom with a plethora of applications in dynamical systems, nanotechnology, photonic crystals and many others [41–46].

What is of the utmost interest to us here is that the mathematical apparatus of quantum graphs offers a wave equation that is not unlike the classical, mechanical one $\ddot{u} = \Delta u$. A wave described by such an equation would share all the "nice" properties from wave mechanics such as a finite speed of propagation [49] which is in fact **not** the case with a typical graph Laplacian approach [28, 29].

Let $G = (V, E)$ be a graph. Let $\mathcal{G}$ be its geometric realisation, i.e. we apply a *metric* onto G such that each edge $e = (u, v)$, connecting vertices u, v, has length 1, an associate coordinate x_e and is fused at its vertices with other edges. Let $\mathcal{V}$ be the vertex counting measure, and $\mathcal{E}$ be the Lebesgue measure on the edges. We can then write the *vertex*-based Laplacian (i.e. the one typically seen in graph theory albeit in a slightly different form) as [123, 125]:

$$u_{tt} d\mathcal{V} = -\Delta u, \tag{1.3}$$

whereas the *edge*-based Laplacian would be:

$$u_{tt} d\mathcal{E} = -\Delta u, \tag{1.4}$$

where u is a square integrable function defined on the graph. Specifically $u(n)$ is the value of u at the node n, and $u(e, x_e)$ is the value of u at the position x_e along the edge e [48]. This second equation is the "proper" wave equation with finite speed propagation that we want to utilise. In order to have a wave propagating through the whole systems we also need to apply suitable boundary conditions. For our purposes we shall use the Neumann

boundary conditions also called "natural":

$$\forall v \in G, \ \sum_{e \ni v} (-1)^{1-x_{e,v}} \nabla u(e, x_{e,v}) = 0, \tag{1.5}$$

and of course we also need the initial conditions. For our purposes we will be sending out a wave packet from a single edge. This wave packet would be a Gaussian one in the form:

$$u(e, x) = \exp\big(- a(x - \mu)^2 \big). \tag{1.6}$$

We choose this particular set up as it has been already studied quite thoroughly [48, 50–52].

The general solution of the wave equation on graph G, provided that the initial condition is Gaussian packet fully localised on a given edge f is derived and presented in detail by Aziz et al. in [48]. Here, we re-write it in terms of integer times, i.e., $t = 0, 1, 2, ...$ so that it fits the case examined in the later chapter. We additionally assume that the graph is unweighted, undirected and non-bipartite. In such a setting, we consider an arbitrary edge $e = \{u, v\}$ that connects two vertices u and v and can be associated with a variable $x_e \in [0, 1]$ that represents coordinate along such an edge. Then the amplitude u of the wave in the middle of edge e can be expressed as

$$u(e, f, t) = u_1(e, f, t) + u_5(e, f, t) + \frac{1}{|E|}, \tag{1.7}$$

where $|E|$ is the number of edges in the graph and u_1 and u_5 are defined as follows

$$\begin{aligned} u_1(e, f, t) &= \sum_{\omega \in \Omega} C(e, \omega) C(f, \omega) \cos(B(e, \omega) + \tfrac{1}{2}\omega) \cos(B(f, \omega) + \omega(\tfrac{1}{2} + t)) \\ u_5(e, f, t) &= 2 \cos(\pi t) \sum_i C_\pi(e, i) C_\pi(f, i) \end{aligned} \tag{1.8}$$

In the above equations ω, $C(e, \omega)$ and $B(e, \omega)$ come from the edge-based eigenvalues and eigenfunctions, which are, respectively ω^2 and $\phi(e, x_e) = \pm C(e, \omega) \cos(B(e, \omega) + \omega x_e)$ of the row-normalised adjacency matrix $\hat{\mathbf{A}}$ of the graph G. Assuming that we know vertex-based eigenvector-eigenvalues pairs ($g(v)$,λ) of matrix $\hat{\mathbf{A}}$ we can express $C(e, \omega)$ and $B(e, \omega)$ as

$$\begin{aligned} C(e, \omega)^2 &= \tfrac{g(v,\omega)^2 + g(u,\omega)^2 - 2g(u,\omega)g(v,\omega)\cos\omega}{\sin^2\omega} \\ \tan B(e, \omega) &= \tfrac{g(v,\omega)\cos\omega - g(u,\omega)}{g(v,\omega)\sin\omega}, \end{aligned} \tag{1.9}$$

while $\omega = \arccos\lambda$. The sign of $C(e, \omega)$ needs to chosen in order to match the phase, in practice it can be achieved by calculating $\mathrm{sgn}[g(v)]|C(e, \omega)|$ It is always true that one

of the eigenvalues is equal to 1 (consequently, $\omega = 0$): this value is responsible for the constant term $1/E$ in Eq. (1.8) so it is not included in further calculations, i.e., it does not belong to Ω set in function u_1. Although $\phi(e, x_e)$ are orthogonal, they still need to be normalised. To fulfil this condition for each $\omega \in \Omega$ we calculate normalisation factor $\rho(\omega)$

$$\rho(\omega) = \sqrt{\sum_e C(e,\omega)^2 \left[\frac{1}{2} + \frac{\sin(2\omega + 2B(e,\omega)) - \sin(2B(e,\omega))}{4\omega}\right]} \tag{1.10}$$

where e runs over all edges in graph G. Then, in order to obtain properly normalised value of $C(e,\omega)$ one needs to divide it by $\rho(\omega)$.

For calculations of C_π one first needs to transform the original undirected graph G into a directed one $D(G)$ by simply replacing each edge $e = \{u, v\}$ with two arcs (u, v) and (v, u). In the next step we create a structure called oriented line graph (OLG), constructed by substituting each arc of $D(G)$ by a vertex (such vertices are connected if the head of one arc meets the tail of another arc). Using the adjacency matrix $\mathbf{A}_{olg}$ of the OLG we solve the eigenproblem $\mathbf{A}_{olg}\mathbf{g}_{olg} = \lambda_{olg}\mathbf{g}_{olg}$ and then restrict ourselves to $\lambda_{olg} = -1$ and corresponding eigenvectors (there should be exactly $|E| - |V|$ linearly independent solutions) that form C_π.

Let us note that if we decide to measure wave amplitude on nodes instead of edges the formula is particularly simple as then

$$u_n(e, f, t) = u_1(e, f, t) + \frac{1}{|E|}, \tag{1.11}$$

and

$$\begin{aligned} u_1(e, f, t) = \sum_{\omega\in\Omega} C(e,\omega)C(f,\omega) \Bigg\{ &\cos\left[\left(t - \frac{1}{2}\right)\omega - B(e,\omega) + B(f,\omega)\right] + \\ &+ \cos\left[\left(t + \frac{3}{2}\right)\omega + B(e,\omega) + B(f,\omega)\right]\Bigg\} \end{aligned} \tag{1.12}$$

If follows that in such a case we do not have to create OLG and thus the calculations are less consuming in regard to both the computational time and resources.

In order to make the above concise description clear, let us follow a very simple example of a graph shown in Fig. 1.2a. In such case, knowing the adjacency matrix $\mathbf{A}$ where $A_{ij} = 1$ if nodes i and j share a link and $A_{ij} = 0$ otherwise, we can write the

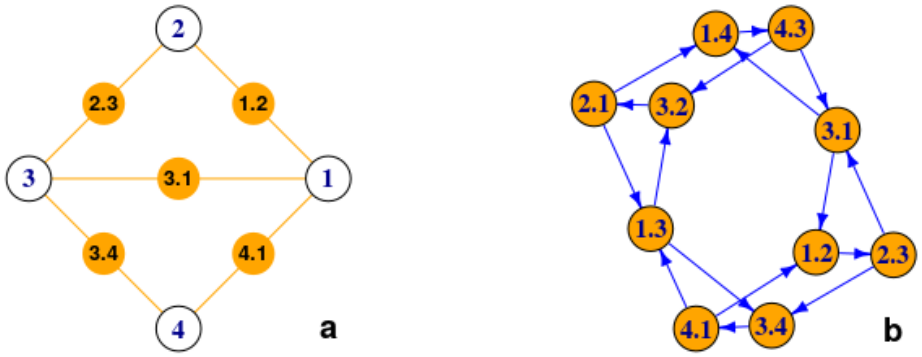

Figure 1.2: (a) An example of a simple graph consisting of $|V| = 4$ nodes and $|E| = 5$ edges. (b) Oriented Line Graph obtained from the graph depicted in panel (a).

row-normalised adjacency matrix $\hat{A}_{ij} = A_{ij} / \sum_k A_{kj}$ as

$$\hat{\mathbf{A}} = \begin{pmatrix} 0 & \frac{1}{3} & \frac{1}{3} & \frac{1}{3} \\ \frac{1}{2} & 0 & 0 & \frac{1}{2} \\ \frac{1}{3} & \frac{1}{3} & 0 & \frac{1}{3} \\ \frac{1}{2} & 0 & \frac{1}{2} & 0 \end{pmatrix}. \tag{1.13}$$

Solving the eigenproblem $\hat{\mathbf{A}}\mathbf{g} = \lambda\mathbf{g}$ one obtains in this case the following eigenvectors

$$\mathbf{g} = \begin{array}{c} \\ 1 \\ 2 \\ 3 \\ 4 \end{array} \begin{array}{c} \begin{array}{cccc} \omega_1 & \omega_2 & \omega_3 & \omega_4 \end{array} \\ \begin{pmatrix} \sqrt{\frac{2}{13}} & \frac{\sqrt{2}}{2} & 0 & -\frac{1}{2} \\ -\frac{3}{\sqrt{26}} & 0 & -\frac{\sqrt{2}}{2} & -\frac{1}{2} \\ \sqrt{\frac{2}{13}} & -\frac{\sqrt{2}}{2} & 0 & -\frac{1}{2} \\ -\frac{3}{\sqrt{26}} & 0 & \frac{\sqrt{2}}{2} & -\frac{1}{2} \end{pmatrix} \end{array} \tag{1.14}$$

and related eigenvalues $\lambda = \left(-\frac{2}{3}, -\frac{1}{3}, 0, 1\right)$. Each column of $\mathbf{g}$ corresponds to different ω and consecutive rows are node numbers. As mentioned before, $\lambda = 1$ is not taken into account in further calculations, so $\omega = \{\omega_1, \omega_2, \omega_3\} = \{\arccos(-\frac{2}{3}), \arccos(-\frac{1}{3}), \frac{\pi}{2}\}$. Now, having calculated $\mathbf{g}$ and ω we are able to obtain $C(e, \omega$ and $B(e, \omega)$ as described in Eq. (1.9). To simplify the outcome we show it as matrices with rows denoted by graph edges

and columns — by ω values:

$$\mathbf{C} = \begin{array}{c} \\ e_{12} \\ e_{13} \\ e_{14} \\ e_{21} \\ e_{23} \\ e_{31} \\ e_{32} \\ e_{34} \\ e_{41} \\ e_{43} \end{array} \begin{array}{c} \begin{array}{ccc} \omega_1 & \omega_2 & \omega_3 \end{array} \\ \begin{pmatrix} -\frac{3\sqrt{26}}{26} & -\frac{3}{4} & \frac{\sqrt{2}}{2} \\ -\frac{1}{13}\sqrt{6}\sqrt{26} & -\frac{\sqrt{3}}{2} & 0 \\ -\frac{3\sqrt{26}}{26} & -\frac{3}{4} & \frac{\sqrt{2}}{2} \\ \frac{3\sqrt{26}}{26} & \frac{3}{4} & -\frac{\sqrt{2}}{2} \\ \frac{3\sqrt{26}}{26} & \frac{3}{4} & -\frac{\sqrt{2}}{2} \\ -\frac{1}{13}\sqrt{6}\sqrt{26} & \frac{\sqrt{3}}{2} & 0 \\ -\frac{3\sqrt{26}}{26} & \frac{3}{4} & \frac{\sqrt{2}}{2} \\ -\frac{3\sqrt{26}}{26} & \frac{3}{4} & \frac{\sqrt{2}}{2} \\ \frac{3\sqrt{26}}{26} & \frac{3}{4} & \frac{\sqrt{2}}{2} \\ \frac{3\sqrt{26}}{26} & \frac{3}{4} & \frac{\sqrt{2}}{2} \end{pmatrix} \end{array} \quad \mathbf{B} = \begin{array}{c} \\ e_{12} \\ e_{13} \\ e_{14} \\ e_{21} \\ e_{23} \\ e_{31} \\ e_{32} \\ e_{34} \\ e_{41} \\ e_{43} \end{array} \begin{array}{c} \begin{array}{ccc} \omega_1 & \omega_2 & \omega_3 \end{array} \\ \begin{pmatrix} \arctan\frac{\sqrt{5}}{2} & -\arctan\frac{\sqrt{2}}{4} & \frac{\pi}{2} \\ -\arctan\sqrt{5} & \arctan\frac{\sqrt{2}}{2} & 0 \\ \arctan\frac{\sqrt{5}}{2} & -\arctan\frac{\sqrt{2}}{4} & -\frac{\pi}{2} \\ 0 & -\frac{\pi}{2} & 0 \\ 0 & \frac{\pi}{2} & 0 \\ -\arctan\sqrt{5} & \arctan\frac{\sqrt{2}}{2} & 0 \\ \arctan\frac{\sqrt{5}}{2} & -\arctan\frac{\sqrt{2}}{4} & \frac{\pi}{2} \\ \arctan\frac{\sqrt{5}}{2} & -\arctan\frac{\sqrt{2}}{4} & -\frac{\pi}{2} \\ 0 & -\frac{\pi}{2} & 0 \\ 0 & \frac{\pi}{2} & 0 \end{pmatrix} \end{array} \tag{1.15}$$

Each column of matrix $\mathbf{C}$ needs to by divided by a corresponding value of $\rho(\omega)$ given by Eq. (1.10), i.e., in the case of the exemplary graph $\rho = \{\frac{15}{13}, \frac{3}{2}, 1\}$. In this way we possess full information needed to evaluate values of u_1.

Figure 1.2b presents an Oriented Line Graph obtained from the graph shown in Fig. 1.2a, its adjacency matrix $\mathbf{A}_{olg}$ being simply

$$\mathbf{A}_{olg} = \begin{array}{c} \\ e_{12} \\ e_{13} \\ e_{14} \\ e_{21} \\ e_{23} \\ e_{31} \\ e_{32} \\ e_{34} \\ e_{41} \\ e_{43} \end{array} \begin{array}{c} \begin{array}{cccccccccc} e_{12} & e_{13} & e_{14} & e_{21} & e_{23} & e_{31} & e_{32} & e_{34} & e_{41} & e_{43} \end{array} \\ \begin{pmatrix} 0 & 0 & 0 & 0 & 1 & 0 & 0 & 0 & 0 & 0 \\ 0 & 0 & 0 & 0 & 0 & 0 & 1 & 1 & 0 & 0 \\ 0 & 0 & 0 & 0 & 0 & 0 & 0 & 0 & 0 & 1 \\ 0 & 1 & 1 & 0 & 0 & 0 & 0 & 0 & 0 & 0 \\ 0 & 0 & 0 & 0 & 0 & 1 & 0 & 1 & 0 & 0 \\ 1 & 0 & 1 & 0 & 0 & 0 & 0 & 0 & 0 & 0 \\ 0 & 0 & 0 & 1 & 0 & 0 & 0 & 0 & 0 & 0 \\ 0 & 0 & 0 & 0 & 0 & 0 & 0 & 0 & 1 & 0 \\ 1 & 1 & 0 & 0 & 0 & 0 & 0 & 0 & 0 & 0 \\ 0 & 0 & 0 & 0 & 0 & 1 & 1 & 0 & 0 & 0 \end{pmatrix} \end{array}. \tag{1.16}$$

We deliberately refrain from showing the full matrix $\eth_{olg}$ of eigenvectors of $\mathbf{A}_{olg}$ as in our case $|E| - |V| = 1$ so there is exactly one eigenvector corresponding to $\lambda = -1$ namely

$$\mathbf{C}_{\pi} = \begin{array}{c} \begin{array}{cccccccccc} e_{12} & e_{13} & e_{14} & e_{21} & e_{23} & e_{31} & e_{32} & e_{34} & e_{41} & e_{43} \end{array} \\ \begin{pmatrix} \frac{\sqrt{2}}{4} & 0 & -\frac{\sqrt{2}}{4} & \frac{\sqrt{2}}{4} & -\frac{\sqrt{2}}{4} & 0 & -\frac{\sqrt{2}}{4} & \frac{\sqrt{2}}{4} & -\frac{\sqrt{2}}{4} & \frac{\sqrt{2}}{4} \end{pmatrix} \end{array}. \tag{1.17}$$

It is now easy to check that if substitute Eq. (1.8) with the calculated matrices $\mathbf{C}$, $\mathbf{B}$, ω and $\mathbf{C}_{\pi}$ and assume that the wave is initially localised on edge $f = \{1, 2\}$ and $t = 0$, the amplitude $u = 1$ for $e = f = \{1, 2\}$ and $u = 0$ in any other case, as expected. The first 10 steps of propagation are depicted in Fig. 1.3 (the wave moves toward $v = 2$).

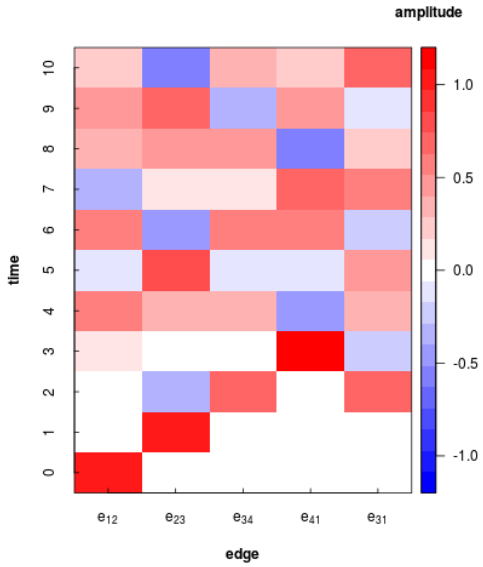

Figure 1.3: Wave propagation on a graph shown in Fig. 1.2a for the first 10 time steps (initial condition: a Gaussian wave fully contained on the edge $f = \{1, 2\}$ moving towards the vertex $v = 2$).

1.4 Other tools and methods

Here we shall describe remaining minor topics that each separately do not really merit their own sections.

For starters let us describe the Principal Components Analysis. These Principal Components are a sequence of projections of the set of data in $\mathbb{R}^p$, mutually uncorrelated and ordered in variance in in $\mathbb{R}^q$ where $q \leq p$ [126]. In other words we transform the feature space such that it becomes orthogonal and each consecutive feature is aligned in the direction maximising the variance of the data and has more variance than the last. We do that by minimising the reconstruction error, i.e. solving:

$$\min_{\mathbf{V}_q} \sum_{i=1}^{N} ||(x_i - \bar{x}) - \mathbf{V}_q \mathbf{V}_q^T (x_i - \bar{x})||^2 \tag{1.18}$$

where $\mathbf{V}_q$ is a $p \times q$ matrix with q orthogonal unit vectors as columns. A $p \times p$ matrix $V_q V_q^T$ is the *transformation matrix* that maps each p-dimensional observation into its q-rank reconstruction. In our case specifically $p = q = 100$ and the examples of transformation matrices are represented as heat-maps in Fig. 3.3 and 3.4 in Chapter 3. In general the PCA is known to be a quick and easy method to (i) perform dimensional reduction, (ii) help to visualise high-dimensional data and (iii) aggregate high-dimensional data into a possibly single measure (see, e.g., [127–129]).

The K-NN classification is a method of the class estimation $\hat{y}(x)$ of a given sample x taken as a majority vote amongst the members of $N_K(x)$ - the neighbourhood of x defined as K points closest to x [126, 130]. To determine which points are closest a metric must be chosen and for the purposes of this paper a Euclidean distance was used. In our case specifically each observation is a graph represented by its WPS, i.e. each graph is a point in a 100-dimensional space.

Fourier analysis allows us to convert a given time dependent signal $f(t)$ onto a frequency domain into $\hat{f}(\omega)$ via a Fourier transform and thus acquire the frequency distribution of the said signal as it becomes a linear combination of the trigonometric functions each corresponding to a particular frequency. A discrete Fourier transform is, as name suggests, a discrete version where the integration is replaced by a summation [131]. Therefore we consider a problem where one wants to express $f(t)$ as a complex Fourier series:

$$\hat{f}(\omega) = \sum_{k=0}^{N-1} f(k) e^{2\pi i \omega / N} \tag{1.19}$$

This procedure, as it stands, would require N^2 operations (where each operation is a complex multiplication followed by a complex addition), however, Cooley and Tukey in [132] presented a method known as the *fast Fourier transform* that allows us to do it in less than $2N \log_2 N$.

A wavelet transform is an analogous procedure to the Fourier transform in the sense that we represent a given signal as an orthonormal series [133]. In case of Fourier those are sine and cosine while in the wavelet those are the eponymous wavelets. A wavelet is a particularly chosen function that is localised, i.e. it has a finite width, and its family can compose an orthonormal basis for the signal - $s(t)$.

$$C(a,b) = \int_{\mathcal{R}} s(t) \frac{1}{\sqrt{a}} \psi\left(\frac{t-b}{a}\right) dt, \;\; a \in \mathcal{R}^+, b \in \mathcal{R} \tag{1.20}$$

In our case the wavelet - ψ - was a Morlet (also known as the Mexican hat) one as per the procedure described in [134] which (simplified) is as follows: perform a continuous wavelet transform (CWT) on the signal, identify the ridge lines by linking local maxima of CWT at each scale level, identify the peaks based on the ridge lines with three rules (quoted verbatim): "(1) The scale corresponding to the maximum amplitude on the ridge line,which is proportional to the width of the peak, should be within a certain range;(2) The SNR should be larger than a certain threshold;(3) The length of ridge lines should be larger than a certain threshold;". Here SNR is a *signal to noise ratio*.

Most simulations, analysis and plotting were conducted with a use of Python and appropriate libraries [135–141] or R [142]. Some simulations were also implemented in Rust [143]. Mathematical analysis and plots were supported by Mathematica [144]. Real world network in Chapter 2 was visualised with Muxviz [145].

Chapter 2

Detecting hidden layers from spreading dynamics

Let us embark into multi-layer networks with a well known and established information propagation model - Susceptible-Infected (SI). While it was originally developed for modelling spreads of viral infections throughout society we choose to say *information* here since one can consider information to spread in a very similar way (it is no coincidence that we call certain videos or memes to have gone viral after all), and viruses can also be thought of as a piece of information. For details on the SI model we refer the Reader to the theoretical introduction earlier in this thesis, see Sec. 1.2.

We shall use this particular model because of its simplicity on one hand and the mechanism of multiple infection opportunities (in comparison with, e.g. an independent cascade model) on the other. The latter makes the combinatorial analysis much more difficult as we will see very soon.

The task before us is thus: having observed a cascade (or multiple cascades) of some spread in a complex network (e.g. a virus in a city or a piece of false information in social media) can we determine whether there are communication channels that are hidden from us? And if so then is there a chance to reverse engineer those connections?

2.1 Cascade likelihood and hidden layer detection

It is already known how to measure the likelihood $P(\Sigma|G,\beta)$ of a cascade in the Susceptible-Infected model [15, 23, 146, 147], however, here we formulate it in terms of a multi-layer graph. Let us have a cascade c from the set of all cascades C represented by a collection of node activation times Σ^c, given a topology G, activation times from all the cascades as $\Sigma = \cup_c \Sigma^c$, and assuming edge activation probabilities β_j per layer j this likelihood is

given by:

$$P(\Sigma|G,\{\beta_j\}) = \prod_{i\in V}\prod_{c\in C} P_i(\tau_i^c|\Sigma^c, G, \{\beta_j\}) \tag{2.1}$$

where V is the set of nodes in graph G. Note that we can use our knowledge about the activation times of each node and compute the probability of node i not being activated by its neighbour k (from layer j) before $\tau_i^c - 1$ under cascade c, which is equal to $\prod_{t=0}^{\tau_i^c-2}(1-\beta_j[\tau_k^c \leq t])$, where $[\heartsuit]$ is the Iverson bracket notation[122] with $[\heartsuit] = 1$ when $\heartsuit$ is true and $[\heartsuit] = 0$ otherwise. Similarly, the probability of the same node not being activated by its neighbour exactly at time $\tau_i^c - 1$ is equal to $(1 - \beta_j[\tau_k^c \leq \tau_i^c - 1])$. Have in mind that $\tau_i^c = t_{max}$ is equivalent to node i not being activated at all. Then each element of the product in Eq. (2.1), being the probability of node activation under a specific cascade, can be computed as follows:

$$P_i(\tau_i^c|\Sigma^c, G, \{\beta_j\}) = \left(\prod_{t=0}^{\tau_i^c-2}\prod_{j}\prod_{k\in\partial_j i}\Big(1-\beta_j[\tau_k^c \leq t]\Big)\right)\times \\ \times\left(1-\prod_{k\in\partial_j i}\Big(1-\beta_j[\tau_k^c \leq \tau_i^c - 1]\Big)[\tau_i^c < t_{max}]\right), \tag{2.2}$$

where $\partial_j i$ represents the neighbourhood of node i in layer j, V the set of all nodes in the graph G, τ_i an activation time of node i, t time and t_{max} the final observation time. That last parameter means that we do not assume that we have observed the cascades in full. This is supposed to model the fact that sometimes we are simply unable to continue to observe the system forever and must seize the measurements even though the propagation has not yet reached all the vertices of the graph.

As seen from Eq. (2.1), adding more cascades reduces the likelihood. Nevertheless increased statistics of cascades makes it easier to find hidden edges, as we show later on. The first major term of Eq. (2.2) represents the probability that the activation signal has not been transmitted by any of the infected neighbours of some node i up until the time $\tau_i - 2$. The second term is the probability that at least one of these neighbours actually did transmit the signal at time $\tau_i - 1$. These two terms combined give us the probability that the node i was activated at a the time τ_i which is exactly what we need in Eq. (2.1).

In practice it is often more convenient to deal with a log-likelihood which is simply the logarithm of Eq. (2.1) and so the numerical analyses from now on will reflect that.

An unobserved layer of propagation may lead to a situation where nodes become active despite not interacting, on the observed network, with any other active node. Such situation leads to the probability described by Eq. (2.1) being equal to zero (log-likelihood

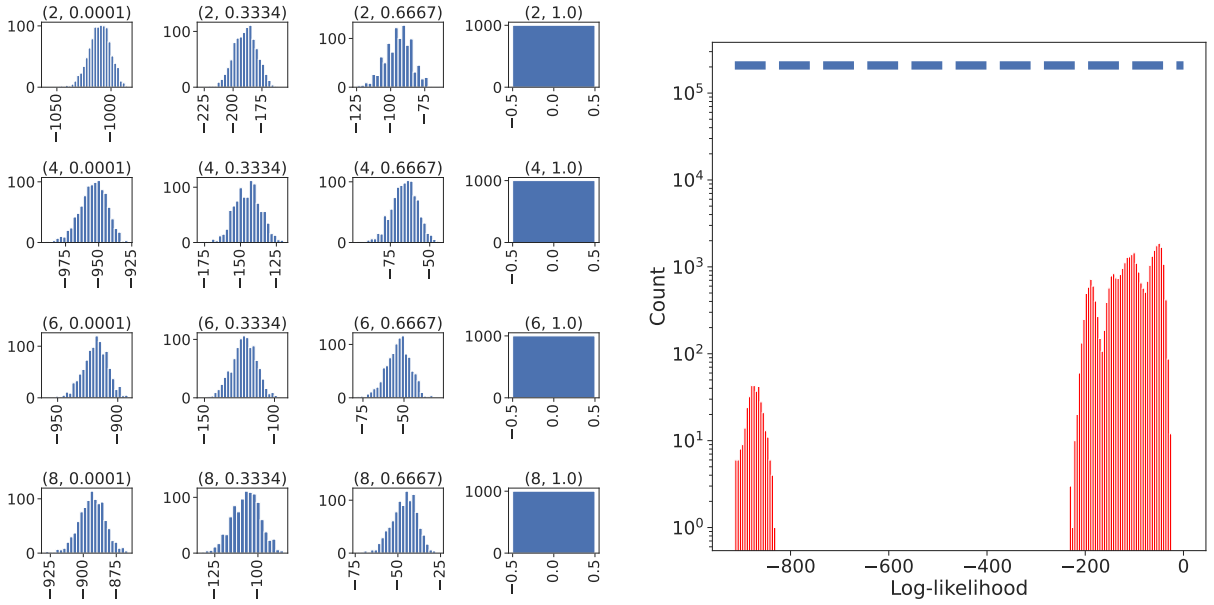

(a) mono-layer variants

(b) bi-layer variants combined

Figure 2.1: Log-likelihood - Eq.(2.1) - histograms of 10^3 independent Susceptible-Infected cascades. Note: likelihood was computed for each cascade separately and it is 10^3 runs per given set of parameters. We used Barabási-Albert graph of size $N = 100$ with $m \in \{1, 2, 3, 4\}$, and infection rate $\beta \in \{0.0001, 0.3334, 0.6667, 1.0\}$. (a) shows results for a single layer network, titles of the subplots represent (k, β). Right column of (a) are all uniquely zeroes. (b) shows an aggregated histogram of 256 different $(k,\ \beta)$ parameters combinations on a bi-layer system.

$\to -\infty$). In such case one can be sure that there exist spreading paths which are not present in the observed layers. For example see Fig. 2.1 where we show log-likelihoods of a mono- (a) and bi-layer (b) Barabási-Albert network [117]. The latter case means that we assume we only know about one layer, observe a cascade and compute the log-likelihood with Eq. (2.1). In (a) we show how the distribution of the log-likelihoods depends on the mean degree (k) and the infection rate (β). Rather intuitively when the β is large and thus the process more stochastic in nature our measure finds the cascades less likely whereas when $\beta = 1$ its logarithm always returns zero. In (b) we show a combined histogram of 256 different combinations of parameters $(k,\ \beta)$ with the dashed line representing the count of (negative) infinities. This is what we have just mentioned - such a result gives us certainty that there is a hidden layer as some observed transmission is simply impossible with our current knowledge of the topology. As one can see such cases highly dominate as the bi-layer model here is not strongly correlated (i.e., there are few overlapping edges between layers). In reality different layers share certain similarities and may be strongly correlated which would decrease the probability

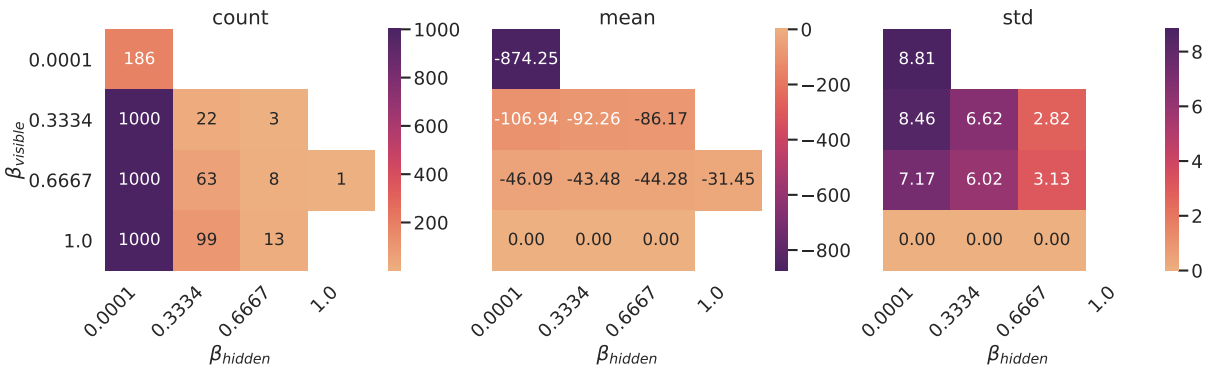

Figure 2.2: Heatmaps of (left) number of cases with finite likelihood, (centre) mean log-likelihood, (right) standard deviation of log-likelihood for the bi-layer case with $k_{visible} = 8$ and $k_{hidden} = 2$ (see Fig 2.1b). Y-axes are infection rates in the visible layer $\beta_{visible}$, X-axes are infection rates in the hidden layers β_{hidden}

of observing a forbidden activation. Real life social networks are a good example of this because of a significant overlap between connections on different social media platforms. Moreover, social connectivity is characterised by high clustering [148] which increases the probability of observed neighbourhood being active, even though the activation came through an unobserved edge. The two distinct histogram regions in (b) are examples of such cascades that had a varied chance of occurring according to the log-likelihood measure. Those are indeed the examples of when it can be ambiguous whether there is a second layer or not. We shall discuss on how to address this issue later on. The fact that there are these two separate clusters of values is a coincidence of our choice of the values of β - the very low values are going to have much lower probabilities attributed to them as already discussed.

To further emphasise how sensitive the likelihood measure is to hidden topology in Fig. 2.2 we show its heatmaps for a selected bi-layer case from those presented in Fig. 2.1b. The likelihood is zero when the cascade contains at least one propagation along an edge that is present in the hidden layer but absent in the visible layer. When $\beta_{hidden} > 10^{-4}$ barely any instances have a non-zero likelihood. We can also see the separation visible earlier due to the infection rate, i.e. the differences in the means and standard deviations between predominantly stochastic or deterministic variants of the propagation process.

While the Barabási-Albert graph can be considered a decent model or real world networks [149] (although perhaps more of an idealised approximation [150]) we have already mentioned that these results were for a not strongly correlated cases. It would be of benefit to analyse scenarios where this correlation is in fact strong. Moreover it would be best if one could in fact control the level of the said correlation. In order to do that we shall introduce our own model of a bi-layer network that shall allow for just that.

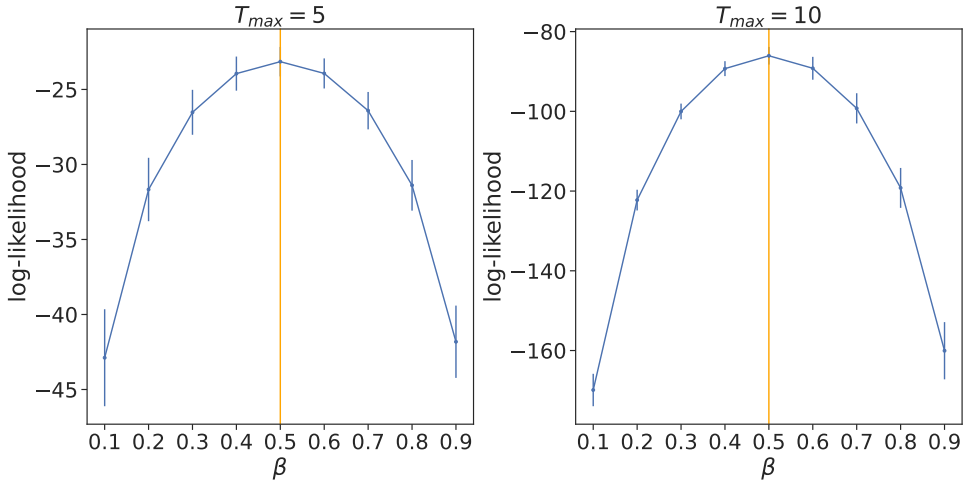

(a) mono-layer

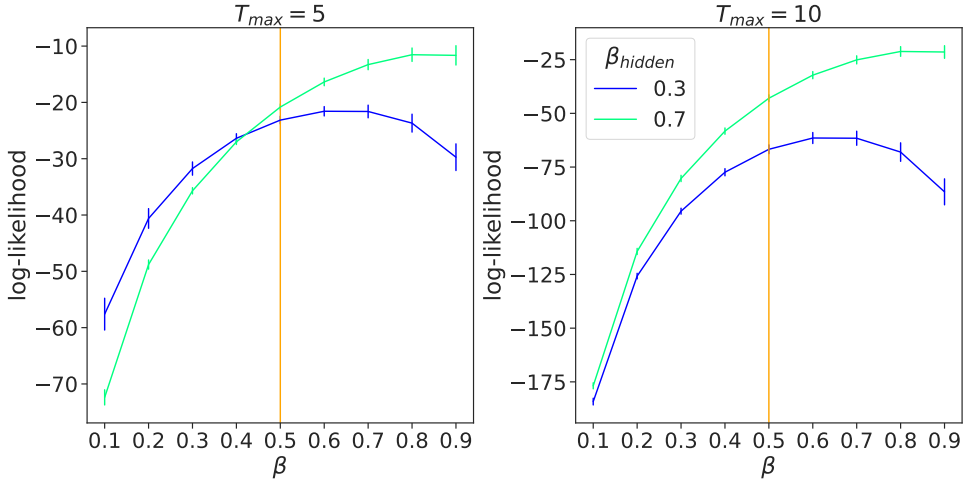

(b) bi-layer

Figure 2.3: Mean log-likelihood in function of β used in (2.1). Bars indicate the standard deviation. Orange vertical line at $\beta = 0.5$ indicates the $\beta_{observed}$ used in all simulations. Each point on plots of (a) represents 10^4 simulations while in (b) 10065 ± 2576 for $t_{max} = 5$ and 7029 ± 380 for $t_{max} = 10$ after removal of infinities (total for each point in both cases is 5×10^4). Bi-layer graph model was generated with $p = 0.01$

.

Let us take any graph, e.g. a square lattice as the first layer (also referred to as visible, observed or top layer) and then apply a rewiring procedure similar to the one introduced by Watts and Strogatz [116] to produce another (hidden or bottom etc.) layer. We can start with a square lattice as an equivalent of real relationships (affected by distance) but we will also explore a scale-free network as a starting layer. The point here is that the correlation between the two layers can now be parametrised by p - the probability of each node being rewired to any random (other) node. To see exactly what how Eq. (2.1) behaves in Fig. 2.3 we present its logarithm in function of a changing β. In (a) we simulate

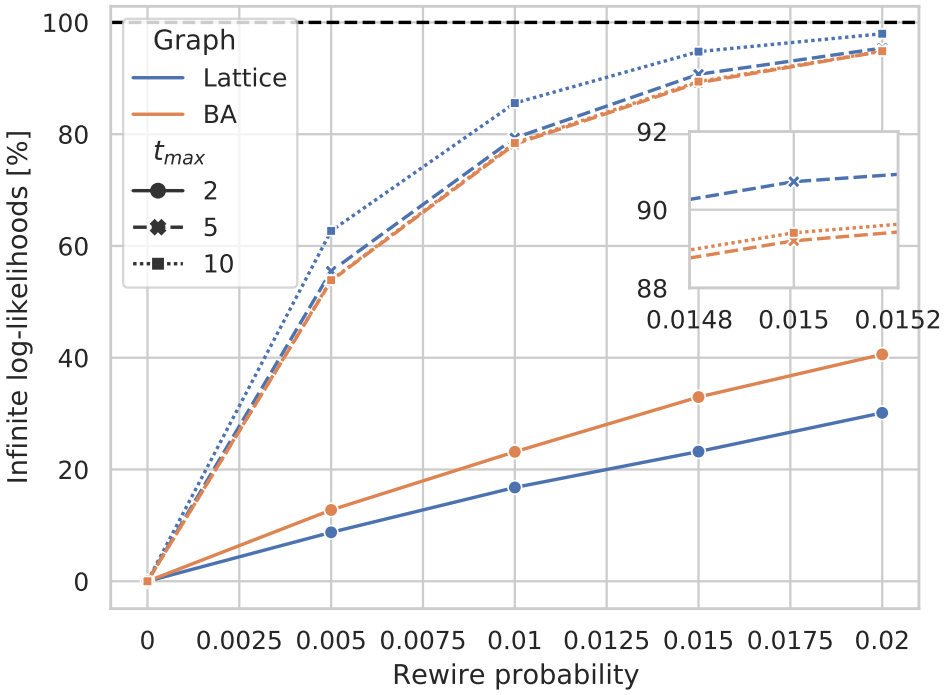

Figure 2.4: The percentage of log-likelihoods resulting with $-\infty$ as a function of the probability of rewiring p. We investigate two different cases of networks: square lattice and Barabási-Albert network for different lengths of cascades. The simulations were made for networks of size $N = 100$ with periodic boundary conditions in the lattice case. The inset zooms in on the curves obtained for $t_{max} > 2$.

the cascades with $\beta = 0.5$ (indicated by an orange vertical line) and then we lie to the measure by inputting a wrong value of β into the equation. What we expect and indeed see is that our measure has a maximum for the correct value. Now if we do a similar experiment with a bi-layer - panel (b) - it becomes very clear what the hidden layer is actually doing from the perspective of the log-likelihood - it shifts the maximum. Again it is not very surprising as we would expect the hidden connections to act as a boost to the propagation - the more connections (or simply faster connections) the higher *effective* β. This solidifies that the formulation we are exploring here brings sufficient merit.

Let us now see how this correlation between layers affects the values of Eq. (2.1). In Fig. 2.4 we show the ratio of log-likelihoods that were infinite as a function of the rewire probability for both a lattice and a Barabási-Albert graph, for three values of t_{max}. What becomes immediately apparent is that unless our observation window is unreasonably small even the tiniest changes to the graph structure result in a vast majority of measurements returning $-\infty$. Do note that the tested graph size was $N = 100$ which means that with a rewire probability $p = 0.01$ we in fact rewire on average a single edge. While it is tempting to leave it at that as it would seem that we have succeeded in

establishing a very reliable way of determining whether a hidden layer exists or not. We have, however, promised to address the ambiguity of a non-infinite results and so we shall do so now.

In order to address such a situation and still be able to evaluate whether a given set of cascades indicates existence of an unobserved layer or not, we assume a single layer model and utilise the Vysochanskij–Petunin (VP) inequality [151] to evaluate whether a given cascade could be generated by such a model.

We expect cascades that involved spreading through unobserved edges have significantly lower likelihood than those in the assumed null model. In the likely case, the distribution is unimodal, we can quantify how distant the value of an observed cascade likelihood is from the value expected from the single-layer model using the VP inequality which states that assuming X is a random variable with unimodal distribution (mean μ, finite and positive variance σ) and $\lambda > \sqrt{\frac{8}{3}}$, we have:

$$\Pr(|X - \mu| \geq \lambda\sigma) \leq \frac{4}{9\lambda^2}, \tag{2.3}$$

which after normalisation $\hat{X} = \frac{|X-\mu|}{\sigma}$ gives:

$$\Pr\left(\hat{X} \geq \lambda\right) \leq \frac{4}{9\lambda^2}. \tag{2.4}$$

Inserting $\lambda = \hat{x}$:

$$\Pr\left(\hat{X} \geq \hat{x}\right) \leq \frac{4}{9\hat{x}^2}, \tag{2.5}$$

which means that an upper bound of probability of obtaining a result $\hat{x}$ or greater from a normalised unimodal distribution describing $\hat{X}$ is:

$$p(\hat{x}) = \min\left(\frac{4}{9\hat{x}^2}, 1\right). \tag{2.6}$$

for $\hat{x} > \sqrt{\frac{8}{3}}$. In our case, x is the likelihood of a cascade given by Eq. (2.1), X is random variable describing the likelihood values for an assumed single layer model. After performing simulations, we calculate μ and σ, and normalise the x value obtaining $\hat{x}$.

In our experience the distributions X in the single-layer case are unimodal and $\hat{x} > \sqrt{\frac{8}{3}}$ with a sufficient observation time (t_{max}) thus the assumptions of the VP hold, however, as we are the ones producing these distributions then it is trivial to inspect whether that is the case before proceeding with the rest of our method. In the event that it is not true, an alternative theorem, analogous to the VP inequality (e.g. the Chebyshev's inequality

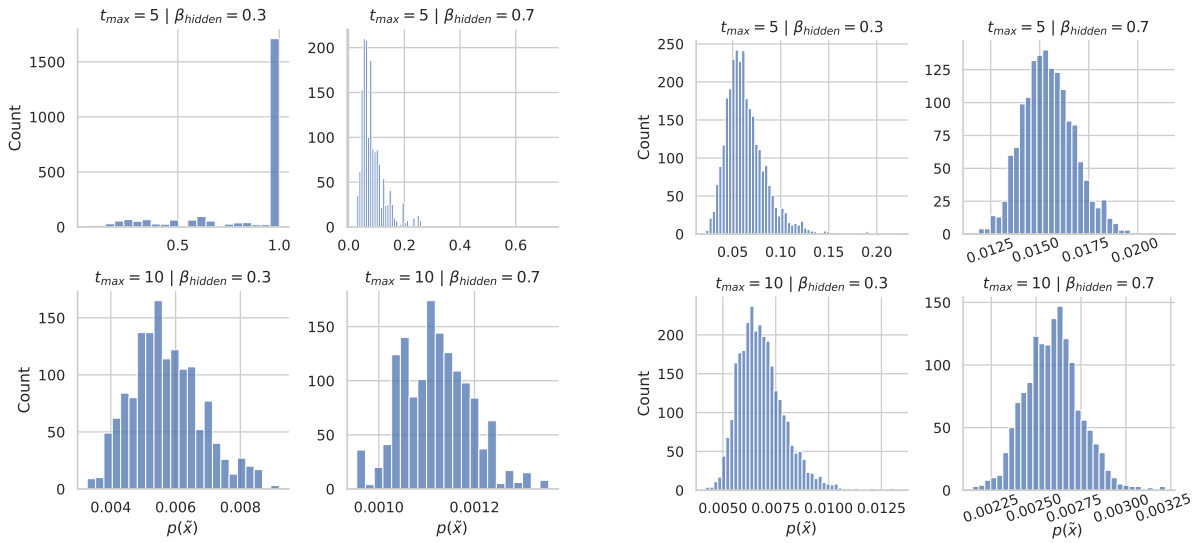

Figure 2.5: Histograms of $p(\hat{x})$ - the probability that the system has only one layer (see Eq. (2.6)) for various combinations of t_{max} and β_{hidden}. Plots on the left are generated for square lattice with rewiring, while the ones on the right are generated for BA network with rewiring. Parameters for all the networks are as follows: $\beta_{observed} = 0.5$, $N = 100$, $p = 0.01$ and $m = 3$ (in case of BA networks). Each histogram was made with 10^4 realisations.

[152]), can be introduced, or even more general approaches such as bootstrapping [153] can be used to determine the confidence level of the observation. Here, we use $p(\hat{x})$ to measure how surprising given cascades are, assuming they were generated by an SI process with known β simulated on a visible layer of the network.

In Fig. 2.5 we present distributions of Eq. (2.6) for various cases of a BA network with rewiring. Aside from the cases where the observation window is small and the infection rate is smaller than in the visible layer (which also means that the effect the hidden layer has on the system dynamics can be insignificant) we get unimodal distributions with a finite standard deviation around a fairly low mean value. What this means is that even when the situation is ambiguous on the first glance when the likelihood of a cascade (2.1) is combined with Eq. (2.6) often can provide us with sufficient certainty about the existence of the hidden layer. On the other hand it can also provide us with the contrary of course. Do note that $p(\hat{x})$ is a measure of how likely the observed cascades are given what we know about the system so no further statistical toolkit is required - one needs simply to declare with what kind of "gamble" they are comfortable with. We observe that in most cases a typical significance level of 0.05 would allow to reject the hypothesis of a singular layer system.

2.2 Finding links in the hidden layer

Now that we have established how to determine whether a hidden layer exists or not we shall go onto the topic of reverse engineering the missing connections. We shall assume to know the topology of the given visible layer and the infection rate of the hidden layer - β_{hidden}. We will try to find the topology by finding cases of node activation that could not be explained by the assumed single layer model. Then in each such case all nodes that were infected in a step preceding the unexplained activation are used to construct a set of possible edges. The details of the procedure are as follows:

1. Let $\mathcal{J}^c(t) = \{i \in \mathcal{N} : \tau_i^c \leq t\}$ be a set of nodes that *are infected* in a simulation step t of cascade c. $\mathcal{N}$ represents the set of nodes in graph G and τ_i^c is the activation time of node i in cascade c. $\Delta\mathcal{J}^c(t) = \{i \in \mathcal{N} : \tau_i^c = t\}$ will be a set of nodes that *became infected* in a simulation step t of cascade c.

2. Using above notation we can introduce a set of nodes that became infected in simulation step t of cascade c but were not a neighbour of any node infected at $t-1$:
$$\mathcal{U}^c(t) = \Delta\mathcal{J}^c(t) \setminus \bigcup_{m \in \mathcal{J}^c(t-1)} \partial m, \tag{2.7}$$
where ∂m is the known neighbourhood of node m.

3. If the likelihood of a cascade is zero then there is at least one hidden edge in a set:
$$\mathcal{E}(i,c) = \left\{ (i,k) : k \in \mathcal{J}^c(\tau_i^c - 1),\ i \in \bigcup_{t=1}^{t_{max}} \mathcal{U}^c(t) \right\}. \tag{2.8}$$
Likelihood of such an edge being the one that was activated to infect i is unknown and difficult to find. However we can say heuristically that the said likelihood is:
$$P^c(i,k) \sim (1 - \beta_{hidden})^{|\tau_i^c - \tau_k^c|}. \tag{2.9}$$

4. Then we must unify the candidates amongst the cascades. Namely if an edge (a, b) was detected in $c = 1$ but not in $c = 2$ we need to associate it with the likelihood of *not being detected* which is similarly non-trivial. Also similarly we can say whatever that likelihood is it must be $\sim (1 - \beta_{hidden})^{|\tau_i^c - \tau_k^c|}$

5. Finally, for each edge e we multiply its likelihoods, therefore obtaining a *joint likelihood* J:

$$J(e) = \prod_c P^c(e). \tag{2.10}$$

6. Edges that maximise J are most likely the hidden edges we seek.

The Eq. (2.9) is a fairly simple yet effective (as we shall see soon) heuristic. The hope for a direct expression for the edge likelihood is rather futile as it is quite easy to follow similar logic as with the derivation of Eq. (2.2) and realise very quickly how complicated such a formula becomes. Hence we rest here with the said heuristic. We are aware that there might be a potential way of finding a better approximation of the edge likelihood via techniques previously utilised by Lokhov et al. [15, 154, 155], however, that goes beyond the scope of our considerations here.

In order to test our propositions we shall need two more pieces: evaluation metrics and a null model. We find that a natural way of determining our success would be to use *sensitivity* that is the ratio between true-positives and all positives. In other words we shall look at the fraction of hidden edges that we have successfully found. As we simulate our systems many times, we take the mean of the sensitivity across all simulations. That on its own, however, we feel does not tell the whole story. Most trivially we could simply demand checking all possible connections and for such a proposition the sensitivity would return 1.0 (or 100% if we so choose). As such we extend upon a metric that the author of this dissertation had helped develop in some past works: $\alpha - \text{CSS}$ [6] which stands for $\alpha-$Credible Set Size. It represents the number of candidates one must investigate in order to have α level of certainty of finding the sought entity. In practice one computes the rank, i.e., the position of the entity they wish to find in the list of the candidates, which is in a descending order in accordance to a given measure the said entity should maximise. The step is repeated many times in order to get a distribution of that rank, and finally, one takes a quantile $q = \alpha$ of that distribution thus acquiring the $\alpha - CSS$ value. In our case the measure is the *joint likelihood* J described above in point 5., and there are multiple entities - edges - thus we have taken the liberty of adapting the said measure such that we take the *highest recorded rank* amongst the hidden edges and follow the rest as usual. I.e., here specifically, we compute J for the appropriate edges (see the procedure description 1.-6. above), order these edges by their $J(e)$ (highest to lowest), find the position of the actual hidden edges (their rank), take the highest recorded rank, repeat 10^4 times, take the quantile $q = 0.95$ of these ranks. We find that this is a good way of evaluating the practicality of our approach. It effectively tells us how many connections we would have

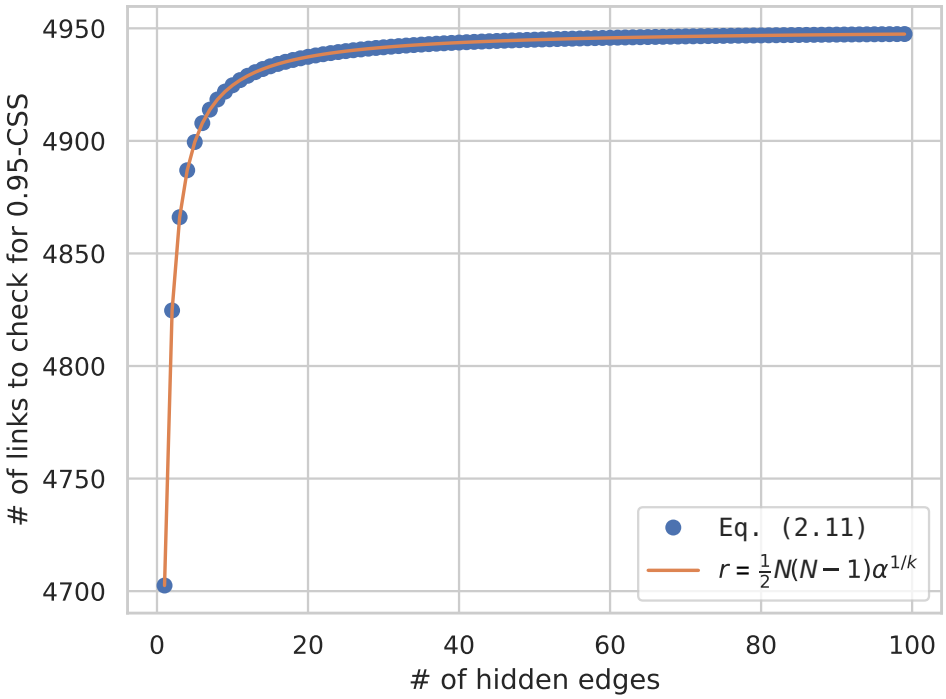

Figure 2.6: The number of edges required to check in order to have 95% certainty, according to the null model, of testing all hidden edges, as a function of number of hidden edges. The plot is done for a network with $N = 100$ nodes but the shape of the curve scales with the size of the network. Comparison is between the numerical solution of Eq. (2.11) and the approximation (2.13).

to test, say via some sort of targeted surveillance or measurements, to achieve α level of certainty of detecting all hidden communication channels.

A null model would quite naturally be random guessing. There are $\binom{N}{2}$ edges to check in a system with N nodes. So for instance, with $N = 100$ that is: $\binom{100}{2} = 4950$ in which case 95% certainty of finding one hidden link requires checking $0.95 \times 4950 = 4703$ (rounded up) edges. In general the number r of links required to check in order to have α certainty, according to the null model, can be obtained from:

$$\frac{\binom{r}{k}}{\binom{\binom{N}{2}}{k}} = \frac{r!}{(r-k)!}\frac{\left(\binom{N}{2}-k\right)!}{\binom{N}{2}!} = \alpha, \tag{2.11}$$

where k is the number of hidden edges and N is the number of nodes.

The curve representing r as a function of k in the case of $N = 100$ nodes is shown in Fig. 2.6. As we show later on our proposition requires substantially less edges to be checked. Since Eq. (2.11) requires to be solved numerically, we also derive an asymptotic approximation as follows: Denote $\binom{N}{2}$ as ξ, then

β_{hidden}	$\beta_{observed}$	*sensitivity*	*0.5-CSS*	*0.95-CSS*
0.3	0.5	0.81	108	322
0.7	0.5	0.85	162	422

Table 2.1: Sensitivity and α-CSS for a square lattice with rewiring ($N = 100$, $t_{max} = 10$, $p = 0.01$). Results obtained for 10^4 realisations per scenario where each scenario had 10 independent cascades from (possibly) different sources.

$$\begin{aligned}\alpha &= \frac{r!}{(r-k!)}\frac{(\xi-k)!}{\xi!} \\ &= \frac{(r-1)(r-2)\dots(r-k)!}{(r-k!)}\frac{(\xi-k)!}{(\xi-1)(\xi-2)\dots(\xi-k)!} \\ &= \frac{(r-1)(r-2)\dots(r-k+1)}{(\xi-1)(\xi-2)\dots(\xi-k+1)} \sim \left(\frac{r}{\xi}\right)^k.\end{aligned} \tag{2.12}$$

We can therefore conclude that

$$r \sim \frac{1}{2}N(N-1)\sqrt[k]{\alpha}. \tag{2.13}$$

The comparison of this result to the numerical solution is shown in Fig. 2.6.

Now we can finally commence testing of our method. Tables 2.1 and 2.2 show the results of applying our method to both lattice and Barabási-Albert networks with hidden layers produced by rewiring (with probability $p = 0.01$). When comparing the two settings one can observe a certain interplay between sensitivity and α-CSS. For lattice based network the sensitivity is significantly higher than in Barabási-Albert case but at the same time scale-free case is characterised by a much lower α-CSS for both $\alpha = 0.5$ and $\alpha = 0.95$. In other words, it is easier to correctly identify hidden edges when we have a locally connected network (lattice) but at the same time a scale-free network requires a smaller set to find all hidden edges (despite reaching a lower sensitivity level). Note that in both cases the observed 0.5-CSS and 0.95-CSS are significantly lower than for the null model where, depending on the number of rewired links, they would be larger than 2475 and 4703 respectively (see Eq. (2.11) for $N = 100$ and $k = 1$ – the higher the k, the more links need to be checked for the null-model). Full distribution of ranks from which the α-CSS was computed is shown for both networks at Fig. 2.7.

As already discussed when the layers are not correlated it is easy to identify that there is a hidden spreading channel. Nevertheless, finding the actual unobserved links may still be challenging. Both Fig. 2.8 and 2.9 show that density of the observed network is an important factor. From the sensitivity perspective it is better to have a denser observed

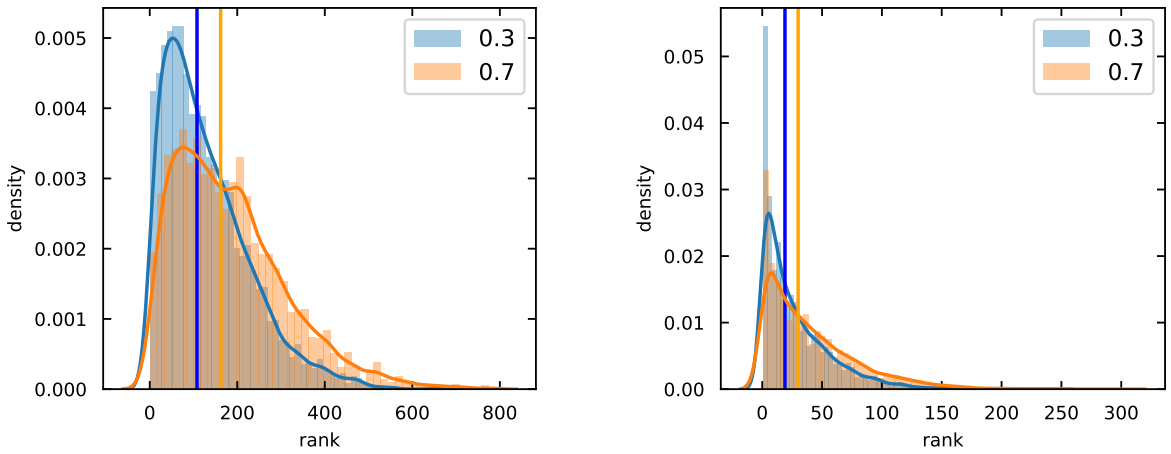

Figure 2.7: Distribution of ranks of hidden edges with medians as vertical lines. Left: lattice with rewiring ($N = 100$, $t_{max} = 10$, $p = 0.01$). Right: BA network with rewiring ($N = 100$, $t_{max} = 10$, $m = 3$, $p = 0.01$). Results obtained with 10^4 realisations per scenario where each scenario had 10 independent cascades from different sources. These results are for those realisations where all hidden edges were detected.

β_{hidden}	$\beta_{observed}$	*sensitivity*	*0.5-CSS*	*0.95-CSS*
0.3	0.5	0.53	19	87
0.7	0.5	0.69	30	116

Table 2.2: Sensitivity and α-CSS for a Barabási-Albert network with rewiring ($N = 100$, $t_{max} = 10$, $m = 3$, $p = 0.01$). Results obtained for 10^4 realisations per scenario where each scenario had 10 independent cascades from (possibly) different sources.

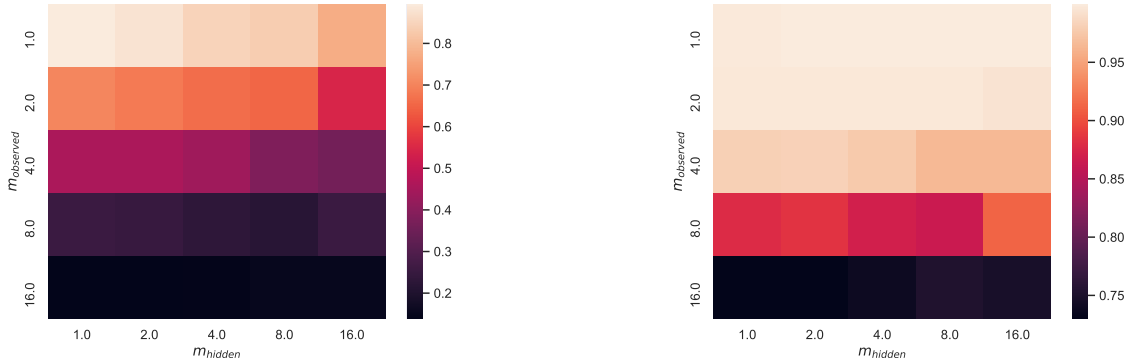

(a) 1000 nodes and 10 cascades

(b) 1000 nodes and 100 cascades

Figure 2.8: The sensitivity as a function of m_{hidden} and $m_{observed}$ for two layer Barabási-Albert network with $\beta_{hidden} = 0.7$, $\beta_{observed} = 0.5$ and $t_{max} = 10$. The results are averaged over 20 independent runs.

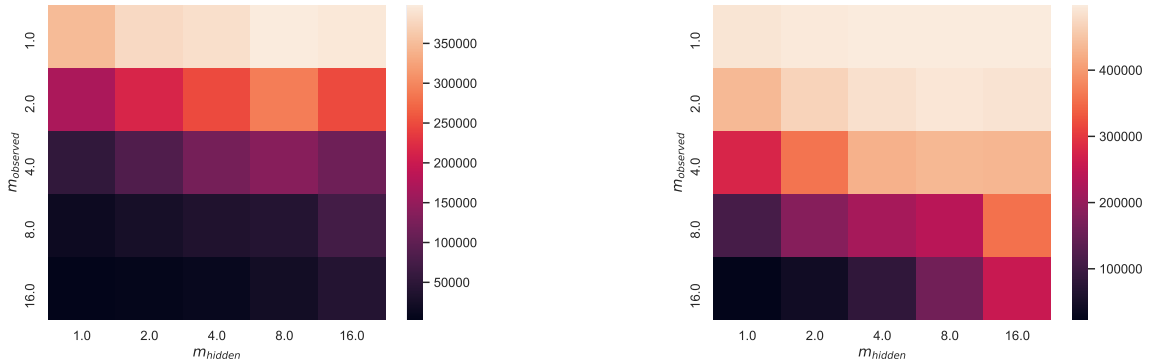

(a) 1000 nodes and 10 cascades

(b) 1000 nodes and 100 cascades

Figure 2.9: The 0.95-CSS as a function of m_{hidden} and $m_{observed}$ for two layer Barabási-Albert network with $\beta_{hidden} = 0.7$, $\beta_{observed} = 0.5$ and $t_{max} = 10$. The results are averaged over 20 independent runs.

network. Unfortunately the 0.95-CSS also grows with the density of known connections, making it more demanding to find all the connections. Additionally, although the effect is weaker, it is beneficial for both measures if the hidden layer is sparser. This aligns with intuition since more hidden connections can make the observed dynamics much more complex and unsurprisingly having more data about the cascades also makes the task easier. The actual dependence between the number of cascades and the sensitivity is shown in Fig. 2.10. For a relatively big BA network we need around 30-40 cascades to reach a fairly satisfactory sensitivity level of around 0.8. Depending on the specifics of the problem such amounts of data may be considered a lot (e.g., in epidemic spreading) or easily available (e.g. information spreading on social media).

On top of synthetic networks we also use real-world data to build a multi-layer network and empirically test our methods. For that purpose we choose the data collected among employees of the Department of Computer Science at Aarhus University [156]. It is a multi-layer network consisting of Facebook friendships, co-authorships, work, leisure (repeated leisure activities) and a lunch layer (regularly eating lunch together). Its full structure is presented in Fig. 2.11 with each layer being shown as a separate network. The whole network has 61 nodes and 620 (unique) edges in total.

Main results for the Aarhus data are shown in Tables 2.3, 2.4 and 2.5, which use respectively Facebook, work and lunch layers as the visible parts of the graph. We omitted the other two possible cases because of their low density of connections. We treat remaining hidden layers as one, aggregated layer as it does not matter how many layers exactly there are in our detection method. Sensitivity and CSS values are consistent with

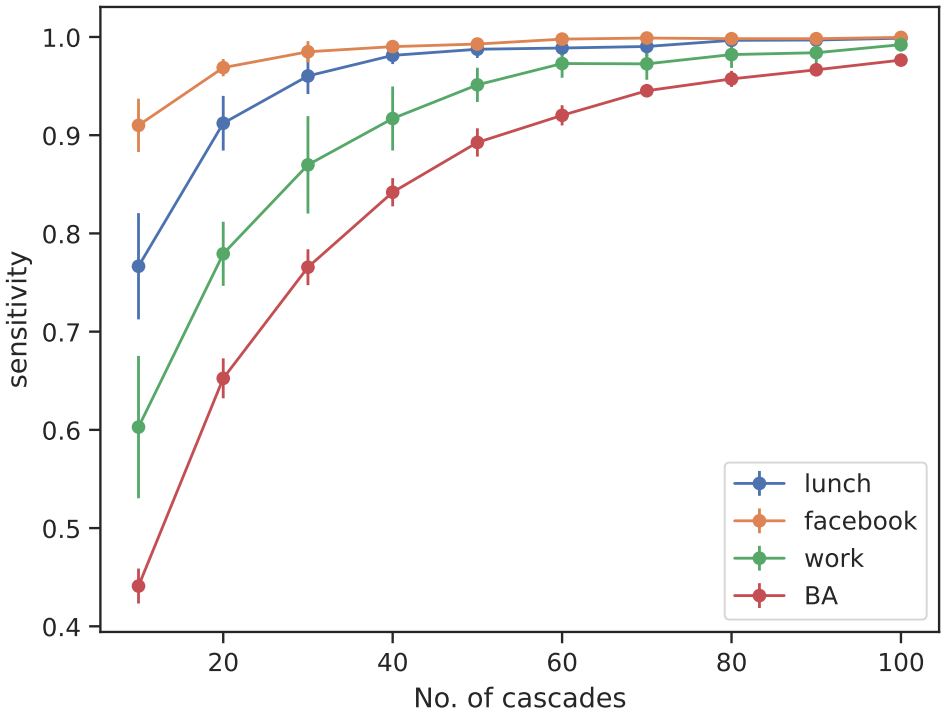

Figure 2.10: The sensitivity as a function of number of cascades for a) two layer Barabási-Albert network with $m = 4$ for both layers, $\beta_{hidden} = 0.7$, $\beta_{observed} = 0.5$, $N = 1000$ and $t_{max} = 10$ (red line); b) Aarhus data with different layers as the observed network (lunch – blue line, facebook – yellow line and work – green line). The results are averaged over 20 independent runs and the error bars represent one standard deviation.

β_{hidden}	$\beta_{observed}$	*sensitivity*	*0.5-CSS*	*0.95-CSS*
0.3	0.5	0.78	1392	1434
0.7	0.5	0.78	1423	1468

Table 2.3: Sensitivity and α-CSS for the Aarhus data, with Facebook layer as the observed network. Results obtained for 10 cascades with $t_{max} = 10$.

synthetic results in the sense that they both grow with the density of the visible layer. It is also apparent that our approach far exceeds the performance of the null model. Independently of which layer will be chosen as the visible one, random guessing would require us to check all possible $\binom{61}{2} = 1830$ links, see Eq. (2.11), with $k \in \{159, 160, 229\}$ for *work*, *lunch*, *facebook* as the visible layer respectively. Our method, on the other hand, needs significantly less than that. Here, k is the number of unique edges in the whole graph (353) minus the number of edges in the visible layer. Note that in order to account for the fact that our method does not always find *all* the links, i.e., sensitivity < 1, one can adjust Eq. (2.11) such that one multiplies k by the expected sensitivity. That, however, barely changes the result, i.e., null model requires maybe one or two edges less than all

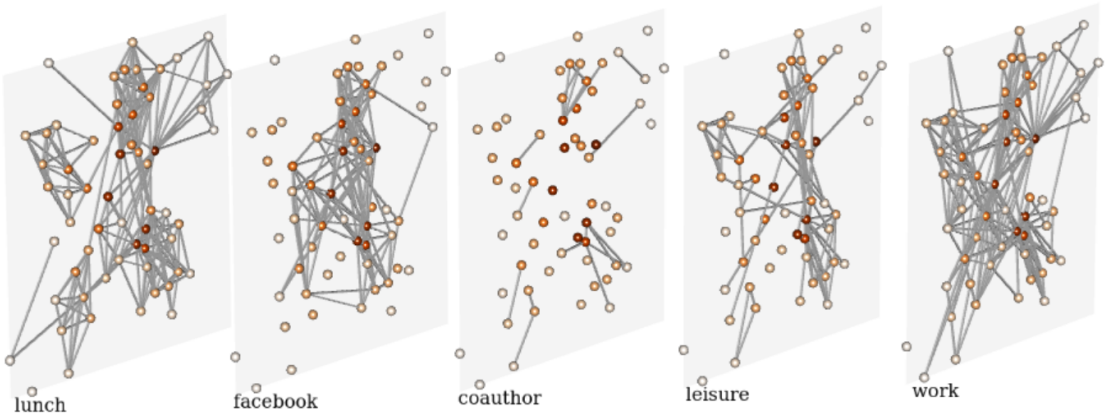

Figure 2.11: Visualisation of the multi-layer network representing the Aarhus data [156]. We utilise this network as a real world example of possible application of our methods. It is quite natural to imagine we know only one of the layers presented here and would like to infer the existence and possibly structure of others. Note that co-author and leisure layers are disconnected and thus we do not use them as visible layers in our analyses as that makes the task of detecting hidden connections potentially much easier.

possible at best. Moreover, our method gets the more successful the more cascades we can observe. A more detailed dependence between sensitivity and the number of cascades is shown in Fig. 2.10, where different colours represent different observed layers. In Fig. 2.12a we show the distributions of ranks for the work layer as the visible network and when comparing them with the synthetic experiments the two distributions for $\beta_{hidden} = 0.3$ and $\beta_{hidden} = 0.7$ are much more symmetric and separated. The distributions of the other two analysed visible layers are qualitatively similar further supporting the merit of our approach, see the results on the "lunch" and "facebook" as observed layer scenarios in Fig. 2.12b and 2.12c.

β_{hidden}	$\beta_{observed}$	*sensitivity*	*0.5-CSS*	*0.95-CSS*
0.3	0.5	0.31	400	536
0.7	0.5	0.42	591	730

Table 2.4: Sensitivity and α-CSS for the Aarhus data, with work layer as the observed network. Results obtained for 10 cascades with $t_{max} = 10$.

We can also test how our layer detection scheme holds for different infection rates and system sizes. By conducting analogous experiments to those presented in Fig. 2.5 we can show the mean and standard deviation of $p(\hat{x})$ from Eq. (2.6) as a function of these variables. We set the visible infection rate $\beta_{visible} = 0.5$, $t_{max} = 10$, and simulate 10^4 times per data point.

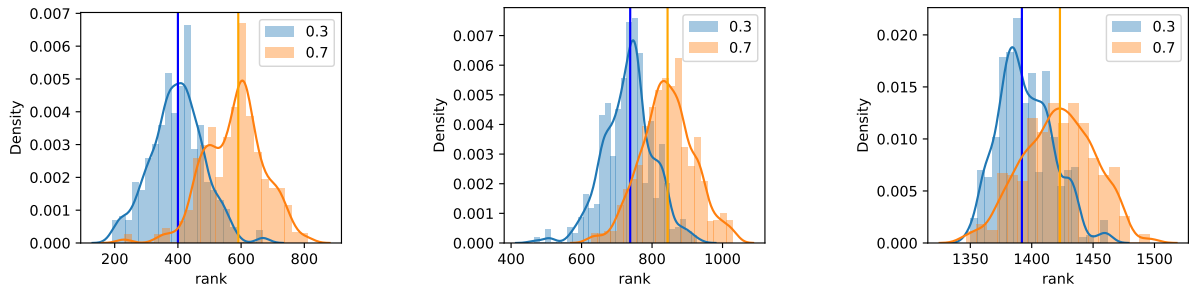

(a) Work (b) Lunch (c) Facebook

Figure 2.12: (a) Distribution of ranks of hidden edges, with medians as vertical lines, for the Aarhus data, with work layer as the observed network. Results obtained for 10 cascades with $t_{max} = 10$, $\beta_{observed} = 0.5$ and two values of β_{hidden} – 0.3 and 0.7, (b) with lunch layer as the observed network, (c) Facebook layer as the observed network.

β_{hidden}	$\beta_{observed}$	*sensitivity*	*0.5-CSS*	*0.95-CSS*
0.3	0.5	0.51	738	837
0.7	0.5	0.56	844	974

Table 2.5: Sensitivity and α-CSS for the Aarhus data, with lunch layer as the observed network. Results obtained for 10 cascades with $t_{max} = 10$.

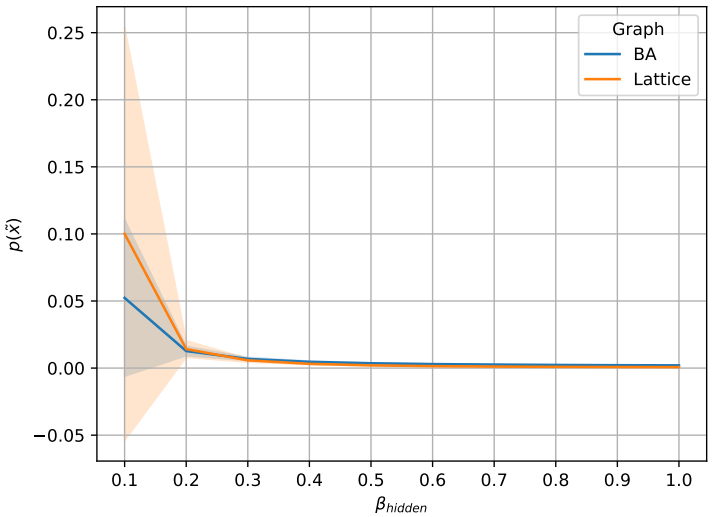

Figure 2.13: Mean probability that the system has only one layer as a function of the infection rate on the hidden layer - β_{hidden} - see Eq. 2.6 and Fig. 2.5. The colour bands represent one standard deviation. Results for two graphs are presented - BA ($m = 3$) and a square lattice with system size $N = 100$, $\beta_{visible} = 0.5$, and $t_{max} = 10$. Each point is the results of 10^4 simulations.

In Fig. 2.13 we show results for a BA graph ($m = 3$) and a square lattice with the infection rate of the hidden layer $\beta_{hidden} \in [0.1, 1.0]$. When β_{hidden} is small we see a

wide spread of the $p(\hat{x})$ values which is not surprising as the probability of a hidden edge being the preferred connection is also small. As the hidden infection rate rises both the expected value and the variance diminish quickly showing that if the hidden layer is significant enough to cause an effect in the whole system then our method will detect it.

In Fig. 2.14 we show how the size of the network, $N \in [50, 500]$, affects the $p(\hat{x})$. On the left we present results for BA ($m = 3$) and on the right for a square lattice. In both cases we choose $\beta_{hidden} = 0.1$ as this is the "worst case" scenario from the previous plot. The blue line shows the mean and one standard deviation of $p(\hat{x})$ while the red shows the ratio of infinite log-likelihoods. For the BA graph the statistic is still sufficient in the tested range, however, for the lattice it is not. On the left we can see that as the size increases the mean and variance diminish which is due to the fact that the larger the graph the more potentially "forbidden" links are possible, and thus the detection of the hidden layer becomes easier. On the right the blue curve shows some wild values and that is because of how quickly the red curve rises up to virtually being equal 1. By the time we reach $N = 500$ only an order of 30 realisations out of 10^4 are finite, rendering the blue curve a bit misrepresentative, as the statistic is insufficient and biased towards cascades very similar to those generated by a single layer model. We show it here for the sake of completeness.

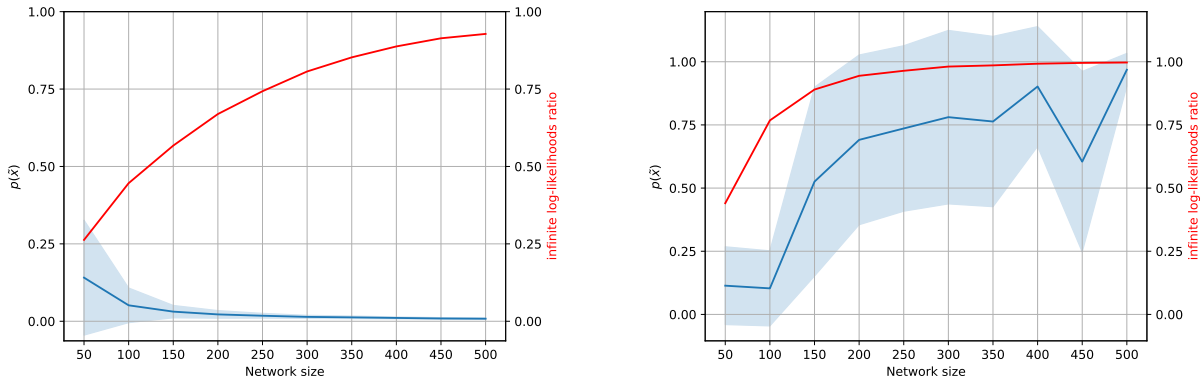

Figure 2.14: Mean probability that the system has only one layer as a function of the system size (blue) - see Eq. 2.6 and Fig. 2.5. The hidden layer infection rate - $\beta_{hidden} = 0.1$. The colour bands represent one standard deviation. Results for two graphs are presented - BA ($m = 3$, left) and a square lattice (right) $\beta_{visible} = 0.5$, and $t_{max} = 10$. Each point is the results of 10^4 simulations. The red curves (Y-axis values on the right side of the plots) represent the ratio of infinite ($-\infty$) log-likelihoods detected in the data (see Fig. 2.4). The wide spread and increasing behaviour for the lattice is the result of a very high infinite log-likelihoods ratio - by the time we reach $N = 500$ only an order of 30 realisations out of 10^4 are finite.

Our methodology can easily be applied to different spreading processes. One example of such process is the Independent Cascade (IC) model. The factorised form of the likelihood, in case of the IC model, is the same as for the Susceptible-Infected model

$$P(\Sigma|G,\{\beta_j\}) = \prod_{i\in V}\prod_{c\in C} P_i(\tau_i^c|\Sigma^c, G, \{\beta_j\}). \tag{2.14}$$

The form of the local probability, however, is different

$$\begin{aligned} P_i(\tau_i^c|\Sigma^c, G, \{\beta_j\}) = \left(\prod_j \prod_{k\in\partial_j i} \Big(1-\beta_j[\tau_k^c \le \tau_i^c - 2]\Big)\right)\times \\ \times\left(1-\prod_j\prod_{k\in\partial_j i}\Big(1-\beta_j[\tau_k^c=\tau_i^c-1]\Big)[\tau_i^c<t_{max}]\right), \end{aligned} \tag{2.15}$$

which is only valid for $\tau_i^c > 0$, otherwise it is equal to one. The plots equivalent to Fig. 2.4 and Fig. 2.7 in the case of the IC model are shown respectively in Fig. 2.15 and Fig. 2.16. Note that these results do not deviate significantly from the SI simulations. This is

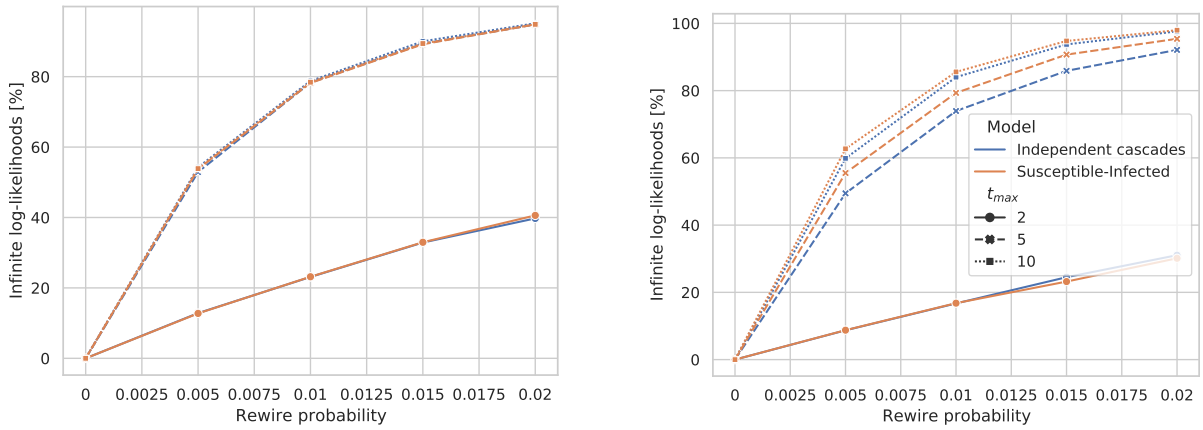

Figure 2.15: The percentage of log-likelihoods resulting with $-\infty$ as a function of the probability of rewiring p. Simulations were conducted using two different spreading models - Susceptible Infected (presented in main text) and Independent Cascades for comparison. We investigate two different cases of networks: a square lattice (right) and the the Barabási-Albert network (left) for different lengths of cascades. The simulations were made for networks of size $N = 100$ with periodic boundary conditions in the lattice case.

interesting for two reasons. First, one could easily produce artificial examples where either IC or SI would be very easier to recover. On one hand it should be easier for IC model to spot any forbidden dynamics, because of the restrictive condition regarding only one time step where spreading is possible for a single node. SI, on the other hand, ensures more statistics, because of the opposite situation (nodes can spread at any time once they are

infected). Second, since these are limiting versions of the SIR model, all other variations (where recovery probability is between 0 and $+\infty$) will also produce similar results. This makes the shown results much more universal, than just for the two analysed models.

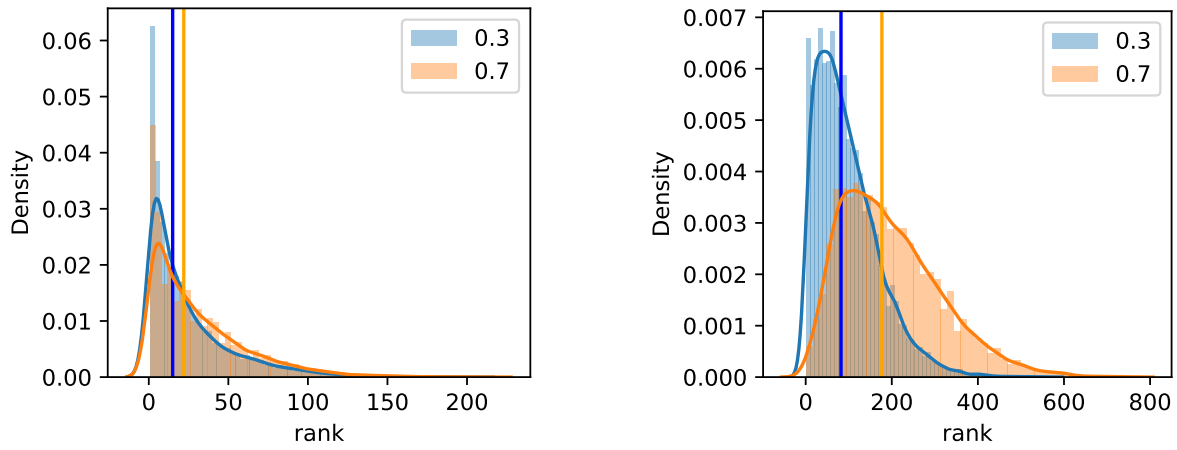

Figure 2.16: Distribution of ranks of hidden edges with medians as vertical lines. Simulations were conducted using the Independent Cascade model for comparison against the results from the main text (which show results for the Susceptible Infected model). Right: lattice with rewiring ($N = 100$, $t_{max} = 10$, $p = 0.01$). Left: BA network with rewiring ($N = 100$, $t_{max} = 10$, $m = 3$, $p = 0.01$). Results obtained with 10^4 realisations per scenario where each scenario had 10 independent cascades from different sources. These results are for those realisations where all hidden edges were detected.

Data from synthetic and empirical networks alike confirm that uncovering the hidden spreading channel is a relatively simple task with our approach - especially when the layers are uncorrelated. It is, however, more difficult to identify specific hidden connections. Despite the general similarities there are some quantitative differences between the results obtained with synthetic and real data. One of the most significant differences is how β_{hidden} relates to the distribution of ranks of hidden edges, influencing the difficulty of hidden connections reconstruction. This effect is much stronger in real world networks than in synthetic ones. It can, however, be explained by the difference in density between hidden and observed networks. In the corresponding plots for synthetic data (see Fig. 2.7) both layers have the same density. Here the hidden layer is denser (it is a sum of four hidden layers) and so changing the hidden spreading probability affects majority of connections.

An important factor in being able to successfully recover the hidden connections turns out to be the density of both the hidden and the observed transmission layers. Specifically, we observe that the denser the hidden layer the harder it is to find the exact connections. An interesting interplay takes place when it comes to the density of the observed layer. On one hand the sensitivity decreases with the density of observed layer, on the other

hand, the α-CSS is also decreasing with the density. This observation, confirmed by both synthetic and real data, means that as the number of connections on a visible layer increases, we are able to identify less hidden edges on average but we need to take into account a smaller set of potential edges in order to find all of the hidden connections.

It should be pointed out that we only focus on the hidden connections which are not overlapping with the observed ones. This means that for correlated layers there might be only few unknown connections whereas the overlapping edges are also influencing the dynamics. Focusing on the more general picture and including the overlapping connections is an interesting subject for future research. Another research direction would be to focus on further improving the hidden connections identification algorithms. These improvements should include both the effectiveness and scalability of proposed methods. The latter is specifically important since real world networks are often quite substantial in size. From the perspective of empirical data it would also be useful to have a way of handling a scenario where different layers have different values of β which may or may not be known. Finally, a more radical generalisations like including temporal networks could also prove to be an interesting research problem.

Chapter 3

Discovering hidden layers in quantum graphs

In the previous chapter we have explored how to detect and reverse engineer hidden edges in a multi-layer network from observations of a well known epidemiological model - Susceptible-Infected. In this chapter we shall consider a different (and perhaps less known) type of propagation model – quantum graphs. Quantum graphs are graphs that have been equipped with a metric (simply put - there is a measure associated with its elements) and a second order differential operator (a Hamiltonian). It is worth noting here that we do not need to use typical Hamiltonians from quantum mechanics - a classical Laplacian also satisfies that definition. Therefore one can think of quantum graphs as of taut strings, fused together at the vertices. For details we refer the Reader to the introductory section 1.3.

The primary question now, however, is why quantum graphs? There has been plenty of examples of their applications yet this field is still fairly fresh and only recently starting to grow. More importantly the consequences of the mathematical formalism seem to be perfectly suited for the purposes of modelling information propagation. It allows us to have a propagating wave through a given complex system whilst the speed of this propagation is *finite* as opposed to diffusive or epidemiological models. As such it is of great interest to us to be able to distinguish amongst mono- and multi-layer topologies and maybe even deduce something about the hidden structures from measurements on the visible layer in a similar fashion to what we have already done for the SI model.

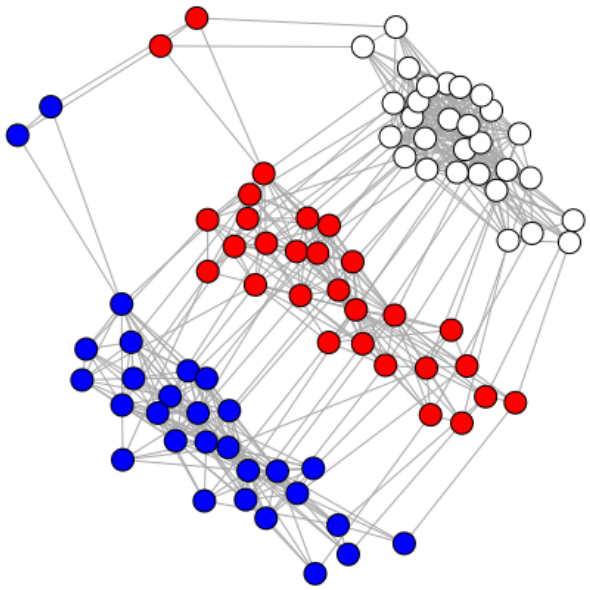

Figure 3.1: Three-layered multiplex representation of the Vickers [157] data.

3.1 Wave definition

Let us begin by defining the details of the system we are going to be studying. We assume a wave packet propagation dynamics on a quantum graph as our model for the dynamical system. Each edge e in the graph G has an associated length $l_e = 1$ and a spatial coordinate variable $x_e \in [0, l_e]$ along the said edge. We use a special case of a Hamiltonian - an edge based Laplacian giving us an edge-based wave equation on a graph in the form:

$$u_{tt} d\mathcal{E} = -\Delta u \tag{3.1}$$

where $\mathcal{E}$ is a Lebesgue measure on the graph's edges [123, 125], and u is a square integrable function defined on the graph. Specifically $u(n)$ is the value of u at the node n, and $u(e, x_e)$ is the value of u at the position x_e along the edge e [48].

We use the Neumann boundary conditions stating that the sum of the outward pointing gradients at every vertex must vanish [48, 123]:

$$\forall v \in G, \ \sum_{e \ni v} (-1)^{1-x_{e,v}} \nabla u(e, x_{e,v}) = 0 \tag{3.2}$$

The initial condition for the wave equation is a Gaussian wave packet:

$$u(e, x) = \exp\big(- a(x - \mu)^2 \big) \tag{3.3}$$

which is fully contained within a single edge with the highest betweenness centrality[158,

159] following the conventions of Aziz et al [48]. We simulate the many-layer system in a multiplex configuration, i.e. we consider a system with a set of $L \geq 1$ interacting layers (mono-layer networks), where each of them has the same set of N nodes but different topologies (set of connections), and each node is connected to its reflection (also sometimes called a replica) in a neighbouring layer (see Fig. 3.1 for a real-world network example and Fig. 3.2 for a wave propagation example on a simple synthetic graph). In its simplest form a multi-layer system can be represented with a set of intra-layer adjacency matrices $\{\mathbf{C}^l\}$ ($\forall_l \mathbf{C}^l \in \mathcal{R}^{N\times N}$), where $\mathbf{C}^l_{i,j} = 1$ when nodes i, j are connected in the layer l and 0 otherwise. Additionally we need a set of inter-layer adjacency matrices $\{\mathbf{B}\}$ ($\mathbf{B} \in \mathcal{R}^{L\times L}$), where the elements $\mathbf{B}_{l_1,l_2}$ signify whether the layers l_1, l_2 are connected (i.e., each node from layer l_1 is connected to its replica in layer l_2). $\{\mathbf{C}^l\}$ and $\{\mathbf{B}\}$ can then be combined into a single adjacency matrix $\mathbf{A} \in \mathcal{R}^{LN\times LN}$. For an example of how that can be done see Sec. 3.5, and for a more elaborate tensor formulation (unnecessary for our purposes here) see Ref.[7]. While the propagation simulations are computed on full systems, for the detection purposes we always only use information from a single layer, i.e., all but one layer are hidden from the perspective of our methods at all times.

Although the idea of travelling waves in the network structure might seem to be academic and considered artificial as being far from typically considered dynamics such as epidemic [4] or opinion spreading [106, 107], it is essential to note that the wave can simply model the information propagating due to interdependences between these concepts [160]. Also in the case of networks, certain propagation dynamics connected to shock waves [161] or excitable nodes [162, 163] have been successfully undertaken. Therefore our study brings very specific applications for a variety of real-world systems.

3.2 Gaussian wave packet signature (WPS)

Gaussian wave packet signature (WPS) is a methodology developed by Aziz et al., [48] that allows to distinguish between various types of graphs. The procedure starts by initiating an edge with a Gaussian wave packet that is completely contained on the said edge (see the left panel in Fig. 3.2). The edge is chosen to be the one with the highest betweenness centrality to assure fastest possible spread of the wave on the graph (although this can, of course, be relaxed in general). The choice of the edge from which the propagation starts does not impact either of the presented methods performance (including our own Fourier transform based described later). All this does is simply speeding up our testing set up, while in practice it would even be possible to apply the methods without knowing (or choosing) the primary edge at all. Additionally this is the choice presented in [48],

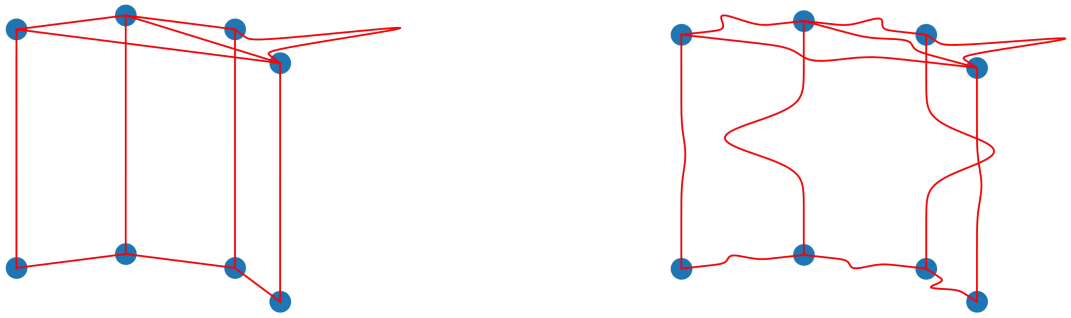

Figure 3.2: Illustration of a wave starting at a specific edge (left, $t = 0$) and then propagating through the multiplex system (right, $t > 0$).

and we follow that for the sake of continuity and ease of comparison. Then on each integer time we measure the amplitude in the centre of every edge $2|E|$ times in total, where $|E|$ is the number of edges in the known layer (see the right panel in Fig. 3.2 and Sec. 1.3 for a detailed description of the way the amplitude is calculated). Again, the number of measurements has been selected for the sake of comparison with [48] where such a value had been used. The difference here is that Aziz et al., assume knowledge of the whole graph and $|E|$ there refers to all edges in the system, whilst for us it refers only to the visible layer. We measure the centre of each edge because at integer times the highest value is in the centre. Finally, we create a histogram with 100 bins of these measurements - this is the WPS of the graph. Aziz et al., show that particular graph types (say Barabási-Albert, Erdős–Rényi etc.) will have similar WPSs yet different in comparison to other types (so e.g. one can differentiate an ER from BA). In order to actually do this differentiation one must build a classifier. In their work a K-nearest neighbours (K-NN) classifier was chosen. From the perspective of the machine learning tools we use here (K-NN, PCA) each histogram bin of the WPS is a dimension in the feature space.

For our purposes we will deviate slightly from this procedure. Namely to us the whole graph is not known and the graph itself is a multiplex. Additionally we assume that the wave propagation is an actual process ongoing through some network. Thus, we assume we have access to a single layer on which a certain spread has happened that can be modelled with a Gaussian wave packet and we suspect there may be hidden layers in the network. The question is - can we detect their presence?

The rest of the procedure is similar, i.e. we create a WPS and we train a classifier on a given type of a graph (e.g. BA) and this time the classes are the number of layers. See

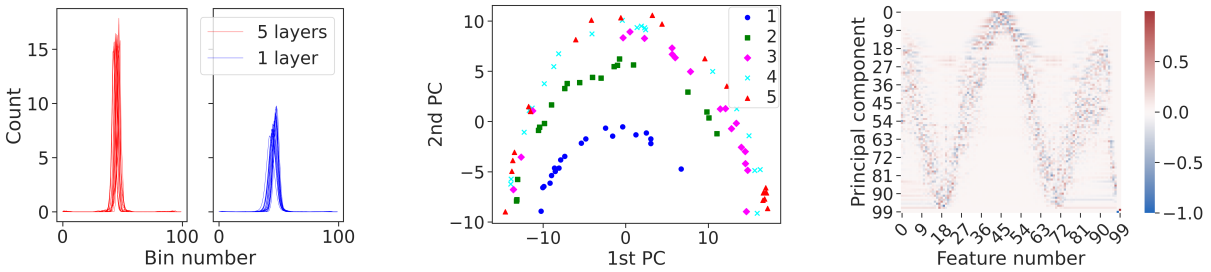

Figure 3.3: Wave packet signatures (left) for various realisations of a Barabási-Albert ($N = 50$, $m = 3$) graph with 5 and 1 layers (measured on one layer only). WPS projected onto a 2D space with PCA (centre) where colours and symbols distinguish the no. of layers. Each point is a different BA graph. PCA transformation matrix (right) showing the contributions of given WPS bins into principal components.

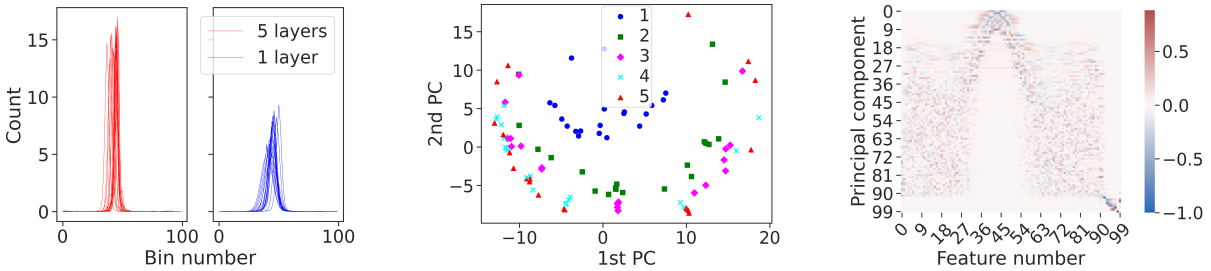

Figure 3.4: Wave packet signatures (left) for various realisations of a Erdős–Rényi ($N = 50$, $\langle k \rangle = 6$) graph with 5 and 1 layers (measured on one layer only). WPS projected onto a 2D space with PCA (centre) where colours and symbols distinguish the no. of layers. Each point is a different ER graph. PCA transformation matrix (right) showing the contributions of given WPS bins into principal components.

Fig. 3.3 and 3.4 where we compare WPSs of a 5-layer BA graph vs 1-layer and a 5-layer ER graph vs 1-layer respectively. One can clearly see that the signatures are distinct. To further illustrate this we use the Principal Component Analysis (PCA, see Sec. 1.4 for details) to project the WPSs onto a 2D space (see the centre pieces of Fig. 3.3, 3.4). There one can see that each class takes a distinct region of space and thus we should be able to discriminate between them. However, it is worth noting that the more layers there are the more tightly packed the observations become, i.e. discriminating between a mono-layer and a penta-layer graph is fairly easy but between a tetra- and a penta- not as much. It is also worth noting that through the PCA we can see that the centre bins carry the most variance in the feature space (see panels on the right in Fig. 3.3, 3.4) and that there are certain distinct structures visible in the higher PCs for both BA and ER graphs.

As mentioned before, we follow Aziz et al., and also choose the K-NN for classification (see Sec. 1.4 for a description of the K-NN method). We build the model on various graphs with between 1 and 5 layers (with values measured only on one of the layers each time,

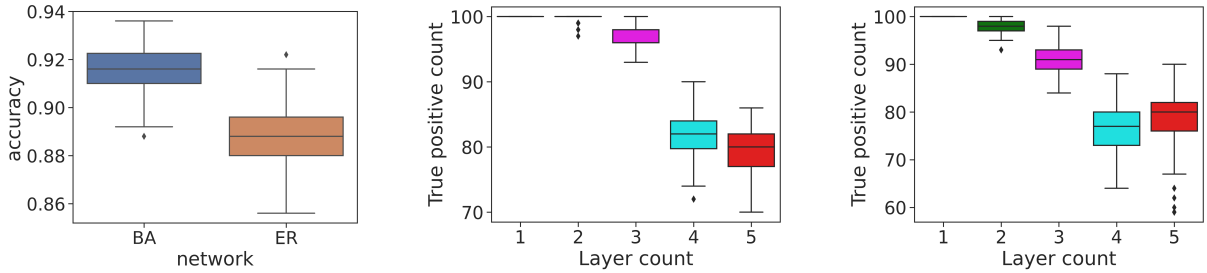

Figure 3.5: K-nearest neighbours classification accuracy of the layer count for a BA and ER graph as box plots (left) based on single layer WPSs. Contingency table diagonal values as box plots for a BA (centre) and ER (right). We simulated 400 independent realisations of a given graph type (BA, $N = 50$, $m = 3$; ER, $N = 50$, $\langle k \rangle = 6$). For each type of graph we conducted 100 rounds of 10-fold cross-validation to determine the K parameter in K-NN withdrawing 100 realisations (25%) for the purposes of the final evaluation. The train/test split was random and stratified.

as explained earlier) and then test it to see if it can recognise how many layers there are in an unknown graph. We conducted our tests for the BA and ER graphs (see Fig. 3.5 for the results of classification). For each type of graph we simulated 500 independent realisations (100 per each number of layers) with the mean degree $\langle k \rangle = 6$ and network size $N = 50$. We take out a 100 randomly chosen, in a stratified manner (i.e. classes are equally represented), realisations out of the data set (this will be the test set). On the training set we conduct 100 rounds of training and then testing. That is in each round we do the training/test split, then a 10-fold cross-validation on the training set to find the best K parameter of the K-NN model and then use that on the test set. We present the results in a form of box plots. In Fig. 3.5 we show the accuracy of the classifier for both the BA and ER. We can see that while for the ER the results are slightly lower than for the BA, in both cases the accuracy is still fairly high with medians of 92 and 89 for BA and ER respectively.

To additionally illustrate the point made earlier that higher numbers of layers are more difficult to be discerned amongst one another we show the diagonal values of the contingency tables from all 100 rounds for the BA (centre panel of Fig. 3.5) and the ER (the right panel of Fig. 3.5). One can clearly see that identifying mono-layer systems is practically 100% accurate and it is the more layered systems that cause trouble for the classifier.

While the classification results seem very promising it is important to note the obvious major disadvantage of this approach. One must build a training set for it to work. With synthetic networks (such as BA or ER graphs) it is easy to generate as many as one wants, therefore creating an extensive training set, and the limitation is purely in the

computing power. When dealing with real world networks one often does not simply have the ability to obtain similar enough graphs to the one currently under observation but with added layers – each real-world network is unique. In such a circumstance perhaps a combination of many different synthetic networks obtained by introducing noise to a real-world network, i.e., rewiring some of the links, creating perturbed versions of the original network could suffice and other, more advanced, classification methods than K-NN could be utilised.

3.3 Fourier transform of the amplitude signal

Here we introduce a new approach to detecting layers on quantum graphs. This completely novel way does not share the same issues as the previous one as it does not rely on building a classifier. Therefore, there is no need to build a training set and deal with all other aspects of the machine learning approach (like the choice of the classifier, tuning hyper-parameters etc.). While obviously not without its own problems, we believe that it is a more powerful and explainable tool while using very similar measurements as the previous method. Similarly to the previous case we assume we can either produce or observe a wave propagation on the graph initiated by a Gaussian wave packet. For efficiency's sake in the simulations we used the edge with the highest betweenness centrality as before and we also measure the amplitudes at integer times in the centres of all edges for $2|E|$ times. While in the WPS method we simply follow the advice of Aziz et al., for the count of measurements in the approach discussed here it is usually rather clear if enough data was collected by a straightforward visual inspection.

Our proposition is as follows, at each integer time compute the sum of all amplitudes in the visible part of the system and treat it as a time dependent signal $S(t)$. Transform the signal into frequency a domain via a fast Fourier transform (see Sec. 1.4 and [132]) - $\hat{S}(f)$ - and look at the spectrum of the signal - $|\hat{S}(f)|^2$.

A mono-layer system will produce a "flat" signal $S(t)$, whilst multi-layer one will exhibit periodic behaviour due to energy leaking in and out of the visible layer from and into other layers. At a sufficiently long measurement time the signal should stabilise and become stationary as long as no perturbation is introduced to the overall network. This transfer of energy induces oscillations in the amplitude sum on the visible layer which in turn create clear peaks in the power spectrum, see Fig. 3.6 for the results from the BA graphs and 3.7 for the ER. The left column shows the signal $S(t)$, centre $|\hat{S}(f)|^2$ and right $|\hat{S}(f)|^2$ in decibels and a log-log scale. Each row has 20 independent realisations plotted on top of each other, with transparency to show that these peaks are fairly consistent,

and different number of layers (1st row are mono-layer systems, 2nd row di-layer etc.). It is quite apparent that there are visible peaks and their count strictly corresponds to the number of layers in the system.

These results already show the advantage of FFT over WPS as it is simpler and does not seem to suffer from struggling to differentiate between highly-layered systems as much. Additionally, it does not require any prior knowledge or learning of the model. It is far from flawless, however. As it is much easier to test on real networks than WPS we applied it to three real world networks [157, 164, 165]. Vickers et al., [157] collected data from 29 7th grade students from Victoria, Australia. Students were asked to nominate classmates in several categories, three of which were used to construct this 3-layer network. These three categories were determined by questions - Who do you get on with in the class? Who are your best friends in the class? Who would you prefer to work with? The graph has 29 nodes and 740 edges in total. Krackhardt [164] took a record of relationship between managers in a high-tech company. The graph has 21 nodes and 312 edges in a 3-layer form. Each layer represents a relationship (advice, friendship, "reports to"). Chen et al., [165] presented a *Caenorhabditis elegans* multiplex connectome network with 3 layers, 279 nodes and 5863 edges. Each layer corresponds to a different synaptic junction: electric, chemical monadic, and polyadic. The results are in Fig. 3.8 where one can see that while we do get peaks in the spectrum and therefore can confidently state that there are hidden layers, it is much less clear how many of them there are. This is most likely due to the fact that these networks are not as clear cut multiplexes as the synthetic systems we discussed earlier. These networks here have various mean degrees in each layer and that also implies varied coupling strength between the layers. Moreover, real world networks can have other characteristics that differ between the layers such as clustering coefficients or degree distributions and the synthetic systems tested simply do not have this property. However, we show in the next section that it is possible to reconstruct the full spectrum of the row-normalised adjacency matrix with this method and therefore determine the number of layers for any system.

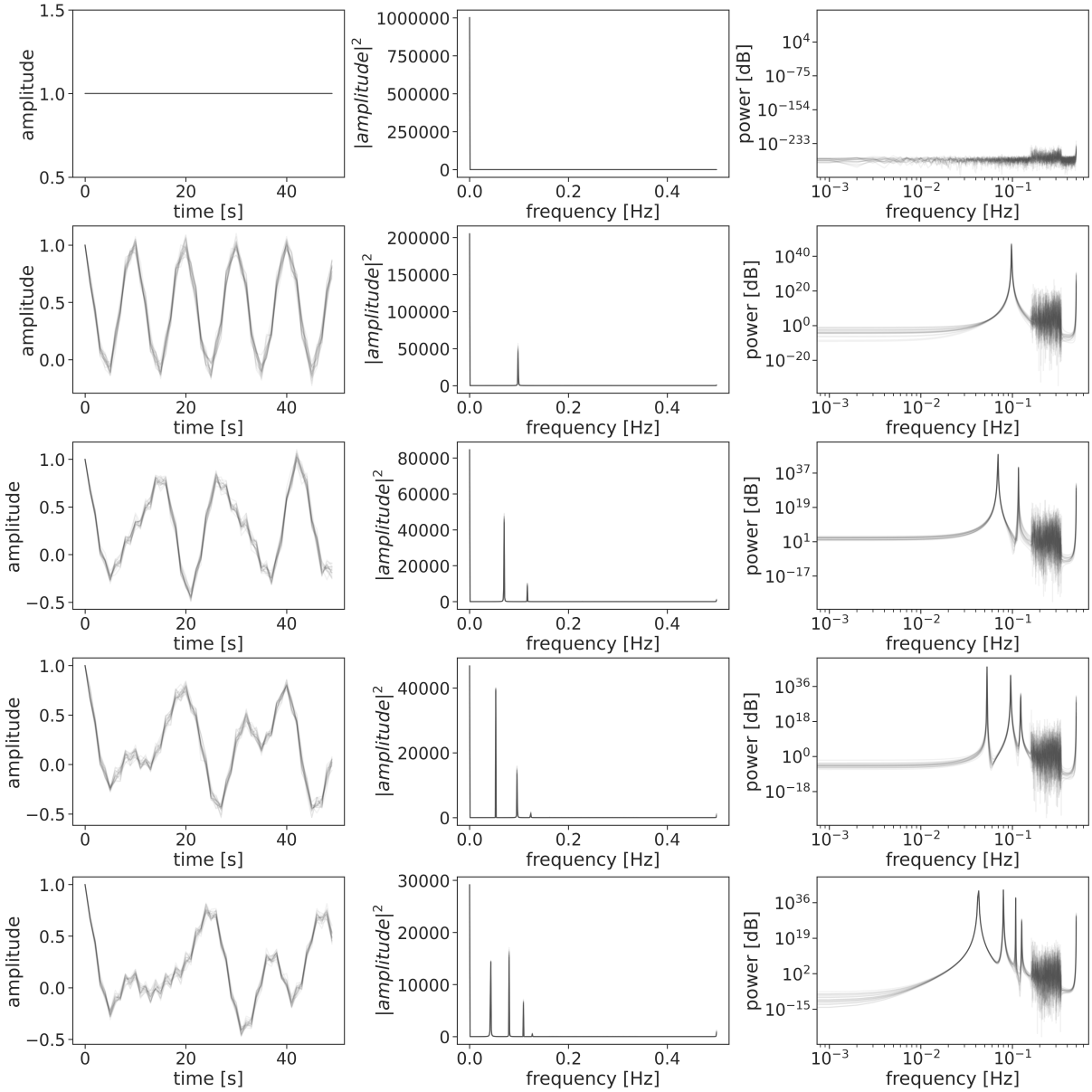

Figure 3.6: Sum of the amplitudes time evolution as measured on the only visible layer (left). A fast Fourier transform of this signal (centre) and its power spectrum (right). Each row represents a different number of layers (1 to 5 going top to bottom). Simulations were conducted on 20 independent realisations of a BA graph ($N = 50$, $m = 3$) per row, overlaid with transparency.

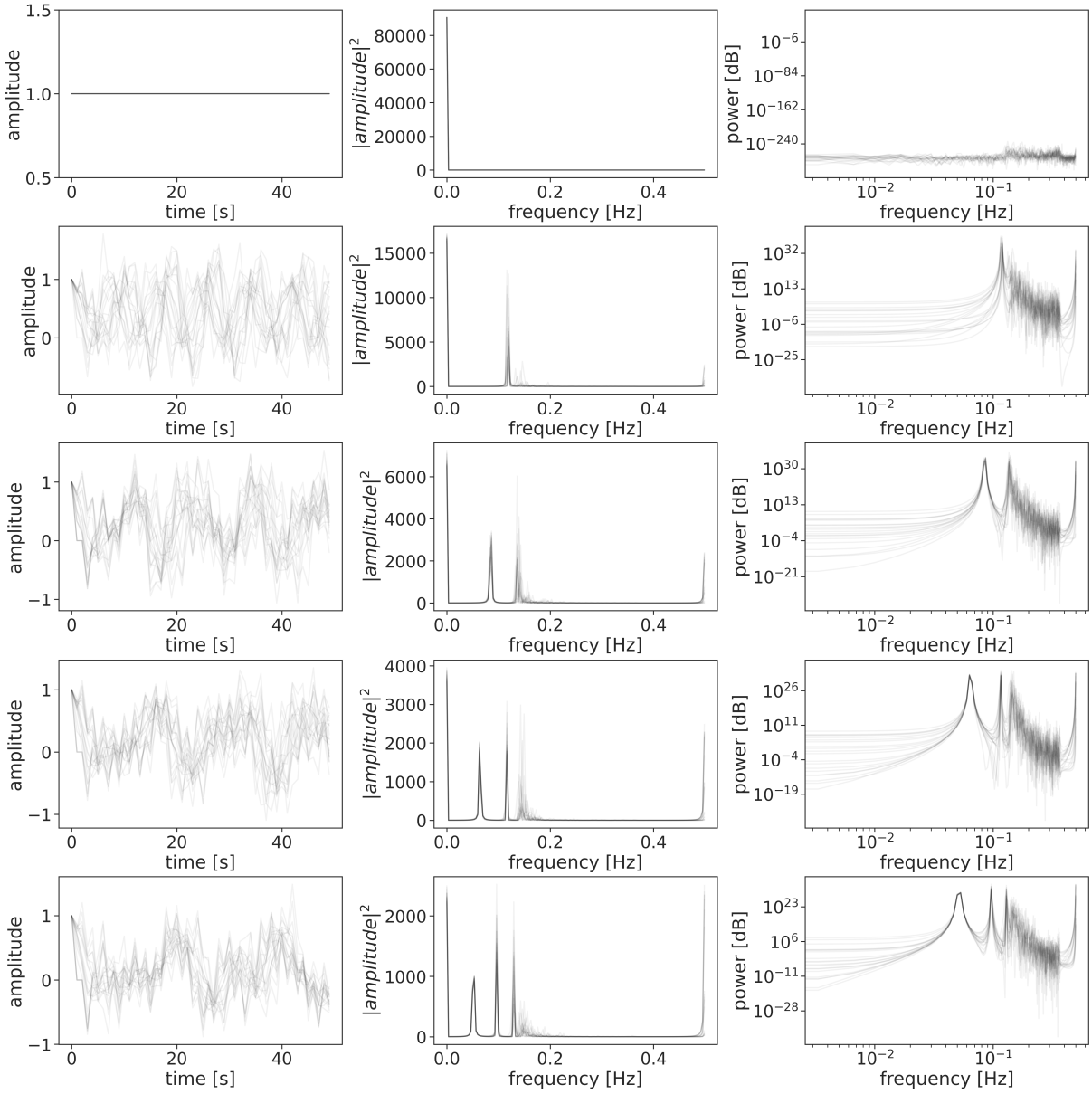

Figure 3.7: Sum of the amplitudes time evolution as measured on the only visible layer (left). A fast Fourier transform of this signal (centre) and its power spectrum (right). Each row represents a different number of layers (1 to 5 going top to bottom). Simulations were conducted on 20 independent realisations of an ER graph ($N = 50$, $\langle k \rangle = 6$) per row, overlaid with transparency.

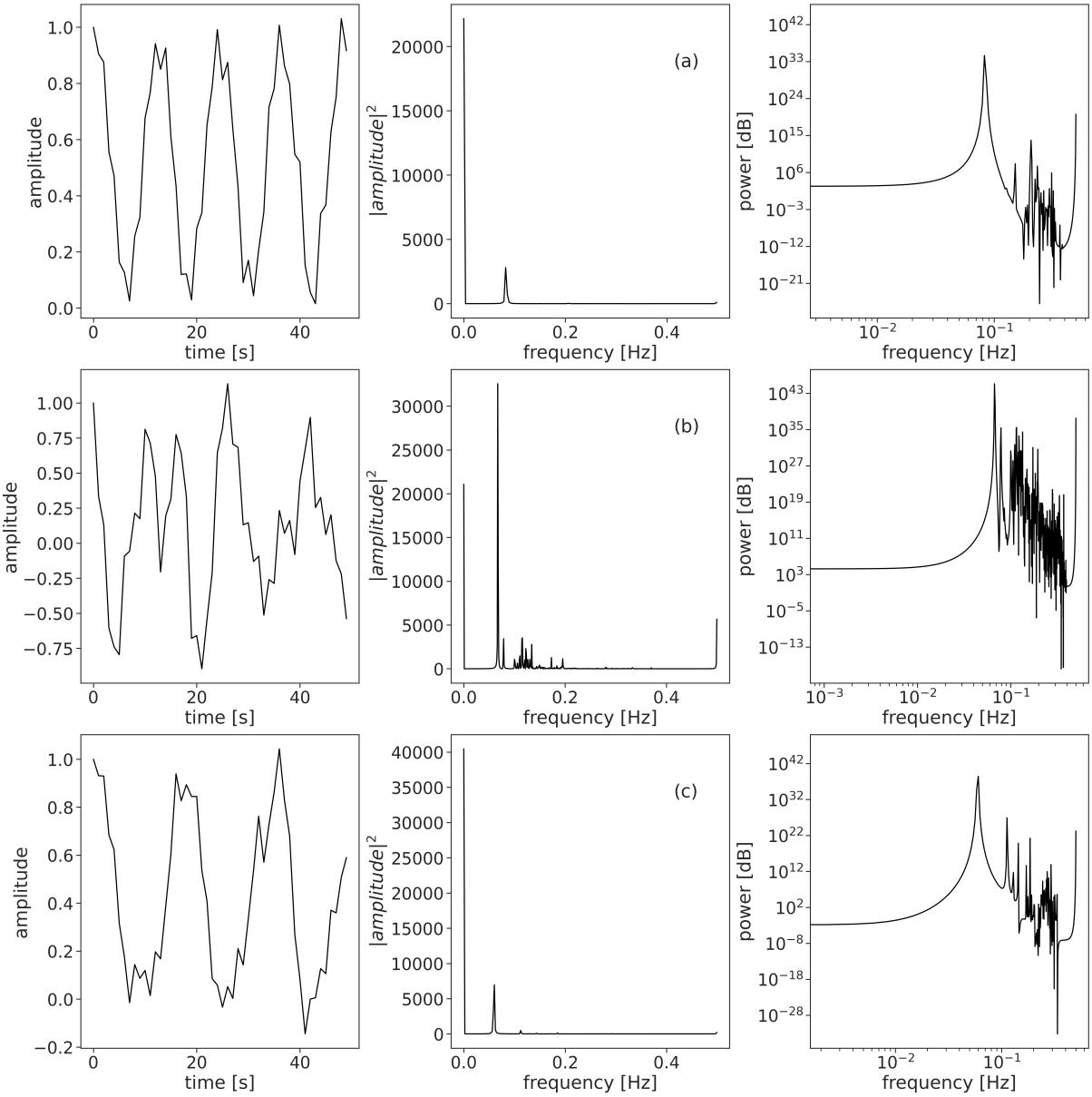

Figure 3.8: Sum of the amplitudes time evolution as measured on the only visible layer (left). A fast Fourier transform of this signal (centre) and its power spectrum (right). Each row represents a different real world network (as indicated by titles - Vickers[157], C.Elegans[165], Krackhardt[164]). Each graph is a 3-layered multiplex.

3.4 Spectrum reconstruction

In this section we show that with a sufficiently long observation it is possible to completely recover all eigenvalues of the row-normalised adjacency matrix of the full system and thus trivially determine the number of hidden layers.

We shift slightly from the previous sections as we no longer take the measurements on the edges but only on the nodes. This makes the problem less computationally intensive and also, in our opinion, makes for a more practical case as it might be sometimes easier to observe just the nodes' states. However, the same analysis here can be applied using edge measurements and the one in the previous sections could be done with the node values only - we chose otherwise as we are stemming from the work of Aziz et al.

Similarly as before we observe the sum of the amplitudes, however, in this case it is important to have enough samples of the signal to provide sufficient resolution in the power spectrum. How long one needs to observe a system will of course depend on the intricacies (and mostly size) of the system in question. As the propagation process is not stochastic the time needed for observation is finite and in our experience not unattainable. The goal is simply to have the complete power spectrum of the signal. Then one takes note of the peaks present - we opted for an automated approach using a wavelet transform [134](see Sec. 1.4). These peaks in the power spectrum are the eigenvalues of the Hamiltonian (divided by 2π) which in turn are directly related to the eigenvalues of the row-normalised adjacency matrix - $\hat{A}$ - such that each eigenvalue $\lambda \notin \{-1, 1\}$ of $\hat{A}$ has the corresponding Hamiltonian eigenvalues $\cos^{-1}(\lambda)$ and $2\pi - \cos^{-1}(\lambda)$. This leads us to two important results, i) the number of frequencies present in the power spectrum $\#f$ is two less than the count of eigenvalues of the adjacency matrix and since we know the layer sizes (i.e. node count per layer - N) as a multiplex structure was assumed the number of layers $K = (\#f+2)/N$, ii) we can in fact recover almost exactly all eigenvalues of $\hat{A}$ as $\cos(2\pi f_i)$ for each frequency peak f_i in the power spectrum.

We present the result of the full spectrum reconstruction in Fig. 3.9 for a complete, BA and real world graph. We chose the complete graph as it has a special case due to the extreme symmetries of the multiplex adjacency matrix and thus the number of peaks directly corresponds to the number of layers unlike more complex cases where the eigenvalues multiplicities behave differently. Of course, this does imply that if due to some particular structures in a given system some eigenvalues have high multiplicity the simple formula $K = (\#f + 2)/N$ will not hold and system specific adjustments would be needed. The reconstructed eigenvalues give an almost perfect match with those of the row-normalised adjacency matrix. Note that the performance here is mostly limited by the

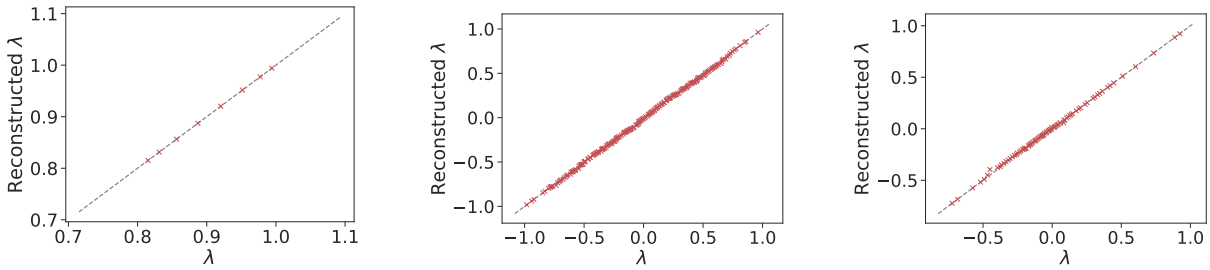

Figure 3.9: Eigenvalues reconstruction from the Fourier spectrum of the nodes' amplitudes sum signal. (Left) an example of a complete graph multiplex with layer size $N = 20$ and number of layers $K = 9$. As it is a special case of an extremely symmetric adjacency matrix there are only as many eigenvalues as there are layers. (Right) a Barabási-Albert graph with $N = 50,\ m = 3,\ K = 4$ has a much more complex spectrum and so does a real world network (right) - Vickers[157] - for both of which we attain an almost perfect match between the recovered and actual eigenvalues. The dashed diagonal line is a visual aid showing "$y = x$".

peak detection method and the resolution in the frequency domain, i.e. the information is there in the spectrum, the only challenge is to recover it efficiently.

In order to explicitly show the correspondence between the eigenvalues of the Hamiltonian and the peaks of the power spectrum we shall now follow in detail (see next section) the case of a full graph, considering the simplest configurations – a monoplex and a duplex network. Our exact analytical solutions prove that for the duplex network of N nodes on each layer, among $2N$ eigenvalues that characterise the system we have only four distinct ones $\boldsymbol{\lambda} = \left\{-\frac{2}{N}, 0, \frac{N-2}{N}, 1\right\}$, the first two having multiplicity of $N - 1$. Figure 3.10 shows that in such a system one recovers just one eigenvalue, i.e., $\lambda = \frac{N-2}{N}$ directly connected to periodicity of the sum of observed amplitudes on the nodes. On the other hand, observing a single node allows for the recovery of the full spectrum (see Fig. 3.11).

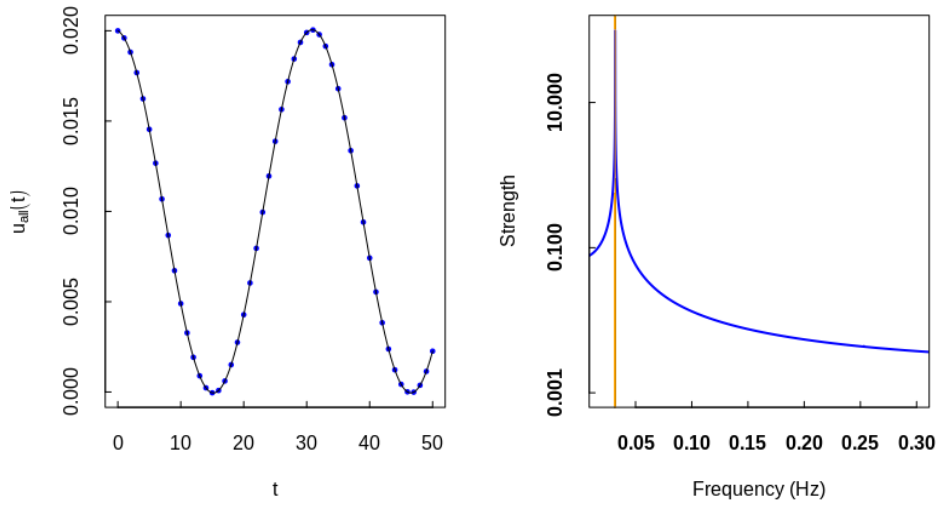

Figure 3.10: (a) Sum of the amplitudes over time in a single layer of the duplex full graph: line comes from Eq. (3.32) and points are numerical simulations. (b) Power spectrum of the signal shown in panel (a) [the series consists of 10000 elements]. Vertical line is frequency equal to $\omega_{2N-1}/2\pi = (N-2)/(2\pi N)$.

3.5 Exact analytical solutions of wave amplitudes in mono- and bi-layer full graphs

3.5.1 Monoplex full graph

Here we will consider a wave propagation on the nodes of a full graph (monoplex) topology, i.e., each node is connected to any other in the network, therefore forming a clique of N nodes. In such a case the adjacency matrix $\mathbf{A}$ is a constant matrix filled with ones except for the diagonal which is filled with zeroes.

It is well known that the spectrum of the full graph consists of values $N-1$ with multiplicity 1 and -1 with multiplicity $N-1$. As we consider the row-normalised matrix which can be characterised as $\hat{\mathbf{A}} = \frac{1}{N-1}\mathbf{A}$ we have

$$\boldsymbol{\lambda} = \{\lambda_1, ..., \lambda_{N-1}, \lambda_N\} = \left\{-\frac{1}{N-1}, ..., -\frac{1}{N-1}, 1\right\} \tag{3.4}$$

and, consequently, $\omega_i = \arccos\left(-\frac{1}{N-1}\right)$ for $i = 1, ..., N-1$. As the full graph is $(N-1)$-regular then $\mathbf{e}$, i.e., all-ones vector is an eigenvector of $\mathbf{A}$ corresponding to λ_N while the other vectors can be written as $\mathbf{e}_i - \mathbf{e}_j$ for $i \neq j$, where $\mathbf{e}_i$ is the vector with 1 in position i and 0 elsewhere, e.g.,

$$\mathbf{g} = \begin{pmatrix} -1 & -1 & -1 & ... & -1 & -1 & 1 \\ 0 & 0 & 0 & ... & 1 & 0 & 1 \\ \vdots & \vdots & \vdots & \ddots & \vdots & \vdots & 1 \\ 0 & 0 & 1 & ... & 0 & 0 & 1 \\ 0 & 1 & 0 & ... & 0 & 0 & 1 \\ 1 & 0 & 0 & ... & 0 & 0 & 1 \end{pmatrix} \tag{3.5}$$

After orthnormalising $\mathbf{g}$ with the Gram-Schmidt procedure and renumbering the matrix so that the first row becomes the last one we obtain the following $N-1 \times N$ eigenvector matrix g_M:

$$\mathbf{g_M} = \begin{pmatrix} 0 & 0 & 0 & 0 & 0 & 0 & 0 & \sqrt{\frac{N-1}{N}} \\ \vdots & \vdots & \vdots & \vdots & \vdots & 0 & \sqrt{\frac{N-2}{N-1}} & -\frac{1}{\sqrt{(N-1)N}} \\ \vdots & \vdots & \vdots & \vdots & 0 & \sqrt{\frac{j}{j+1}} & \cdots & \vdots \\ \vdots & \vdots & \vdots & 0 & \ddots & -\frac{1}{\sqrt{j(j+1)}} & \cdots & \vdots \\ \vdots & \vdots & 0 & \ddots & \cdots & \vdots & \cdots & \vdots \\ \vdots & 0 & \sqrt{\frac{3}{4}} & \cdots & ... & -\frac{1}{\sqrt{j(j+1)}} & \cdots & -\frac{1}{\sqrt{(N-1)N}} \\ 0 & \sqrt{\frac{2}{3}} & -\frac{1}{\sqrt{3\cdot 4}} & \cdots & ... & -\frac{1}{\sqrt{j(j+1)}} & \cdots & -\frac{1}{\sqrt{(N-1)N}} \\ \sqrt{\frac{1}{2}} & -\frac{1}{\sqrt{2\cdot 3}} & -\frac{1}{\sqrt{3\cdot 4}} & \cdots & ... & -\frac{1}{\sqrt{j(j+1)}} & \cdots & -\frac{1}{\sqrt{(N-1)N}} \\ -\frac{1}{\sqrt{1\cdot 2}} & -\frac{1}{\sqrt{2\cdot 3}} & -\frac{1}{\sqrt{3\cdot 4}} & \cdots & ... & -\frac{1}{\sqrt{j(j+1)}} & \cdots & -\frac{1}{\sqrt{(N-1)N}} \end{pmatrix} \tag{3.6}$$

Note that we deliberately omit the eigenvector corresponding to ω_N which consists of N values $1/\sqrt{N}$ gathered in the column vector

$$\mathbf{C}_M = \left(\frac{1}{\sqrt{N}}, ..., \frac{1}{\sqrt{N}} \right)^T \tag{3.7}$$

as it does not play any role in further calculations.

Let us now assume, that the wave is initially contained on edge $f = e_{uv}$. We are bound to obtain two expressions: one showing the amplitude of the wave at the node v which can be simply calculated as $u_n(f, f, t)$ and the other one, showing the sum of the

amplitudes for all nodes which can be expressed as

$$u_{all} = u_n(e_{vu}, f, t) + \sum_{i=1,..,N, i\neq u} u_n(e_{ui}, f, t). \tag{3.8}$$

We will further assume, without losing any generality, that $f = e_{12}$. Such a setting greatly simplifies further calculations of u_n as in this case the only non-zero inputs come from eigenvalues ω_{N-2} and ω_{N-1}. For any other ω_i with $i = 1, ..., N-3$ we have $C(f, \omega_i) = 0$. Respective coefficients C and B for ω_{N-2} and ω_{N-1} are gathered in Table 3.1

edge e	$C(e, \omega_{N-2})$	$B(e, \omega_{N-2})$	$C(e, \omega_{N-1})$	$B(e, \omega_{N-1})$
e_{12}	$\sqrt{\frac{N-1}{N}}$	$-\frac{\pi}{2}$	$\sqrt{\frac{N-1}{N}}$	0
e_{1k}	$\sqrt{\frac{N-1}{N}}\frac{1}{N-2}$	$\frac{\pi}{2}$	$\sqrt{\frac{N-1}{N}}$	0
e_{21}	$\sqrt{\frac{N-1}{N}}$	$-\arctan\left(\frac{1}{\sqrt{N(N-2)}}\right)$	$-\sqrt{\frac{N-1}{N}}$	$\arctan\left(\sqrt{N(N-2)}\right)$

Table 3.1: Coefficients C and B for the full graph case; in the third row $k = 2, ..., N$.

As mentioned in the introduction section 1.3, in order to have a proper form of the eigenfunction ϕ one needs to calculate the normalisation factor $\rho(\omega)$. Next we show how to obtain $\rho(\omega_{N-1})$: Eq. (1.10) states that it is necessary to sum of over all the edges in the networks, however in the case of ω_{N-1} there are only two different terms. The first one ρ_1 comes from $(N-1)$ pairs $e_{12}, e_{13}, ..., e_{1N}$ the second one ρ_2 from all the other $\frac{1}{2}(N-1)(N-2)$ pairs, i.e., $e_{23}, ..., e_{2N}, e_{34}, ..., e_{N-1N}$ so

$$\rho(\omega_{N-1}) = \sqrt{(N-1)\rho_1 + \frac{1}{2}(N-1)(N-2)\rho_2} \tag{3.9}$$

The values of C and B for ρ_1 are shown in Table (3.1) – taking into account that $B = 0$, the value of ρ_1 simplifies to:

$$\rho_1 = \frac{N-1}{N}\left[\frac{1}{2} + \frac{\sin\left[2\arccos\left(-\frac{1}{N-1}\right)\right]}{4\arccos\left(-\frac{1}{N-1}\right)}\right]. \tag{3.10}$$

Substituting $\sin(2\arccos x)$ with $2x\sqrt{1-x^2}$ we arrive at

$$\rho_1 = \frac{N-1}{N}\left[\frac{1}{2} - \frac{2\frac{\sqrt{N(N-2)}}{(N-1)^2}}{4\arccos\left(-\frac{1}{N-1}\right)}\right]. \tag{3.11}$$

In the case of ρ_2 the values C and B can be written as

$$C(e_{ik}, \omega_{N-1}) = -\sqrt{\frac{2}{N(N-2)}} \tag{3.12}$$

$$B(e_{ik}, \omega_{N-1}) = -\arctan\sqrt{\frac{N}{N-2}} \tag{3.13}$$

for $i = 2, ..., N-1$ and $k = i+1, ..., N$ which results in the following form of ρ_2:

$$\rho_2 = \frac{2}{N(N-2)}\left[\frac{1}{2} + \frac{\sin\left[2\arccos\left(-\frac{1}{N-1}\right) - 2\arctan\sqrt{\frac{N}{N-2}}\right] + \sin\left(2\arctan\sqrt{\frac{N}{N-2}}\right)}{4\arccos\left(-\frac{1}{N-1}\right)}\right]. \tag{3.14}$$

Here, making use of the fact that $\arccos x = 2\arctan\frac{\sqrt{1-x^2}}{1+x}$ we arrive at

$$\rho_2 = \frac{2}{N(N-2)}\left[\frac{1}{2} + \frac{2\frac{\sqrt{N(N-2)}}{N-1}}{4\arccos\left(-\frac{1}{N-1}\right)}\right]. \tag{3.15}$$

After substituting Eq. (3.9) with ρ_1 and ρ_2 given by Eqs. (3.11) and (3.15) and performing some short algebra we arrive simply at

$$\rho(\omega_{N-1}) = \sqrt{\frac{N-1}{2}}. \tag{3.16}$$

With similar calculations it possible to show that $\rho(\omega_{N-2}) = \rho(\omega_{N-1})$ (in fact, this the case for any ω_i other than ω_N).

edge e	$C(e, \omega_{N-2})$	$B(e, \omega_{N-2})$	$C(e, \omega_{N-1})$	$B(e, \omega_{N-1})$
e_{12}	$\frac{N}{\sqrt{2(N-1)(N+2)}}$	$\frac{\pi}{2}$	$-\sqrt{\frac{N^2-2}{2(N-1)(N+2)}}$	$-\arctan\left(\frac{1}{N-1}\sqrt{\frac{N-2}{N+2}}\right)$
e_{1k}	$\frac{N}{N-2}\frac{1}{\sqrt{2(N-1)(N+2)}}$	$-\frac{\pi}{2}$	$-\sqrt{\frac{N^2-2}{2(N-1)(N+2)}}$	$-\arctan\left(\frac{1}{N-1}\sqrt{\frac{N-2}{N+2}}\right)$
e_{21}	$-\frac{1}{\sqrt{2(N-1)(N+2)}}$	$-\arctan\left(\frac{2}{\sqrt{N^2-4}}\right)$	$\sqrt{\frac{N^2-2}{2(N-1)(N+2)}}$	$\arctan\left((N+1)\sqrt{\frac{N-2}{N+2}}\right)$

Table 3.2: Coefficients C and B for the duplex full graph case; in the third row $k = 2, ..., N$.

We can now use the above calculated values of C, B and ρ to express the wave amplitude at the nodes of the full graph by the means of Eq. (1.12) in Sec. 1.3 (note that in order to simplify the equation we use the transformation of time $t \to t + \frac{1}{2}$, thus $t = 0$ means that the wave has arrived at the first node). We shall start with $u_n(e_{12}, e_{12}, t)$ as

edge e	$C(e,\omega_{2N-3})$	$B(e,\omega_{2N-3})$	$C(e,\omega_{2N-2})$	$B(e,\omega_{2N-2})$	$C(e,\omega_{2N-1})$	$B(e,\omega_{2N-1})$
e_{12}	$\sqrt{\frac{N-2}{2(N-1)}}$	$-\frac{\pi}{2}$	$\sqrt{\frac{(N-1)^2+1}{2N(N-1)}}$	$\arctan\left(\frac{1}{N-1}\right)$	$-\sqrt{\frac{1}{2(N-1)}}$	$-\arctan\left(\sqrt{\frac{1}{(N-1)}}\right)$
e_{1k}	$\sqrt{\frac{1}{2(N-2)(N+1)}}$	$\frac{\pi}{2}$	$\sqrt{\frac{(N-1)^2+1}{2N(N-1)}}$	$\arctan\left(\frac{1}{N-1}\right)$	$-\sqrt{\frac{1}{2(N-1)}}$	$-\arctan\left(\sqrt{\frac{1}{(N-1)}}\right)$
e_{21}	$\sqrt{\frac{N-2}{2(N-1)}}$	0	$-\sqrt{\frac{(N-1)^2+1}{2N(N-1)}}$	$\arctan(N-1)$	$-\sqrt{\frac{1}{2(N-1)}}$	$-\arctan\left(\sqrt{\frac{1}{(N-1)}}\right)$

Table 3.3: Coefficients C and B for the duplex full graph case (cntd).

the simplest case:

$$\begin{aligned} u_n(e_{12},e_{12},t) &= \sum_{i=\{N-2,N-1\}} \frac{C^2(e_{12},\omega_i)}{2\rho^2(\omega_i)}\left[\cos(\omega_i t)+\cos(\,(t+2)\omega+2B(e_{12},\omega_i)\,)\right]+\frac{1}{E} \\ &= \frac{1}{2\rho^2(\omega_{N-2})}\frac{N-1}{N}\left[\cos t\omega_{N-2}+\cos[(t+2)\omega_{N-2}-\pi]\right]+ \\ &+ \frac{1}{2\rho^2(\omega_{N-1})}\frac{N-1}{N}\left[\cos t\omega_{N-1}+\cos[(t+2)\omega_{N-1}]\right]+\frac{2}{N(N-1)} \end{aligned} \tag{3.17}$$

Making use of Eq. (3.16) and the fact that $\cos(x-\pi) = -\cos(x)$ as well as denoting $\omega_{N-2} = \omega_{N-1} = \omega$ we arrive simply at

$$u_n(e_{12},e_{12},t) = \frac{2}{N}\cos(t\omega)+\frac{2}{N(N-1)} \tag{3.18}$$

with $\omega = \arccos\left(-\frac{1}{N-1}\right)$. In the same manner one can show that

$$u_n(e_{1k},e_{12},t) = \frac{1}{N(N-2)}\left((N-3)\cos(t\omega)+(N-1)\cos((t+2)\omega)\right)+\frac{2}{N(N-1)} \tag{3.19}$$

for $k = 3,...,N$ and

$$u_n(e_{21},e_{12},t) = -\frac{2}{N(N-1)}\left(\cos(t\omega)+\sqrt{N(N-2)}\sin((t+2)\omega)\right)+\frac{2}{N(N-1)} \tag{3.20}$$

In this way, Eqs. (3.18)-(3.20) fully determine the wave amplitude at every node in the considered monoplex full graph. They can now be put into Eq. (3.8) to show that

$$u_{all}^M(t) = \frac{2}{N-1} \tag{3.21}$$

which proves that the sum of the node amplitudes is constant for any value of t.

3.5.2 Duplex full graph

In this part we consider a full graph duplex, i.e., a network consisting of two cliques (full graphs) of N nodes each connected in such a way that the node i from the first clique links with node $i+N$ from the second one ($i = 1, ..., N$). Assuming that $\mathbf{A}_N$ is an $N \times N$ adjacency matrix of a full graph (as in the previous section) and $\mathbf{I}_N$ is an $N \times N$ identity matrix, we can describe the topology of a full graph duplex with its $2N \times 2N$ adjacency matrix $\mathbf{A}_d$

$$\mathbf{A}_d = \begin{pmatrix} \mathbf{A}_N & \mathbf{I}_N \\ \mathbf{I}_N & \mathbf{A}_N \end{pmatrix} \tag{3.22}$$

Owing to the symmetry of the system (each node has exactly N neighbours - $N-1$ in the layer it belongs to and one that connects it to the second layer) the row-normalised matrix can be characterised simply as $\hat{\mathbf{A}}_d = \frac{1}{N}\mathbf{A}_d$.

In such a setting we can obtain the following orthonormalised $2N \times 2N$ matrix of the eigenvectors for the duplex network

$$\mathbf{g}_D = \frac{1}{\sqrt{2}} \begin{pmatrix} -\mathbf{g}_M & \mathbf{g}_M & \mathbf{C}_M & \mathbf{C}_M \\ \mathbf{g}_M & \mathbf{g}_M & -\mathbf{C}_M & \mathbf{C}_M \end{pmatrix} \tag{3.23}$$

where $\mathbf{g}_M$ and $\mathbf{C}_M$ are the matrices given by Eqs (3.6) and (3.7), and the corresponding set of $2N$ eigenvalues is

$$\begin{aligned} \boldsymbol{\lambda} &= \{\lambda_1, ..., \lambda_{N-1}, \lambda_N, ..., \lambda_{2N-2}, \lambda_{2N-1}, \lambda_{2N}\} = \\ &= \left\{-\frac{2}{N}, ..., -\frac{2}{N}, 0, ..., 0, \frac{N-2}{N}, 1\right\} \end{aligned} \tag{3.24}$$

and, consequently, $\omega_1 = ... = \omega_{N-1} = \arccos\left(-\frac{2}{N}\right)$, $\omega_N = ... = \omega_{2N-2} = \frac{\pi}{2}$, $\omega_{2N-1} = \arccos\left(\frac{N-2}{N}\right)$

As in the previous case we assume that the wave is initially placed on the edge $f = e_{12}$ and our goal is to find the wave amplitudes on each of the nodes $1, ..., N$ as well as the total amplitude on a given layer. Again, the choice of the initial edge is a direct consequence of the structure of $\mathbf{g}_D$ as it restricts the set of eigenvalues needed to calculate u_n to ω_{N-2}, ω_{N-1}, ω_{2N-3}, ω_{2N-2} and ω_{2N-1} – all others result in $C(f, \omega) = 0$. The values of C and B necessary to compute $u_n(e_{12}, e_{12}, t)$, $u_n(e_{1k}, e_{12}, t)$ for $k = 2, ..., N$ and $u_n(e_{21}, e_{12}, t)$ obtained from $\mathbf{g}_D$ are summed up in Tables 3.2 and 3.3. Following similar calculations as in the monoplex case one can show that the normalisation factor is

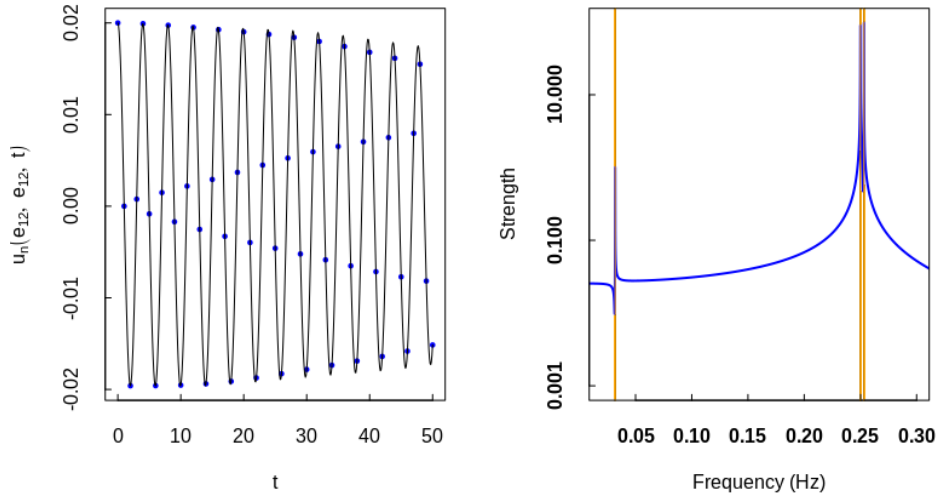

Figure 3.11: (a) the amplitude at the node $v = 2$ over time in the duplex full graph: lines come from Eq. (3.26) with coefficients $\mathbf{c}^{12}$ and $\mathbf{s}^{12}$ and points are numerical simulations. (b) the power spectrum of the signal shown in panel (a) [the series consists of 10000 elements]. The vertical lines are drawn for frequencies equal to $\omega_1/2\pi$, $\omega_N/2\pi$ and $\omega_{2N-1}/2\pi$.

$$\begin{aligned} \rho(\omega_{N-2}) = \rho(\omega_{N-1}) = \rho(\omega_{2N-3}) = \\ = \rho(\omega_{N-2}) = \rho(\omega_{2N-1}) = \sqrt{\frac{N}{2}} \end{aligned} \tag{3.25}$$

Using the above-calculated values of C, B and ρ it is possible to give exact solutions for the amplitude at any node v as

$$u_n(e_{uv}, e_{12}, t) = \frac{1}{N^2}\left[1 + \sum_i (c_i^{uv} \cos \omega_i t + s_i^{uv} \sin \omega_i t)\right] \tag{3.26}$$

where

$$\begin{aligned} \omega &= \{\omega_1, \omega_N, \omega_{2N-1}\} \\ &= \left\{\arccos\left(-\frac{2}{N}\right), \frac{\pi}{2}, \arccos\left(\frac{N-2}{N}\right)\right\} \end{aligned} \tag{3.27}$$

and the respective coefficients for $u_n(e_{12}, e_{12}, t)$ are given by

$$\mathbf{c}^{12} = \{N-1, N-1, 1\} \tag{3.28}$$
$$\mathbf{s}^{12} = \left\{-\sqrt{\frac{N-2}{N+2}}, 1, -\frac{1}{\sqrt{N-1}}\right\}$$

while in the case of $u_n(e_{1k}, e_{12}, t)$, $k = 2, ..., N$ they are

$$\mathbf{c}^{1k} = \{-1, -1, 1\} \tag{3.29}$$
$$\mathbf{s}^{1k} = \left\{\sqrt{\frac{N+2}{N-2}}, 1, -\frac{1}{\sqrt{N-1}}\right\}$$

and for $u_n(e_{21}, e_{12}, t)$, $k = 2, ..., N$ we have

$$\mathbf{c}^{21} = \{-1, -1, 1\} \tag{3.30}$$
$$\mathbf{s}^{21} = \left\{-(N+1)\sqrt{\frac{N-2}{N+2}}, -(N-1), -\frac{1}{\sqrt{N-1}}\right\}$$

Finally by calculating

$$u^D_{all}(t) = u_n(e_{12}, e_{12}, t) + (N-2)u_n(e_{1k}, e_{12}, t) + u_n(e_{21}, e_{12}, t) \tag{3.31}$$

we arrive at the expression giving the sum of the amplitudes over all nodes in a single layer in the duplex full graph which reads

$$u^D_{all}(t) = \frac{1}{N}\left[1 + \cos\left(t\omega_{2N-1}\right) - \frac{1}{\sqrt{N-1}}\sin\left(t\omega_{2N-1}\right)\right]. \tag{3.32}$$

Formula (3.26) indicates that in the case of a single node all three eigenvalues $\arccos\left(-\frac{2}{N}\right)$, $\frac{\pi}{2}$ and $\arccos\left(\frac{N-2}{N}\right)$ can be recovered by observing the wave amplitude over time at such a node. Indeed, the outcomes of the power spectrum shown in Fig. 3.11 confirm this claim. It should be noted, though, that once N is sufficiently large, two eigenvalues $\arccos\left(-\frac{2}{N}\right)$ and $\frac{\pi}{2}$ will tend to merge and $\frac{N-2}{N}$ shall approach 1, giving in result two frequencies: 1/4 and 0. On the other hand Eq. (3.26) clearly shows that if the sum of the amplitudes in a single layer is observed then we are able to recover only one eigenvalue, namely $\omega = \arccos\left(\frac{N-2}{N}\right)$, this fact is depicted in Fig. 3.10.

In summary, in this chapter we have explored the framework of quantum graphs in context of detecting hidden layers. The main question we tried to answer was this: what can we infer about the underlying topological structure by observing an ongoing dynamic that can be modelled by a propagating wave on a graph? We approached this question two fold - with i) machine learning and ii) signal processing and analysis of edge-based Laplacian properties. We have outlined the viability and potential challenges associated with both propositions and established an answer to the posed question. One can indeed make deductions about the existence and even topological features of hidden layers in quantum graphs, however, limitations to what can be reverse engineered do exist and are discussed further in the last chapter of this work.

Chapter 4

Bi-layer-induced phenomena in the echo chambers and polarisation model

Thus far we have established methods of detecting hidden layers having observed some sort of information dynamics on a complex network. As we have already discussed in the introduction the effects of hidden layers in terms of viral propagation are well known and are also being considered in opinion dynamics. In this chapter we shall look upon an example of the latter by taking an established model of a social phenomenon and show the possible implications of introducing an additional layer into the system.

4.1 Echo chambers and polarisation model

Let us begin by introducing the mono-layer model, first described by Baumann et al., [70]. This echo chambers and polarisation model consists of N agents each with a real, continuous opinion variable $x_i(t) \in \mathbb{R}$. The sign determines the nature of opinion (e.g. for/against) while the value the magnitude of conviction to it. The opinion dynamics are driven exclusively by the interactions between agents and are described by a system of coupled ordinary differential equations presented in [70]:

$$\frac{dx_i}{dt} = -x_i + K \sum_{j=1}^{N} A_{ij}(t) \tanh(\alpha x_j), \tag{4.1}$$

where $K > 0$ is the *social interaction strength* and $\alpha > 0$ determines the degree of non-linearity (also called *controversialness*). The rationale behind this very equation is built on the mechanism of informational influence theory with guarantees of monotonic

influence and a cap on extreme opinions while also not being dissimilar to previously used non-linear functions in chaotic systems [166–169].

The matrix A is an $N \times N$ adjacency matrix in an activity-driven (AD) temporal network model [170–173]. This is a model where there is no statically set social network but in each time step an agent can become active with *propensity* $a_i \in [\epsilon, 1]$. The propensities are drawn from a power law distribution [170, 172] defined as follows:

$$F(a) = \frac{1-\gamma}{1-\epsilon^{1-\gamma}} a^{-\gamma}. \tag{4.2}$$

Once the agent is activated it makes m random connections with other agents and as is standard in AD models the connections are uniformly random. In [70] there is additionally an element of homophily as it is expected to be necessary to create polarisation effects [174, 175], however, since we will be considering a bi-layer model later on this is not the case for us.

The interactions in social media can often be asymmetric and so it is not always true that $A_{ij} = A_{ji}$. However, in this model there is a mechanism of *reciprocity* where each agent j that has received a connection from an active agent i can reciprocate the connection with probability r.

Main phenomena in this model are three distinct steady state phases and a possibility of a clustering effect (echo chambers). These three phases are *neutral consensus* where all agents' opinions converge on zero, *radicalisation* where all agents shift towards one of two possible extremes and *polarisation* where two oppositely polarised groups emerge. Bauman et al., provide a formula for the critical controversialness using the mean field approximation (in the absence of homophily) as:

$$\alpha_c = \frac{1}{(1+r)Km\langle\alpha\rangle} \tag{4.3}$$

Our goal here is to extend this model such that we have more than one layer interacting (we shall limit ourselves to a bi-layer scenario) and determine the existence and potentially the importance of such layered interactions.

4.2 Methodology

First we briefly introduce some assumptions and formulations present in both analytical and numerical considerations later on. Analytically, we shall approach the problems using the mean field theory [176, 177]. As such we will replace the summation over neighbours

with an averaged neighbourhood effect on any given agent. For that we shall need the average activity which is given by:

$$\langle a \rangle = \frac{1-\gamma}{2-\gamma}\frac{1-\epsilon^{2-\gamma}}{1-\epsilon^{1-\gamma}}. \tag{4.4}$$

Similarly as in [70] we assume that processes related to topology changes as described by matrices $A_{ij}(t)$ are much faster than changes of opinions $x_i(t)$ (and $y_i(t)$ introduced later in this chapter) and as mentioned before we substitute the summations terms over A_{ij} mean values of these matrices, denoted further on as c

$$c \stackrel{def}{=} \langle A_{ij}(t) \rangle_{t,a} = \frac{1}{2} m(1+r)\langle a \rangle. \tag{4.5}$$

Note the $\frac{1}{2}$ which is a consequence of the existence of two layers and the assumption that agents do not have an explicit preference to connect with members of either layer.

As far as simulations are concerned, we conduct them, unless stated otherwise, with these parameter values: network size $N = 1000, \gamma = 2.1, \epsilon = 0.01, m = 10, r = 0.5, K = 1, \alpha = 1$. Note that as a consequence of these values the parameter $c \approx 0.306$. The systems of equations in the agent based simulations were integrated using an explicit fourth order Runge-Kutta method with a time step $dt = 0.05$. The temporal adjacency matrix A_{ij} is computed at each integration step. Mean field equations where no analytical solution was possible were integrated using an embedded Runge-Kutta 5(4)[69, 178]. Following the rationale in [70, 179] the AD network is updated on each integration step as to separate the timescales of connections and opinion dynamics.

4.3 External Bias

Let us open the bi-layer considerations with a seemingly simple case where the second layer can be modelled as a linear additive term to Eq. (4.1). This external bias can represent a cumulative effect of another group or maybe just the medium itself within which the system operates. Let us denote it as B and that it is either supporting X or working in opposition to X.

In such case we can say that:

$$\dot{x}_i = -x_i + K\sum_{j}^{N} A_{ij}(t)\tanh(\alpha x_j) + B, \tag{4.6}$$

and by averaging x_i and denoting $c_B = 2c$ we get (recall Eq. (4.5))

$$\langle \dot{x} \rangle = -\langle x \rangle + K c_B \tanh(\alpha \langle x \rangle) + B. \tag{4.7}$$

For such a system it becomes apparent that if $K\alpha c_B < 1$ then there is only one steady state solution of (4.7), however, for $K\alpha c_B > 1$ two scenarios are possible. When the magnitude of the external bias B is smaller than some critical value B_c then equation (4.7) possesses two stable and one unstable fixed point. It means the group can possess a polarisation towards or against the external bias B. When B is larger than some critical B_c then the equation (4.7) possesses only one solution and the polarisation directed against the external bias is not possible. It means that at some critical B_c a discontinuous transition takes place (see Fig. 4.1).

The critical value of the external bias - B_c - can be obtained from the stability analysis [180]. The Jacobian of the system (4.6) can be written as:

$$J|_{x_i=x_c} = \begin{bmatrix} -1 & K\alpha c_B \ \operatorname{sech}^2(\alpha x_c) & \dots \\ K\alpha c_B \ \operatorname{sech}^2(\alpha x_c) & -1 & \dots \\ \vdots & & \end{bmatrix}, \tag{4.8}$$

with the largest eigenvalue

$$\lambda_{max} = -1 + \frac{N-1}{N} K\alpha c_B \ \operatorname{sech}^2(\alpha x_c), \tag{4.9}$$

Combining the condition for the steady state of (4.7) (i.e. substituting $\langle \dot{x} \rangle = 0$) and the condition for the sign change of the largest eigenvalue λ_{max} (4.9) we get a solution for the critical value of the external bias B_c:

$$\begin{cases} B_c = x_c - K c_B \ \tanh(\alpha x_c) \\ x_c = \frac{1}{\alpha} \cosh^{-1}\left(\sqrt{\frac{N-1}{N} K\alpha c_B}\right) \overset{N\to\infty}{\sim} \frac{1}{\alpha} \cosh^{-1}\left(\sqrt{K\alpha c_B}\right). \end{cases} \tag{4.10}$$

In Fig. 4.1 we show that a phase transition occurs from the system's state to that of the bias. E.g. if the system converges on a positive (average) opinion and we set the bias to a negative and sufficiently large value the system will suddenly jump to the opposite side. In Fig. 4.1a we present an example of that. We wait until the system reaches its steady state and then activate the bias with an opposite sign. If the value is below the critical one the system merely shifts slightly towards zero, however, if $|B| > B_c$ a sudden jump occurs. In Fig. 4.1b we show this in the (B, α) phase space. The mean field approach - Eq. (4.10) - allows us to predict this behaviour, however, there is a discrepancy in the

actual value of the critical point. This is most likely due to finite nature of the simulated system as is usual for the mean field theory.

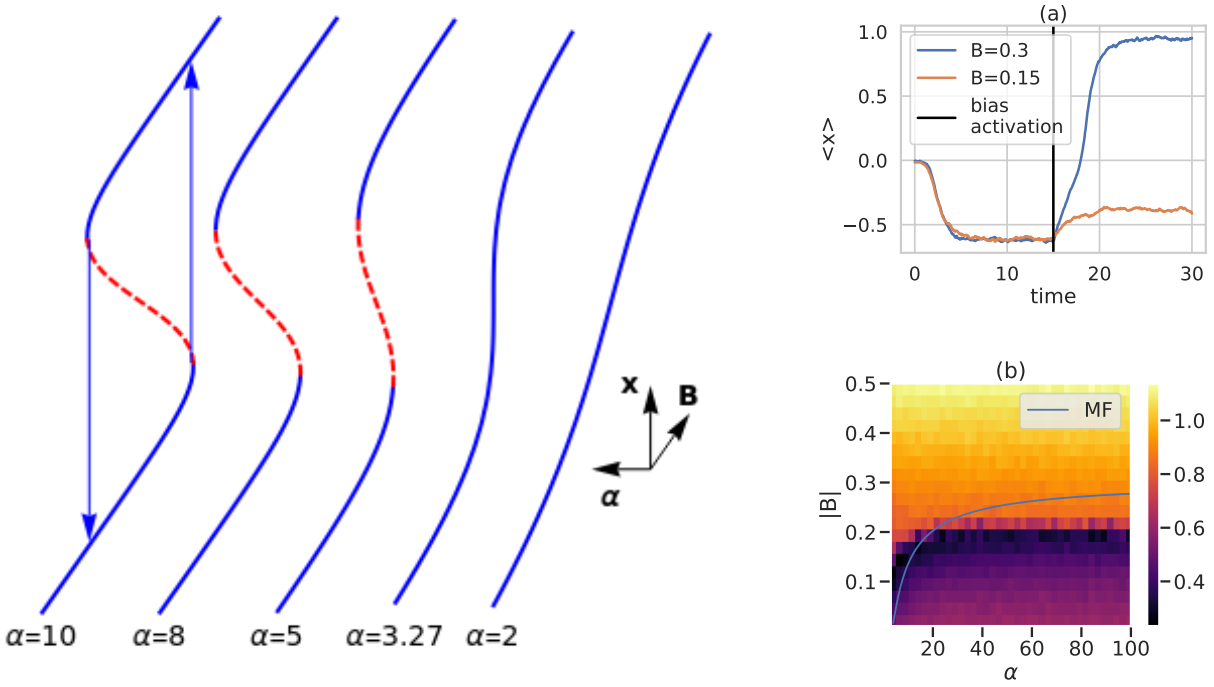

Figure 4.1: Left - bifurcation and hysteresis loop in the system of external bias: for $\alpha > 1/(Kc_B)$ the system is bi-stable and once a critical value of B_c is reached there is a switch from a polarisation against the field to towards it (an vice-versa for $-B_c$). Also in such a case, we cannot reach a neutral solution ($x = 0$) for any $B > 0$. For $\alpha < 1/(Kc_B)$ we have only one stable solution and such effects do not take place. Right - phase transition under the influence of an external bias. The top panel - (a) - shows two examples of an average opinion of the system as a function of time. One trajectory is for a value of external bias above the critical threshold and the other below. A solid vertical line signifying the moment we enable the external bias is present. The bottom panel - (b) - shows the (B, α) phase space, where colour is $\langle|\text{opinion}|\rangle$, with a visible phase transition to an opposite opinion and the mean field approximation - Eq. (4.10).

We can consider this case study as illustrative of how for example a propaganda may or may not be successful. We use propaganda here as a neutral term without concerning ourselves whether it is good or bad as one can easily imagine either. Such a scenario boils down to the strength of the campaign in question, however, it is not simply the stronger you push the more supporters you get. The dynamics of change are non-linear and the transition very sudden. This implies that it may be rather difficult to react to the propaganda machine in time to stop the society from drastically shifting its stance.

4.4 Symmetric coupling

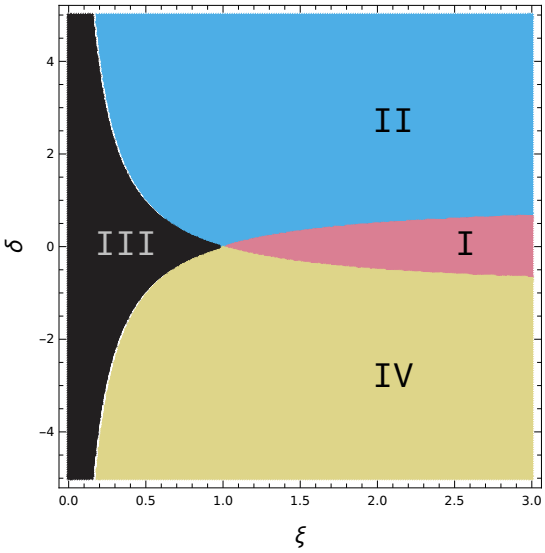

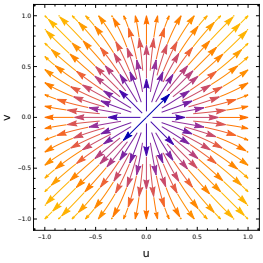

(a) Phase I portrait - source / repellent - in **pink**.

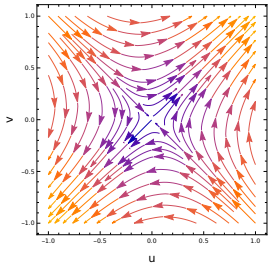

(b) Phase II portrait - saddle - in **blue**.

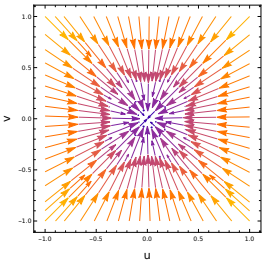

(c) Phase III portrait - sink / attractor - in **black**.

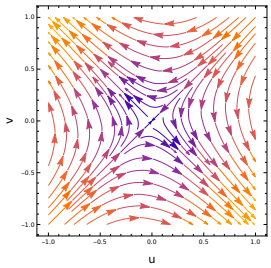

(d) Phase IV portrait - saddle - in **gold**.

Figure 4.2: Phase diagram of system (4.12) - left. Four distinct phases are visible defined by the signs of the eigenvalues (4.13). On the right corresponding phase portraits of each phase. In (a) we have the phase represented in **pink** on the left - a bi-stable phase. It is a typical case of a source or a repellent. In (b) we have a portrait corresponding to **blue** with an apparent saddle (radicalisation), (c) shows the sink or attractor phase (**black**, neutral consensus), and (d) another saddle in **gold** (polarisation).

We have just shown how the second layer even in a simply form of a linear external bias added can have profound implications for the dynamics of the system. In the next three sections we shall explore the implications of adding an actual, physical second layer with its own set of agents and their opinions $y_i(t)$. Let us define the bi-layer model as:

$$\begin{cases} \dot{x}_i = -x_i + K \sum_{j}^{N/2} A_{ij}(t) \tanh(\alpha x_j) + \delta K \sum_{j}^{N/2} A_{ij}(t) \tanh(\alpha y_j) \\ \dot{y}_i = -y_i + K \sum_{j}^{N/2} A_{ij}(t) \tanh(\alpha y_j) + \delta K \sum_{j}^{N/2} A_{ij}(t) \tanh(\alpha x_j), \end{cases} \tag{4.11}$$

where δ is the coupling parameter. In a sense what we create here is a situation where the layers are either at odds with one another ($\delta < 0$) or are supportive of each other ($\delta > 0$). One can of course write a more general form with different parameters for within

and without layer interactions (so e.g. instead of K have $K_{xx}, K_{xy}, K_{yx}, K_{yy}$) and we shall explore some of such scenarios later on, however, since the possibilities are nearly endless one must choose to stop at some point and so here we opt for more of a "ground up" approach. In order to make further analysis slightly less cumbersome let us introduce new coordinates $u = \alpha\langle x\rangle, v = \alpha\langle y\rangle$ and parameter $\xi = K\alpha c$ giving us the mean field formulas for the expected values for each of the layers as:

$$\begin{cases} \dot{u} = -u + \xi \tanh u + \delta\xi \tanh v \\ \dot{v} = -v + \xi \tanh v + \delta\xi \tanh u. \end{cases} \tag{4.12}$$

This system of equations (4.12) has a fairly trivial Jacobian at $(u, v) = (0, 0)$ with eigenvalues

$$\lambda_{1,2} = -1 + \xi(1 \pm \delta). \tag{4.13}$$

In Fig. 4.2 we present phase diagram and appropriate portraits. There are four distinct phases possible in this system depending on the values of $(\xi,\ \delta)$. If both eigenvalues are *negative* then we are in region of a stable steady state solution - an attractor or a sink (**black** on the phase diagram). The phase portrait of this situation is presented in the panel (a). What this means is that the system will always reach a consensus and in our case specifically - a neutral one, i.e. $\forall i\ x_i = y_i = 0$ as $t \to \infty$. When both $\lambda_{1,2}$ are *positive* we have a case of a repellent (or a source, shown in **pink**). In this case the neutral consensus is an unstable solution and the system will escape from it onto one of two stable solutions - a radicalised consensus or polarisation. Both of these also have their own respective regions in the phase diagrams and are typical saddles, i.e. one eigenvalue is positive and the other negative. When $\lambda_1 > 0\ \ \&\ \ \lambda_2 < 0$ we are in the **blue** phase - a radicalised consensus. While the exact steady state value can vary all agents eventually fall in line, i.e. $\forall i\ x_i = y_i \neq 0$ as $t \to \infty$. In **gold** region we have $\lambda_1 < 0\ \ \&\ \ \lambda_2 > 0$ and the stable solution is the polarised state - no consensus at all is possible, each layer maintains its position opposite to the other layer's, namely $\langle x\rangle = -\langle y\rangle\ (\neq 0)$ as $t \to \infty$. Example trajectories of these can be seen in Fig. 4.3.

Similarly to the external bias case by looking at when λ_{max} changes signs and the steady states we can derive the equations for the critical value δ_c. We can have either $x_c = -y_c (\neq 0)$ in the steady state and since $\mathrm{sech}^2(x)$ is an even function we need not

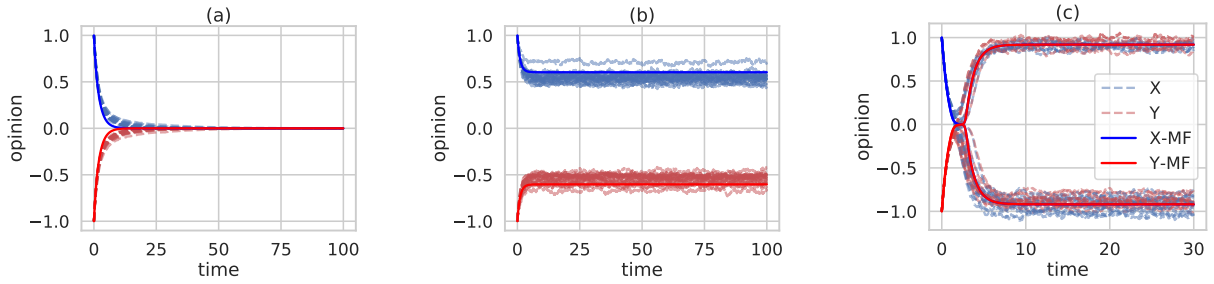

Figure 4.3: Example trajectories of the groups' average opinions as they change in time. Dashed lines represent agent based simulations and there are 20 independent realisations shown. Solid lines are the result of the mean field approximation (-MF). In all cases we start from a polarised state and in (a) we are below the critical value with $\xi = 0.26, \delta = -1$ and both groups converge on a neutral opinion while in - (b) - above it with $\xi = 1.2, \delta = -1$ and groups remain in their respective opinions in opposition to each other. Finally (c) - $\xi = 3.1, \delta = 2$ and a radicalised consensus forms.

worry about the sign or simply $x_c = y_c (\neq 0)$ and thus:

$$\begin{cases} \delta_c = \pm \left(\frac{1}{\xi} \cosh^2(u_c) - 1 \right) \\ u_c = \xi(1 \mp \delta_c) \tanh(u_c), \end{cases} \tag{4.14}$$

which is a bit more challenging set of equations than previously and there is no closed form solution, and therefore needs to be solved numerically.

Alongside the aforementioned Fig. 4.3 showing a reasonable agreement of agent-based simulations and the mean field approximation in terms of opinion change in time, we also show the phase transitions in Fig. 4.4. There we present how the steady state of the system's opinion changes in function of the control parameter ξ. While the mean field does not perfectly match the simulations and the critical points are slightly shifted, and more so for large values of ξ, qualitatively the theory is very successful at describing the behaviour of the system.

We can interpret the **III**-IV transition as a case of a typical echo chamber situation in context of two rivalling groups such as political parties. If the animosity from one to the other or mutually is strong enough then no consensus is possible - while the groups may not be as radical as in initially they will always persist in their view opposite to the other. This essentially shows that prejudice has the potential to lock society into a predetermined antagonistic state. On the other hand we have the IV-II transition that stands somewhat in contrast to the opposition scenario described above. Let us imagine that we can somehow influence the attitudes of the layers such that we soften the animosities towards more amicable and maybe even eventually slightly cordial side of

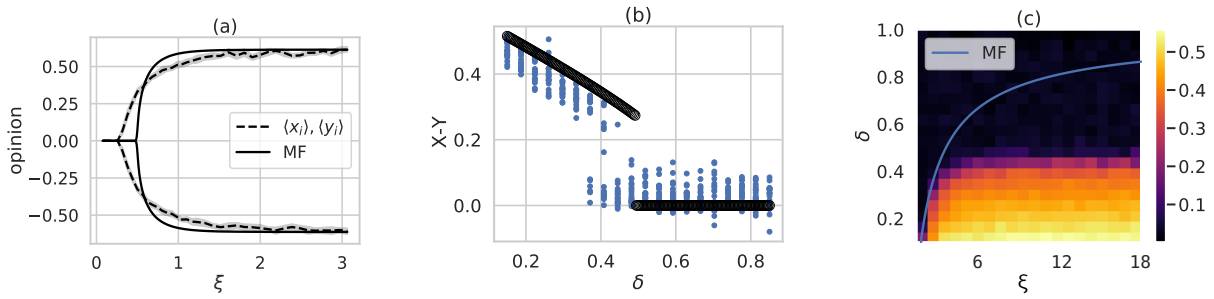

Figure 4.4: (a) Phase transition from the symmetric consensus to the opposite polarisation of opinions in different layers X and Y with visible small discrepancy between mean field approximation and agent-based simulations while the asymptotic behaviour having a very good agreement. ABM simulations are shown with 95% confidence interval as the error bands. (b) polarisation to radicalisation transition shown as the difference of opinions between layers in function of the parameter δ. (c) heatmap of (ξ, δ) phase space, with colour representing $|\langle x\rangle - \langle y\rangle|$.

things then would that be enough? Or do we need to completely flip peoples attitudes to make consensus possible. Our model suggests that it can be enough, indeed. This implies that while prejudice can cause society to split there is also room for hope as not so drastic changes in attitudes can cause the layers to merge in opinion albeit not a neutral one. The **III-I** and **III-II** transitions somewhat reduce to what has already been described in [70] and are as such are not of particular interest to us right now.

4.5 Asymmetric coupling

By *asymmetric* we mean here that we no longer have a single δ like in Eq. (4.11) by introducing δ_{xy}, δ_{yx}. Let us proceed straight to the mean field formulation getting:

$$\begin{cases} \dot{u} = -u + \xi \tanh u + \delta_{xy}\xi \tanh v \\ \dot{v} = -v + \xi \tanh v + \delta_{yx}\xi \tanh u. \end{cases} \tag{4.15}$$

However, we keep the *signs* of δ_{xy}, δ_{yx} to be the same such that $\sqrt{\delta_{xy}\delta_{yx}} \in \mathcal{R}_+$. We can then look at the condition for the largest eigenvalue λ_{max} of the Jacobian changing its sign giving us:

$$\delta_{yx} = \left(1 - \frac{1}{\xi}\right)^2 \frac{1}{\delta_{xy}}, \tag{4.16}$$

which is the formula for the boundary between the neutral consensus phase and either radicalised consensus or polarisation depending on the sings of δ_{xy}, δ_{yx}. Comparison of this with numerical simulations can be seen in Fig. 4.5 where we present the $(\delta_{xy}, \delta_{yx})$ space

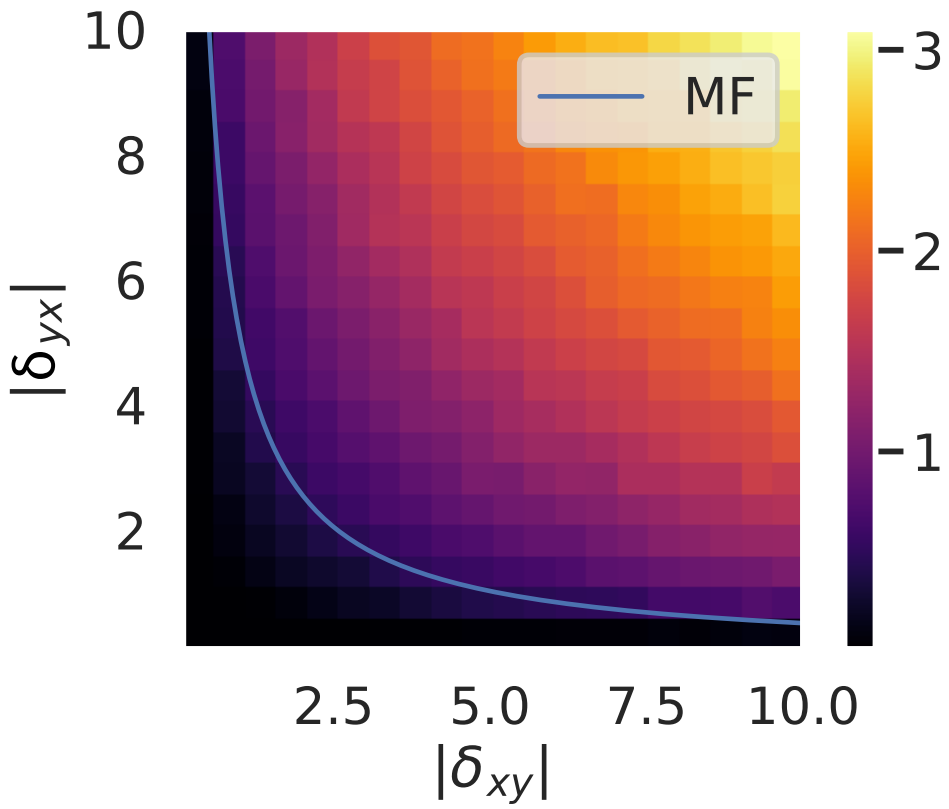

Figure 4.5: The asymmetric coupling parameters phase space $(|\delta_{xy}|, |\delta_{yx}|)$ in a form of a heat map, where the colour represents $\langle|\text{opinion}|\rangle$, with a visible transition from neutral consensus to polarisation. MF is Eq. (4.16)

in form of a heatmap where colour represents the mean of the absolute value of opinions in the system (i.e. $\langle|\text{opinion}|\rangle$). We can see a very satisfactory agreement between the formula and the agent-based simulations.

4.6 Anti-symmetric coupling

By *anti-symmetric* we mean the case where $\delta_{xy}\delta_{yx} < 0$ and therefore the eigenvalues:

$$\lambda_{1,2} = -1 + \xi \pm \xi\sqrt{\delta_{xy}\delta_{yx}} \tag{4.17}$$

are complex with $\text{Re}(\lambda_{1,2}) = -1 + \xi$ and $\text{Im}(\lambda_{1,2}) = \pm\xi\sqrt{|\delta_{xy}\delta_{yx}|}$. The fact the the eigenvalues are complex with non-zero real parts means that we are dealing with a Poincaré–Andronov–Hopf bifurcation [180, 181]. Therefore the condition $\text{Re}(\lambda_{1,2}) = 0$ gives us the critical value of the control parameter ξ at which the bifurcation occurs. In our case it is simply $\xi_{crit} = 1$. Traditionally in the so called normal form the parameter is defined in

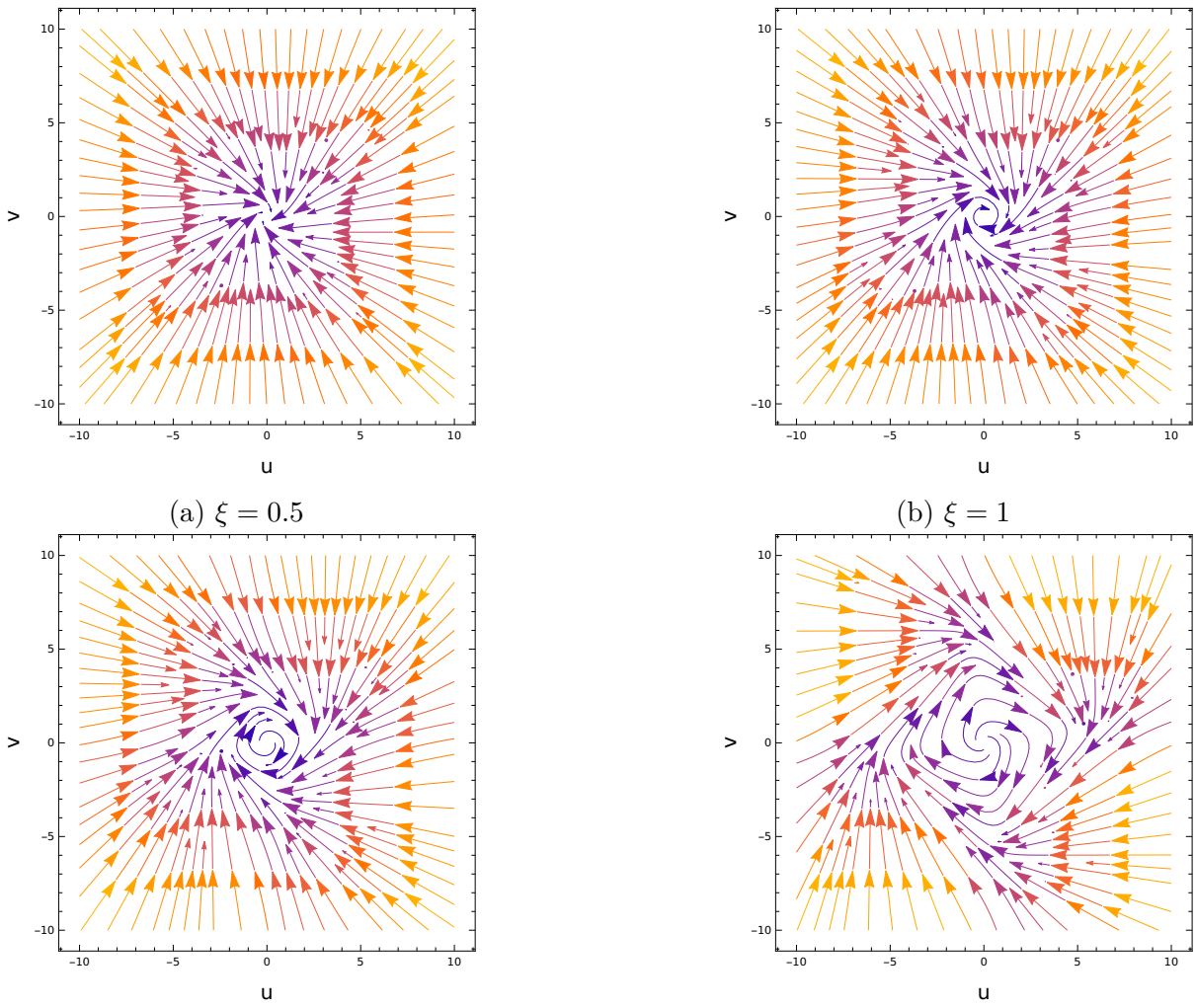

(a) $\xi = 0.5$

(b) $\xi = 1$

(c) $\xi = 1.5$

(d) $\xi = 3$

Figure 4.6: Phase portraits of the Eq. (4.15) showing the behaviour below and above critical point determined by the real part of the Jacobian eigenvalues (4.17). For $\xi - 1 \geq 0$ the system is attracted to an orbit whilst when $\xi - 1 < 0$ it collapses into the point $(0, 0)$.

such a way that the bifurcation occurs when the control parameter vanishes, however, we are not here to delve into the details of the Poincaré–Andronov–Hopf (P-A-H) and thus shall not trouble ourselves with that. We can see in Fig. 4.6 that the system has a stable limit cycle above the critical value which means this is a *supercritical* P-A-H bifurcation. This tells us that what we expect to see in the system are oscillations (dampened below the critical value and sustained above) and indeed in Fig 4.7 we can see some example agent based simulations compared to the mean field approximation. Both show the expected behaviour, albeit again, the mean field critical point is not exactly right - in (b) the mean field is still dampened while the ABM is not. It is also informative to look at some trajectories in the space described before by the portraits - see Fig. 4.8. There we

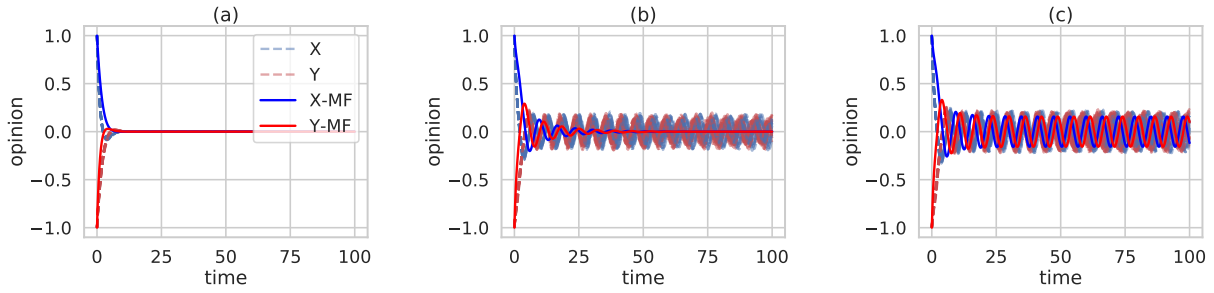

Figure 4.7: Example trajectories in the asymmetric coupling parameters scenario for $\xi = \{0.31, 0.92, 1.1\}$ respectively left to right. 20 independent agent based simulation results are shown as dashed lines with solid lines representing the mean field (MF) approximation. Two distinct behaviours are visible - sustained and dampened oscillations.

can see again the behaviour described above and how qualitatively our analyses are in very good agreement with simulations.

Another matter we can explore here is that of the oscillations frequency as Hopf theorem provides as with the angular frequency of the orbit at the critical point $\omega_{crit} = \xi\sqrt{|\delta_{xy}\delta_{yx}|}$. In our case it corresponds to an ordinary frequency $f_{crit} \approx 0.159$. Since the system we are analysing is highly non-linear we cannot expect the mean field approximation (or Hopf theorem for that matter) to give us the exactly right answer, however, in Fig. 4.9 we can see a good qualitative match yet again. It is worth noting that should the oscillations be of a linear kind we would expect their frequency to grow with ξ but here we see it decrease (in the supercritical region). At the same time the amplitude rises with ξ and this might be the clue as to why the frequency behave in such a way. One could say that the amplitude here plays the role of a sort of barrier for the system to overcome and so the higher the barrier the longer it takes to be overtaken thus the frequency of the oscillations increases.

While this scenario might be slightly less obvious to interpret we do believe there are certain parallels to be drawn here. It may seem as though one group is a *trend setter* while the other represents *followers*. In such a case there can be a very similar sort of a feedback dynamic that we observe in our model. One group - the followers - is positively oriented towards the other - the trend setters - as they look up to them and would like to be, act, think like them etc. On the other hand, the setters share a negative attitude towards the followers in this context. While they might appreciate the following they would very much want to move away from it in terms of the opinion in question. This leads to this chasing and oscillating behaviour. However, should the attitudes magnitudes *within* the groups be not strong enough the dynamic simply dies down as neither the followers are not as interested in following nor setters in trend setting.

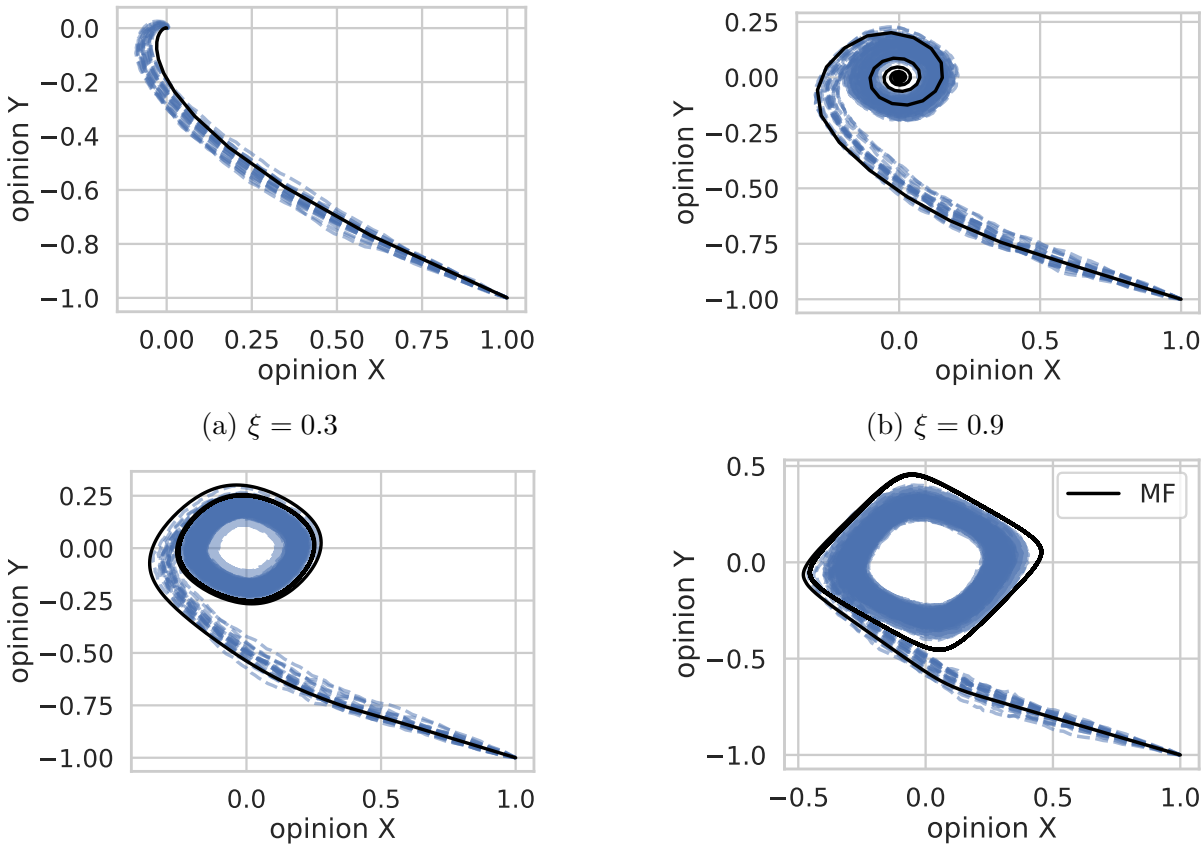

(a) $\xi = 0.3$

(b) $\xi = 0.9$

(c) $\xi = 1.2$

(d) $\xi = 3.1$

Figure 4.8: Y(X) trajectories in the asymmetric coupling scenario for $\xi = \{0.3, 0.9, 1.2, 3.1\}$ with dashed lines representing 20 independent realisations of the agent based simulation and solid lines showing the mean field solution. We observe in detail that the system has two possible attractors - a point ($\xi < 1$) and an orbit ($\xi \geq 1$). For $\xi \geq 1$ the point (0,0) becomes unstable and trajectories starting from it would also end in an orbit.

To sum up, in this chapter we have explored four different case studies of a bi-layer temporal echo chambers and polarisation model. We looked upon an existing single layer model and extended it onto a multi layered paradigm and thus acquired new complex behaviours that were previously absent. We saw a case that could potentially model how devastating (or simply effective) a propaganda machine can be as the transitions to a completely opposite opinion could be very sudden and unexpected. We found evidence that a seemingly trivial one parameter coupling can lead to many new transitions between neutral and radical consensus, and a polarised society. We also discovered that even intricate oscillating behaviours are possible when two separate and anti-symmetrically coupled layers are present. This underlines the importance of the previous two chapters that dealt with detecting the layered structure of some hypothetical systems. Real world

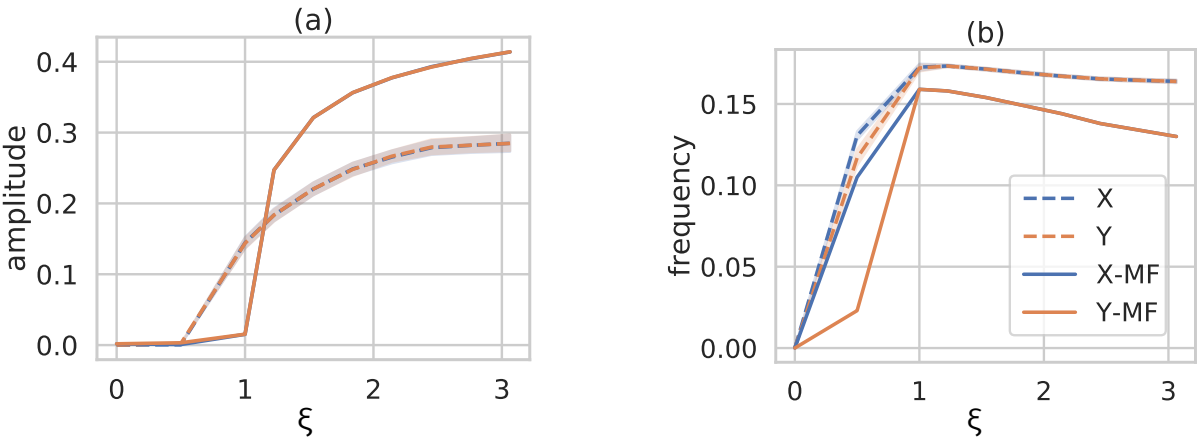

Figure 4.9: Oscillation frequencies and amplitudes. Dashed lines represent an average of 20 independent realisations of agent based simulations with a 95% confidence interval present as the error bands. Solid lines show the mean field solution.

systems are complex and layered and in order to model them appropriately we need to be able to determine what layers are hidden from us and what implications they can carry.

Chapter 5

Conclusions

This work is the conclusion of the following three articles:

- [1] **Gajewski, Ł. G.**, Chołoniewski, J., & Wilinski, M., *Detecting Hidden Layers from Spreading Dynamics on Complex Networks.* Phys. Rev. E 104(2), 2021, 024309. Supported by National Science Centre, Poland Grant No. 2015/19/B/ST6/02612.
- [2] **Gajewski, Ł. G.**, Sienkiewicz, J., & Hołyst, J. A., *Discovering hidden layers in quantum graphs.* Phys. Rev. E 104(3), 2021, 034311. Supported by POB Research Centre Cybersecurity and Data Science of Warsaw University of Technology within the Excellence Initiative Program - Research University (IDUB)
- [3] **Gajewski, Ł. G.**, Sienkiewicz, J., & Hołyst, J. A. (2021). *Phase transitions and oscillations in a temporal bi-layer echo chambers model.* arXiv preprint arXiv:2101.03430. Supported by an IDUB against COVID-19 project granted by Warsaw University of Technology under the program Excellence Initiative: Research University (IDUB), under review in Phys. Rev. E,

in which we analyse dynamics on complex networks and propose methods of detecting hidden structures by simply observing the states of agents and their relationships in the system. We also show how profound can the consequences be if a hidden layer exists using an example of echo chambers and polarisation model.

More specifically, we focused on identifying both the existence and the structure of a hidden spreading layer by observing a diffusion process unravelling on a graph. We provide methods for i) determining whether a hidden layer exists and ii) estimating what links are present in that layer. Our approach is based on an exact formula for the likelihoods of an observed cascade given knowledge of the system's topology. Using the said likelihood and the fact its distribution can be assumed to be unimodal we established a practical and

effective way of discerning the existence of a hidden layer. Furthermore using a series of heuristics we obtain an algorithm for estimating the joint likelihood of a given (hidden) edge taking part in the observed cascade therefore providing a tool for assessing which nodes are most likely to exchange information via channel we do not know of that is vastly superior to random guessing.

We tested our proposition on both synthetic and empirical data sets and found that detecting hidden spreading channel is a relatively simple task with our approach - especially when the layers are uncorrelated. On the other hand, reverse engineering of hidden connections can be a bit more of a challenge yet not impossible. The difficulty of this task does depend heavily on the densities of both observed and hidden layers and their relationship. The denser the hidden layer the harder it is to find the exact connections. An interesting interplay takes place when it comes to the density of the observed layer. On one hand the sensitivity decreases with the density of observed layer, but the α-CSS is also decreasing with the density which may be slightly counter intuitive. While our propositions have their limitations and do not account for several effects like e.g. overlapping connections neither have we focused on optimising it for very large networks, it does show a lot of success in synthetic and real data sets alike. Moreover, some generalisations such as including temporal networks could also prove to be an interesting research problem for the future. While we do hope to address some of the above topics in the near future we feel that methods presented here already provide effective and practical tools for real world applications.

We have also explored the paradigm of quantum graphs as a potential tool for studying multi-layer networks. The particular problem we are interested in is determining whether there are hidden layers of communication in the system, that we cannot fully observe, by taking measurements of the ongoing dynamics in a single layer that we can observe. We proposed and tested two methods - one based upon a Gaussian wave packet signature (WPS) that was introduced previously by Aziz *et al.* to discriminate between various types of mono-layer systems, and the other on observing the power spectrum of the wave amplitudes.

WPS is a method where a Gaussian wave packet, either observed or purposefully produced, initiates the propagation from a single edge and we take the measurements of the amplitudes at every edge at integer times for a sufficiently large number of times. Such data is then histogrammed to produce the signature. This signature has the property of being similar within a category of graphs while varied without. That is, e.g., signatures of the ER graphs are similar to one another but different from the BA graphs, or for our purposes, mono-layer graphs have different signatures than multi-layer ones etc. This in

turn can be utilised by machine learning models, such as K-nearest neighbours, to build a model capable of discriminating between graphs with different numbers of layers. This approach suffers from several issues, however. Most prominently, it requires a training sample. This can be very difficult to obtain in real-world scenarios and while perhaps a well varied synthetic data set could suffice, at this point it is mere speculation. The choice of an appropriate machine learning scheme and its construction is also a non-trivial task. Additionally, as the number of layers grows, differentiating between such networks becomes increasingly difficult since the signatures become less varied.

We also introduce an approach that utilises a discrete Fourier transform (DFT) instead of a machine learning model. Instead of histogramming the measurements as before, one computes the sum of the amplitudes on the visible layer at each integer time. This constitutes a signal that at sufficient time scales should become stationary. In a mono-layer system the signal will simply be a constant value due to energy conservation. However, should other layers be present in the system, from the perspective of the mono-layer there will be oscillations as the energy will flow out and back into it. We can inspect those oscillations with the use of the DFT and look at the power spectrum. The spectrum will exhibit characteristic peaks absent in the mono-layer networks. The number of these peaks strictly corresponds with the number of layers in the synthetic scenarios tested. This approach is significantly advantageous over the WPS as it does not require building a learning sample and is in general much simpler. Furthermore, it does not really suffer in terms of differentiating, e.g., tetra- from penta-layer systems, etc. Although it shows much promise in synthetic scenarios, it does not perform as well in real-world networks. It does indeed indicate clearly that there are hidden layers but the number of them can be rather tricky to discern. This is perhaps not that surprising considering that real-world networks are much more "messy" in some way than synthetic examples. Layers vary in size, degree distribution, clustering coefficients and so on and so forth, while, e.g., a penta-layer BA graph shares all characteristics between layers even though the exact connections are different. Those and other features of real-world systems could also affect the coupling amongst the layers that most certainly will affect the nature of the amplitude signal.

In such cases (i.e., where peak count after a brief observation is not enough) we show that simply a longer observation time is required. As the signal is not stochastic and oscillation periods are finite it does not seem unfeasible to observe enough of the signal to determine its power spectrum with sufficient resolution. Then each peak in the spectrum corresponds to the Hamiltonian eigenvalues that in turn are related to the eigenvalues of the row-normalised adjacency matrix via a simple formula. With this we showed that it

is indeed possible to recover all these eigenvalues and thus trivially determine the number of layers in the system.

It is worth underlining here that a row-normalised adjacency matrix is in fact the so called right stochastic matrix of a given graph and while it goes beyond the scope of this thesis, there exist methods of reconstructing the whole matrix from its spectrum [182–186] which we suspect should be quite feasible considering we already assume knowing part of it (one layer and inter-layer structure). That in turn could also open the door to the adjacency matrix itself. Recovering all the connections exactly may not be possible, however, having a matrix iso-spectral to the adjacency matrix is also very valuable as having this spectrum allows for determining many important properties of the system [187, 188].

The issue of – how long the observation time should be – still remains, however. In the experiments presented in this work, we needed more observation points using the Fourier approach than with the machine learning one. In the real-world example used in this work, the necessary measurement time to get the almost perfect match seen at the right panel of Fig. 3.9 is fairly substantial – we simulated the system for 11520 time steps to be exact. While lower values would not mean no match at all, the low power components do become less discernible. This is due to the fact that some frequencies may be difficult to observe because of the particular intricacies of a given system, while some eigenvalues are going to be detectable more easily since more power is associated with them. In order to observe all frequencies, in an idealised scenario, we should observe at least two periods of the signal (one could also possible suffice but we shall assume two). Therefore, the total observation time should be $4\pi/\arccos(\lambda_2)$, where λ_2 is the eigenvalue with the second largest magnitude of the stochastic matrix. In general, i.e., for any system, for any stochastic matrix, it is not possible to give one formula for the behaviour of λ_2[189]. In special cases it is possible to provide an analytical expression and, e.g., for a full graph duplex we would need $4\pi/\arccos((N-2)/N)$ measurements which is clearly much fewer than in case of the machine learning approach – $N(N-1)$ (note that it does not hold for networks like Vickers). The latter has also been rather arbitrarily chosen by Aziz et al., and further more, one could also ask how big the training test must be to achieve a certain level of accuracy. This, similarly to assessing the necessary number of measurements, is rarely, if ever, possible to be known a priori. This points to an another possible advantage of our Fourier approach (despite requiring more observation time in some systems), which is that since we do not require training of the model we can in fact start recovering the spectrum "online", i.e., with very few measurements and simply keep adding them and improving the results as the time passes. As we continue our measurements it will also

usually become clear which frequency peaks are stable and whether all of them are already expressed via a visual inspection of the signal or the spectrum.

We find that both methods presented here - the WPS and FFT - show enough success in these simple scenarios we tested to merit further study, such as in noisy (or stochastic) systems, for instance. They each have their pros and cons that we hopefully managed to outline clearly as well as the potential room for improvement of their applicability and understanding of waves on quantum graphs alike.

While we find our approach to be very promising it is also important to outline the potential further study areas as we could not possibly have covered everything in this thesis. It would be of substantial interest to investigate how the described system behaves when distinct community structures (as in, e.g., a stochastic block model [190]) are present. We suspect that it is feasible to detect the communities themselves, however, discerning these communities from layers can pose an additional challenge. Furthermore, we have tested a particular form of multi-layer networks with distinct symmetries, yet other, more complicated types exist, such as networks of networks [118] and multi-layer graphs with complex inter-layer connections [9]. These are especially interesting and considerably more difficult as the inter-layer structures themselves can vary wildly. Finally, there is also a matter of node membership in specific layers. Depending on the particulars of the studied real-world scenarios it can be of interest to be able to ascertain where a given node belongs. We suspect that this may also be possible, as from our experience single-node time series can also contain a substantial amount of information. We hope to address these issues in our future work.

Finally, we have presented a temporal bi-layer echo chamber and polarisation model on complex networks inspired by the mono-layer model introduced by Baumann et al. We recognise that there is both a precedent and apparent value in studying scenarios where two clearly cut groups - or layers in a network - are interacting with one another. Understanding how layered complex networks evolve in various environments in context of opinion dynamics can help us better prepare for tackling issues that potentially threaten our democracies such as misinformation campaigns or echo chambers. In the context of this thesis, the presented socio-physical model serves as an argument for the importance of the layer detection methods developed in prior chapters since it shows new behaviour appearing as a consequence of a layered topology.

We formulate the dynamics equations for the bi-layer system and then provide a mean field analysis that uncovers interesting possible scenarios. The nature of system's behaviour is different depending on the coupling between the layers. We can see several interesting case studies such as opposite polarisation where the groups do not like each

other, opinion oscillations where one group likes the other, however, the feeling is not mutual, external bias where we consider the other group as an external bias acting upon a mono-layer system, and where there is an attraction between the groups, however, perhaps not as strong as withing them.

In the opposite polarisation scenario we observe that a coexistence of two groups with different (opposite) opinions is possible. The system undergoes a phase transition from a neutral consensus - where the two layers' opinions merge at zero - to a polarised state - where the two groups coexist each of them having their own opinion, opposite to the other groups. The details of the transition and asymptotic behaviour of the system are predicted by a mean field approximation with which we predict the critical values of control parameter ξ and the coupling parameters δ_{xy}, δ_{yx}. In both cases the mean field approach gives us a satisfying fit to agent-based simulations.

When the coupling parameters are set anti-symmetrically, in the sense that one is positive and one negative, we detect a transition from dampened to sustained oscillations of the layers' opinions. In a way one might say that one group is "chasing" the other with their opinions, while the other is trying to get away. We additionally find that the oscillations are highly non-linear as the frequency *decreases* with control parameter as opposed to *increasing* as one would expect from a linear oscillator. At the same time the amplitude rises with the control parameter. We believe the amplitude here plays the role of a sort of barrier for the system to overcome and so the higher the barrier the longer it takes to be overtaken thus the frequency of the oscillations increase.

In the case of a single layer with an external bias present we postulate that it might be possible to model either a background of some sort or the second layer for that matter as simply a cumulative effect in the form of such an external bias. We find that there exists a critical value of the said bias that when the system is subject to it a sudden change to an opposite opinion is possible. For small values of the control parameter we find a decent match of mean field approach and agent-based simulations, however, for larger values the two diverge in the prediction as to when the transition should occur, most likely due to the finite size of the simulated system.

When the two layers are weakly yet positively coupled we see not very dissimilar behaviour to the one with the external bias. Namely there exists a critical value of the coupling parameter that causes the system to experience a sudden shift in the opinions. In this case we observe that there is a transition from an oppositely polarised state to a polarised consensus (or a radicalised state) where all agents (from both layers) share similar and non-zero opinion. Similarly to the previous case the match between the mean field theory and simulations is qualitatively satisfying, however, for larger values of the

control parameter the predictions as to when the transition should happen diverge from the results of numerical experiments.

With each scenario we have drawn parallels to real world to illustrate what these results could mean for understanding the dynamics of our societies. We understand that there are limitations with both the model and the approach in general as it can be often difficult to construct reproducible experiments in sociological context, however, we firmly believe that seeing where certain assumptions can lead us is an important and crucial building block of science.

The main achievements of this work are two-fold: i) new tools for uncovering hidden structures in multi-layer networks, and ii) evidence that these tools are in fact very much needed. The former is provided for two very distinct families of models that differ not only in their information dynamic but also the layering structure itself. For this purpose, we leverage cascade likelihood formulae for epidemiological models, as well as machine learning and signal analysis tools in the realm of quantum graphs to achieve this goal. The latter is accomplished by extending an echo chambers and polarisation model onto a layered topology and showing that this change – adding a layer – can result in a new and unexpected behaviour, thus arguing that it is crucial to be able to detect such layered structures. Thus, we have succeeded in what we set out to achieve.

In the end we hold a firm belief that our analyses throughout this text have been thorough, insightful and led to profound observations, and practical, applicable propositions of tools to be of use in real world scenarios. We sincerely hope that after consuming this work the dear Reader shares that belief as well.

Bibliography

1. Gajewski, Ł. G., Chołoniewski, J. & Wilinski, M. Detecting hidden layers from spreading dynamics on complex networks. *Phys. Rev. E* **104,** 024309. https://link.aps.org/doi/10.1103/PhysRevE.104.024309 (2 Aug. 2021).

2. Gajewski, Ł. G., Sienkiewicz, J. & Hołyst, J. A. Discovering hidden layers in quantum graphs. *Phys. Rev. E* **104,** 034311. https://link.aps.org/doi/10.1103/PhysRevE.104.034311 (3 Sept. 2021).

3. Gajewski, Ł. G., Sienkiewicz, J. & Hołyst, J. A. Phase transitions and oscillations in a temporal bi-layer echo chambers model. *arXiv preprint arXiv:2101.03430* (2021).

4. Paluch, R., Gajewski, Ł. G., Suchecki, K. & Hołyst, J. A. Impact of interactions between layers on source localization in multilayer networks. *Physica A: Statistical Mechanics and its Applications* **582,** 126238. https://www.sciencedirect.com/science/article/pii/S0378437121005112%20https://linkinghub.elsevier.com/retrieve/pii/S0378437121005112 (2021).

5. Paluch, R., Gajewski, Ł., Suchecki, K., Szymański, B. & Hołyst, J. A. in *Simplicity of Complexity in Economic and Social Systems* 21–41 (Springer International Publishing, Nov. 2020). https://doi.org/10.1007%5C%2F978-3-030-56160-4_2.

6. Paluch, R., Gajewski, Ł. G., Hołyst, J. A. & Szymanski, B. K. Optimizing sensors placement in complex networks for localization of hidden signal source: A review. *Future Generation Computer Systems* **112,** 1070–1092 (2020).

7. De Domenico, M. *et al.* Mathematical formulation of multilayer networks. *Physical Review X* **3,** 041022 (2013).

8. Kivelä, M. *et al.* Multilayer networks. *Journal of complex networks* **2,** 203–271 (2014).

9. Boccaletti, S. *et al.* The structure and dynamics of multilayer networks. *Physics Reports* **544,** 1–122 (2014).

10. De Domenico, M., Solé-Ribalta, A., Omodei, E., Gómez, S. & Arenas, A. Ranking in interconnected multilayer networks reveals versatile nodes. *Nature communications* **6,** 1–6 (2015).

11. De Domenico, M., Granell, C., Porter, M. A. & Arenas, A. The physics of spreading processes in multilayer networks. *Nature Physics* **12,** 901–906 (2016).

12. De Arruda, G. F., Rodrigues, F. A. & Moreno, Y. Fundamentals of spreading processes in single and multilayer complex networks. *Physics Reports* **756,** 1–59 (2018).

13. Barrat, A., Barthelemy, M. & Vespignani, A. *Dynamical processes on complex networks* (Cambridge university press, 2008).

14. Pastor-Satorras, R., Castellano, C., Van Mieghem, P. & Vespignani, A. Epidemic processes in complex networks. *Reviews of modern physics* **87,** 925 (2015).

15. Lokhov, A. *Reconstructing parameters of spreading models from partial observations* in *Advances in Neural Information Processing Systems* (2016), 3467–3475.

16. Wilinski, M. & Lokhov, A. Y. Scalable Learning of Independent Cascade Dynamics from Partial Observations. *arXiv preprint arXiv:2007.06557* (2020).

17. Leskovec, J. & Krause, A. Inferring networks of diffusion and influence. *In KDD10* (2010).

18. Woo, J., Ok, J. & Yi, Y. *Iterative learning of graph connectivity from partially-observed cascade samples* in *Proceedings of the Twenty-First International Symposium on Theory, Algorithmic Foundations, and Protocol Design for Mobile Networks and Mobile Computing* (2020), 141–150.

19. Pouget-Abadie, J. & Horel, T. *Inferring Graphs from Cascades: A Sparse Recovery Framework* in *Proceedings of the 24th International Conference on World Wide Web* (2015), 625–626.

20. Abrahao, B., Chierichetti, F., Kleinberg, R. & Panconesi, A. *Trace complexity of network inference* in *Proceedings of the 19th ACM SIGKDD international conference on Knowledge discovery and data mining* (2013), 491–499.

21. Gripon, V. & Rabbat, M. *Reconstructing a graph from path traces* in *2013 IEEE International Symposium on Information Theory* (2013), 2488–2492.

22. Gomez-Rodriguez, M., Leskovec, J. & Krause, A. Inferring networks of diffusion and influence. *ACM Transactions on Knowledge Discovery from Data (TKDD)* **5,** 1–37 (2012).

23. Netrapalli, P. & Sanghavi, S. Learning the graph of epidemic cascades. *ACM SIGMETRICS Performance Evaluation Review* **40,** 211–222 (2012).

24. Braunstein, A., Ingrosso, A. & Muntoni, A. P. Network reconstruction from infection cascades. *Journal of the Royal Society Interface* **16,** 20180844 (2019).

25. Gajewski, Ł., Suchecki, K. & Hołyst, J. Multiple propagation paths enhance locating the source of diffusion in complex networks. *Physica A: Statistical Mechanics and its Applications* **519,** 34–41 (2019).

26. Paluch, R., Lu, X., Suchecki, K., Szymański, B. K. & Hołyst, J. A. Fast and accurate detection of spread source in large complex networks. *Scientific reports* **8,** 1–10 (2018).

27. Paluch, R., Gajewski, Ł. G., Suchecki, K. & Hołyst, J. A. Source location on multilayer networks. *arXiv preprint arXiv:2012.02023* (2020).

28. Gomez, S. *et al.* Diffusion dynamics on multiplex networks. *Physical review letters* **110,** 028701 (2013).

29. Sole-Ribalta, A. *et al.* Spectral properties of the Laplacian of multiplex networks. *Physical Review E* **88,** 032807 (2013).

30. Chmiel, A. & Sznajd-Weron, K. Phase transitions in the q-voter model with noise on a duplex clique. *Physical Review E* **92,** 052812 (2015).

31. Chmiel, A., Sienkiewicz, J. & Sznajd-Weron, K. Tricriticality in the q-neighbor Ising model on a partially duplex clique. *Physical Review E* **96,** 062137 (2017).

32. Chmiel, A., Sienkiewicz, J., Fronczak, A. & Fronczak, P. A Veritable Zoology of Successive Phase Transitions in the Asymmetric q-Voter Model on Multiplex Networks. *Entropy* **22,** 1018 (2020).

33. Lacasa, L. *et al.* Multiplex decomposition of non-Markovian dynamics and the hidden layer reconstruction problem. *Physical Review X* **8,** 031038 (2018).

34. Guimerà, R. & Sales-Pardo, M. Missing and spurious interactions and the reconstruction of complex networks. *Proceedings of the National Academy of Sciences* **106,** 22073–22078 (2009).

35. De Bacco, C., Power, E. A., Larremore, D. B. & Moore, C. Community detection, link prediction, and layer interdependence in multilayer networks. *Physical Review E* **95,** 042317 (2017).

36. Kuchment, P. Quantum graphs: I. Some basic structures. *Waves in Random media* **14.** Publisher: Taylor & Francis, S107–128. ISSN: 0959-7174 (2004).

37. Kuchment, P. Quantum graphs: II. Some spectral properties of quantum and combinatorial graphs. *Journal of Physics A: Mathematical and General* **38.** Publisher: IOP Publishing, 4887. ISSN: 0305-4470 (2005).

38. Kuchment, P. Quantum graphs: an introduction and a brief survey. *arXiv preprint arXiv:0802.3442* (2008).

39. Berkolaiko, G. & Kuchment, P. *Introduction to quantum graphs* Issue: 186. ISBN: 0-8218-9211-8 (American Mathematical Soc., 2013).

40. Pauling, L. The diamagnetic anisotropy of aromatic molecules. *The Journal of Chemical Physics* **4,** 673–677 (1936).

41. Kuchment, P. Graph models for waves in thin structures. *Waves in random media* **12,** R1–R24 (2002).

42. Biamonte, J., Faccin, M. & De Domenico, M. Complex networks from classical to quantum. *Communications Physics* **2.** Publisher: Nature Publishing Group, 1–10. ISSN: 2399-3650 (2019).

43. Exner, P. & Post, O. *Quantum networks modelled by graphs* in *AIP Conference Proceedings* **998** (2008), 1–17.

44. Faccin, M., Migdał, P., Johnson, T. H., Bergholm, V. & Biamonte, J. D. Community detection in quantum complex networks. *Physical Review X* **4.** Publisher: APS, 041012 (2014).

45. Faccin, M., Johnson, T., Biamonte, J., Kais, S. & Migdał, P. Degree distribution in quantum walks on complex networks. *Physical Review X* **3.** Publisher: APS, 041007 (2013).

46. Cuquet, M. & Calsamiglia, J. Entanglement percolation in quantum complex networks. *Physical review letters* **103.** Publisher: APS, 240503 (2009).

47. Bianconi, G. The topological Dirac equation of networks and simplicial complexes. *Journal of Physics: Complexity* **2,** 035022. `https://doi.org/10.1088/2632-072x/ac19be` (Sept. 2021).

48. Aziz, F., Wilson, R. C. & Hancock, E. R. A wave packet signature for complex networks. *Journal of Complex Networks* **7,** 346–374. ISSN: 2051-1329. `https://doi.org/10.1093/comnet/cny023` (2020) (June 2019).

49. Kostrykin, V., Potthoff, J. & Schrader, R. Finite propagation speed for solutions of the wave equation on metric graphs. *Journal of Functional Analysis* **263.** Publisher: Elsevier, 1198–1223. ISSN: 0022-1236 (2012).

50. Aziz, F., Wilson, R. C. & Hancock, E. R. *Analysis of wave packet signature of a graph* in *International Conference on Computer Analysis of Images and Patterns* (2013), 128–136.

51. Aziz, F., Wilson, R. C. & Hancock, E. R. *Graph characterization using gaussian wave packet signature* in *International Workshop on Similarity-Based Pattern Recognition* (2013), 176–189.

52. Wilson, R. C., Aziz, F. & Hancock, E. R. Eigenfunctions of the edge-based Laplacian on a graph. *Linear Algebra and its Applications* **438,** 4183–4189. ISSN: 0024-3795. http://www.sciencedirect.com/science/article/pii/S0024379513000566 (2013).

53. Pesenson, I. Analysis of band-limited functions on quantum graphs. *Applied and Computational Harmonic Analysis* **21.** Publisher: Elsevier, 230–244. ISSN: 1063-5203 (2006).

54. Pesenson, I. Band limited functions on quantum graphs. *Proceedings of the American Mathematical Society* **133,** 3647–3655. ISSN: 0002-9939 (2005).

55. Exner, P. & Barseghyan, D. Spectral analysis of Schrödinger operators with unusual semiclassical behavior. *Acta Polytechnica* **53.** ISSN: 1805-2363 (2013).

56. Cattaneo, C. The spectrum of the continuous Laplacian on a graph. *Monatshefte für Mathematik* **124.** Publisher: Springer, 215–235. ISSN: 0026-9255 (1997).

57. Kac, M. Can one hear the shape of a drum? *The american mathematical monthly* **73,** 1–23 (1966).

58. Gordon, C., Perry, P. & Schueth, D. Isospectral and isoscattering manifolds: a survey of techniques and examples. *Contemporary Mathematics* **387,** 157–180 (2005).

59. Band, R., Sawicki, A. & Smilansky, U. Scattering from isospectral quantum graphs. *Journal of Physics A: Mathematical and Theoretical* **43,** 415201 (2010).

60. Band, R., Sawicki, A. & Smilansky, U. Note on the Role of Symmetry in Scattering from Isospectral Graphs and Drums. *Acta Physica Polonica A* **120** (2011).

61. Hul, O. *et al.* Are Scattering Properties of Graphs Uniquely Connected to Their Shapes? *Phys. Rev. Lett.* **109,** 040402. https://link.aps.org/doi/10.1103/PhysRevLett.109.040402 (4 July 2012).

62. Smilansky, U. Delay-time distribution in the scattering of time-narrow wave packets.(I). *Journal of Physics A: Mathematical and Theoretical* **50,** 215301 (2017).

63. Smilansky, U. & Schanz, H. Delay-time distribution in the scattering of time-narrow wave packets (II)—quantum graphs. *Journal of Physics A: Mathematical and Theoretical* **51,** 075302 (2018).

64. Robinson, M. *Inverse problems in geometric graphs using internal measurements* 2010. arXiv: `1008.2933 [math.MG]`.

65. Hołyst, J. A., Kacperski, K. & Schweitzer, F. in *Annual Reviews Of Computational PhysicsIX* 253–273 (World Scientific, 2001).

66. Castellano, C., Fortunato, S. & Loreto, V. Statistical physics of social dynamics. *Reviews of modern physics* **81,** 591 (2009).

67. Galam, S. *Sociophysics: A Physicist's Modeling of Psycho-political Phenomena* (Springer, 2016).

68. Galam, S. Modeling the Forming of Public Opinion: An approach from Sociophysics. *Global Economics and Management Review* **18,** 2–11 (2013).

69. Sen, P. & Chakrabarti, B. K. *Sociophysics: an introduction* (Oxford University Press, 2014).

70. Baumann, F., Lorenz-Spreen, P., Sokolov, I. M. & Starnini, M. Modeling Echo Chambers and Polarization Dynamics in Social Networks. *Physical Review Letters* **124.** ISSN: 1079-7114 (Jan. 2020).

71. Cota, W., Ferreira, S. C., Pastor-Satorras, R. & Starnini, M. Quantifying echo chamber effects in information spreading over political communication networks. *EPJ Data Science* **8,** 35 (2019).

72. Törnberg, P. Echo chambers and viral misinformation: Modeling fake news as complex contagion. *PLOS ONE* **13,** 1–21 (Sept. 2018).

73. Sasahara, K. *et al.* Social influence and unfollowing accelerate the emergence of echo chambers. *Journal of Computational Social Science.* ISSN: 2432-2725. `http://dx.doi.org/10.1007/s42001-020-00084-7` (Sept. 2020).

74. Del Vicario, M. *et al.* The spreading of misinformation online. *Proceedings of the National Academy of Sciences* **113,** 554–559. eprint: `https://www.pnas.org/content/113/3/554.full.pdf`. `https://www.pnas.org/content/113/3/554` (2016).

75. Vosoughi, S., Roy, D. & Aral, S. The spread of true and false news online. *Science* **359,** 1146–1151. ISSN: 0036-8075 (2018).

76. Bessi, A. *et al.* Trend of Narratives in the Age of Misinformation. *PLOS ONE* **10,** 1–16 (2015).

77. Shao, C. *et al.* Anatomy of an online misinformation network. *PLOS ONE* **13,** 1–23 (2018).

78. Shao, C., Ciampaglia, G. L., Flammini, A. & Menczer, F. Hoaxy. *Proceedings of the 25th International Conference Companion on World Wide Web - WWW '16 Companion* (2016).

79. Shao, C. *et al.* The spread of low-credibility content by social bots. *Nature Communications* **9,** 4787. ISSN: 2041-1723 (Nov. 2018).

80. DiMaggio, P., Evans, J. & Bryson, B. Have American's social attitudes become more polarized? *American journal of Sociology* **102,** 690–755 (1996).

81. Fiorina, M. P. & Abrams, S. J. Political Polarization in the American Public. *Annual Review of Political Science* **11,** 563–588 (2008).

82. Mouw, T. & Sobel, M. E. Culture wars and opinion polarization: the case of abortion. *American Journal of Sociology* **106,** 913–943 (2001).

83. McCright, A. M. & Dunlap, R. E. The Politicization of Climate Change and Polarization in the American Public's Views of Global Warming, 2001–2010. *The Sociological Quarterly* **52,** 155–194 (2011).

84. Lin, T. Z. & Tian, X. Audience Design and Context Discrepancy: How Online Debates Lead to Opinion Polarization. *Symbolic Interaction* **42,** 70–97 (2019).

85. Conover, M. D. *et al.* Political polarization on twitter. *Icwsm* **133,** 89–96 (2011).

86. Conover, M. D., Gonçalves, B., Flammini, A. & Menczer, F. Partisan asymmetries in online political activity. *EPJ Data Science* **1,** 6 (2012).

87. Hanna, A. *et al. Partisan Alignments and Political Polarization Online: A Computational Approach to Understanding the French and US Presidential Elections* in *Proceedings of the 2nd Workshop on Politics, Elections and Data* (Association for Computing Machinery, San Francisco, California, USA, 2013), 15–22. ISBN: 9781450324182.

88. Brady, W. J., Wills, J. A., Jost, J. T., Tucker, J. A. & Van Bavel, J. J. Emotion shapes the diffusion of moralized content in social networks. *Proceedings of the National Academy of Sciences* **114,** 7313–7318 (2017).

89. Weber, I., Garimella, V. R. K. & Batayneh, A. *Secular vs. islamist polarization in egypt on twitter* in *Proceedings of the 2013 IEEE/ACM international conference on advances in social networks analysis and mining* (2013), 290–297.

90. Baumann, F., Lorenz-Spreen, P., Sokolov, I. M. & Starnini, M. Emergence of polarized ideological opinions in multidimensional topic spaces. *Physical Review X* **11,** 011012 (2021).

91. Schweighofer, S., Schweitzer, F. & Garcia, D. A Weighted Balance Model of Opinion Hyperpolarization. *Journal of Artificial Societies and Social Simulation* **23,** 5. ISSN: 1460-7425 (2020).

92. Chen, T., Li, Q., Yang, J., Cong, G. & Li, G. Modeling of the Public Opinion Polarization Process with the Considerations of Individual Heterogeneity and Dynamic Conformity. *Mathematics* **7.** ISSN: 2227-7390 (2019).

93. Kurahashi-Nakamura, T., Mäs, M. & Lorenz, J. Robust clustering in generalized bounded confidence models. *Journal of Artificial Societies and Social Simulation* **19** (2016).

94. Banisch, S. & Olbrich, E. Opinion polarization by learning from social feedback. *The Journal of Mathematical Sociology* **43,** 76–103 (2019).

95. Macy, M., Deri, S., Ruch, A. & Tong, N. Opinion cascades and the unpredictability of partisan polarization. *Science Advances* **5** (2019).

96. Górski, P. J., Bochenina, K., Hołyst, J. A. & D'Souza, R. M. Homophily Based on Few Attributes Can Impede Structural Balance. *Phys. Rev. Lett.* **125,** 078302. https://link.aps.org/doi/10.1103/PhysRevLett.125.078302 (7 Aug. 2020).

97. Waldner, D. & Lust, E. Unwelcome Change: Coming to Terms with Democratic Backsliding. *Annual Review of Political Science* **21,** 93–113. https://doi.org/10.1146/annurev-polisci-050517-114628 (2018).

98. Wiesner, K. *et al.* Stability of democracies: a complex systems perspective. *European Journal of Physics* **40,** 014002. https://doi.org/10.1088%5C%2F1361-6404%5C%2Faaeb4d (Nov. 2018).

99. Suchecki, K. & Hołyst, J. A. Ising model on two connected Barabasi-Albert networks. *Physical Review E* **74.** ISSN: 1550-2376 (July 2006).

100. Suchecki, K. & Hołyst, J. A. Bistable-monostable transition in the Ising model on two connected complex networks. *Phys. Rev. E* **80,** 031110 (3 Sept. 2009).

101. Krueger, T., Szwabiński, J. & Weron, T. Conformity, Anticonformity and Polarization of Opinions: Insights from a Mathematical Model of Opinion Dynamics. *Entropy* **19.** ISSN: 1099-4300 (2017).

102. Chmiel, A. & Sznajd-Weron, K. Phase transitions in the q-voter model with noise on a duplex clique. *Phys. Rev. E* **92,** 052812 (5 Nov. 2015).

103. Choi, J. & Goh, K.-I. Majority-vote dynamics on multiplex networks with two layers. *New Journal of Physics* **21,** 035005 (2019).

104. Lambiotte, R. & Ausloos, M. Coexistence of opposite opinions in a network with communities. *Journal of Statistical Mechanics: Theory and Experiment* **2007,** P08026 (2007).

105. Lambiotte, R., Ausloos, M. & Hołyst, J. Majority model on a network with communities. *Physical Review E* **75,** 030101 (2007).

106. Chmiel, A., Sienkiewicz, J. & Sznajd-Weron, K. Tricriticality in the q -neighbor Ising model on a partially duplex clique. *Physical Review E* **96** (2017).

107. Chmiel, A., Sienkiewicz, J., Fronczak, A. & Fronczak, P. A Veritable Zoology of Successive Phase Transitions in the Asymmetric q-Voter Model on Multiplex Networks. *Entropy* **22.** `https://www.mdpi.com/1099-4300/22/9/1018` (2020).

108. Ye, Y. *et al.* Effect of heterogeneous risk perception on information diffusion, behavior change, and disease transmission. *Physical Review E* **102,** 1–10 (2020).

109. Alvarez-Zuzek, L. G., La Rocca, C. E., Iglesias, J. R. & Braunstein, L. A. Epidemic spreading in multiplex networks influenced by opinion exchanges on vaccination. *PLOS ONE* **12,** 1–14. `https://doi.org/10.1371/journal.pone.0186492` (2017).

110. Albert, R. & Barabási, A.-L. Statistical mechanics of complex networks. *Reviews of modern physics* **74,** 47 (2002).

111. Newman, M. *Networks* (Oxford university press, 2018).

112. Boccaletti, S., Latora, V., Moreno, Y., Chavez, M. & Hwang, D.-U. Complex networks: Structure and dynamics. *Physics reports* **424,** 175–308 (2006).

113. Dorogovtsev, S. N., Goltsev, A. V. & Mendes, J. F. Critical phenomena in complex networks. *Reviews of Modern Physics* **80,** 1275 (2008).

114. Masuda, N., Porter, M. A. & Lambiotte, R. Random walks and diffusion on networks. *Physics reports* **716,** 1–58 (2017).

115. Erdős, P. & Rényi, A. On the evolution of random graphs. *Publ. Math. Inst. Hung. Acad. Sci* **5,** 17–60 (1960).

116. Watts, D. J. & Strogatz, S. H. Collective dynamics of 'small-world'networks. *nature* **393,** 440–442 (1998).

117. Barabási, A.-L. & Albert, R. Emergence of scaling in random networks. *science* **286,** 509–512 (1999).

118. Aleta, A. & Moreno, Y. Multilayer Networks in a Nutshell. *Annual Review of Condensed Matter Physics* **10,** 45–62 (2019).

119. De Arruda, G. F., Cozzo, E., Peixoto, T. P., Rodrigues, F. A. & Moreno, Y. Disease localization in multilayer networks. *Physical Review X* **7,** 011014 (2017).

120. Pinto, P. C., Thiran, P. & Vetterli, M. Locating the source of diffusion in large-scale networks. *Physical review letters* **109,** 068702 (2012).

121. Kempe, D., Kleinberg, J. & Tardos, É. *Maximizing the spread of influence through a social network* in *Proceedings of the ninth ACM SIGKDD international conference on Knowledge discovery and data mining* (2003), 137–146.

122. Graham, R. L., Knuth, D. E., Patashnik, O. & Liu, S. Concrete mathematics: a foundation for computer science. *Computers in Physics* **3,** 106–107 (1989).

123. Friedman, J. & Tillich, J.-P. Wave equations for graphs and the edge-based Laplacian. *Pacific Journal of Mathematics* **216.** Publisher: Mathematical Sciences Publishers, 229–266. ISSN: 0030-8730 (2004).

124. Hurt, N. E. *Mathematical physics of quantum wires and devices: From spectral resonances to Anderson localization* (Springer Science & Business Media, 2013).

125. Friedman, J. & Tillich, J.-P. Calculus on graphs. *arXiv preprint cs/0408028* (2004).

126. Hastie, T., Tibshirani, R. & Friedman, J. *The elements of statistical learning: data mining, inference, and prediction* (Springer Science & Business Media, 2009).

127. Gajewski, Ł., Chołoniewski, J. & Hołyst, J. Key Courses of Academic Curriculum Uncovered by Data Mining of Students' Grades. *Acta Physica Polonica, A.* **129** (2016).

128. Sienkiewicz, J., Soja, K., Hołyst, J. A. & Sloot, P. M. Categorical and geographical separation in science. *Scientific reports* **8,** 1–12 (2018).

129. Chołoniewski, J. *et al.* A calibrated measure to compare fluctuations of different entities across timescales. *Scientific Reports* **10,** 20673. ISSN: 2045-2322. `https://doi.org/10.1038/s41598-020-77660-4` (Nov. 2020).

130. Stevens, K. N. *et al. Nearest Neighbor Pattern Classification* 1953.

131. Arfken, G. B. & Weber, H. J. *Mathematical methods for physicists* 1999.

132. Cooley, J. W. & Tukey, J. W. An algorithm for the machine calculation of complex Fourier series. *Mathematics of computation* **19,** 297–301 (1965).

133. Daubechies, I. *Ten lectures on wavelets* (SIAM, 1992).

134. Du, P., Kibbe, W. A. & Lin, S. M. Improved peak detection in mass spectrum by incorporating continuous wavelet transform-based pattern matching. *Bioinformatics* **22,** 2059–2065. ISSN: 1367-4803. eprint: `https://academic.oup.com/bioinformatics/article-pdf/22/17/2059/767773/btl355.pdf`. `https://doi.org/10.1093/bioinformatics/btl355` (July 2006).

135. *Python* `https://www.python.org/`. Accessed: 2021-02-05.

136. Pedregosa, F. *et al.* Scikit-learn: Machine Learning in Python. *Journal of Machine Learning Research* **12,** 2825–2830 (2011).

137. McKinney, W. *Data Structures for Statistical Computing in Python* in *Proceedings of the 9th Python in Science Conference* (eds van der Walt, S. & Millman, J.) (2010), 56–61.

138. Harris, C. R. *et al.* Array programming with NumPy. *Nature* **585,** 357–362. `https://doi.org/10.1038/s41586-020-2649-2` (Sept. 2020).

139. Hagberg, A. A., Schult, D. A. & Swart, P. J. *Exploring Network Structure, Dynamics, and Function using NetworkX* in *Proceedings of the 7th Python in Science Conference* (eds Varoquaux, G., Vaught, T. & Millman, J.) (Pasadena, CA USA, 2008), 11–15.

140. Hunter, J. D. Matplotlib: A 2D graphics environment. *Computing in Science & Engineering* **9,** 90–95 (2007).

141. Waskom, M. & the seaborn development team. *mwaskom/seaborn* version latest. Sept. 2020. `https://doi.org/10.5281/zenodo.592845`.

142. *The R Project for Statistical Computing* `https://www.r-project.org/`. Accessed: 2021-02-05.

143. *Rust* `https://www.rust-lang.org/`. Accessed: 2021-02-05.

144. Wolfram Research, I. *Mathematica, Version 12.1* Champaign, IL, 2020.

145. Domenico, M. D., Porter, M. A. & Arenas, A. MuxViz: a tool for multilayer analysis and visualization of networks. *Journal of Complex Networks* **3,** 159–176. https://doi.org/10.1093/comnet/cnu038 (Oct. 2014).

146. Myers, S. A. & Leskovec, J. On the convexity of latent social network inference. *arXiv preprint arXiv:1010.5504* (2010).

147. Rodriguez, M. G., Balduzzi, D. & Schölkopf, B. Uncovering the temporal dynamics of diffusion networks. *arXiv preprint arXiv:1105.0697* (2011).

148. White, H. C., Boorman, S. A. & Breiger, R. L. Social structure from multiple networks. I. Blockmodels of roles and positions. *American journal of sociology* **81,** 730–780 (1976).

149. Clauset, A., Shalizi, C. R. & Newman, M. E. Power-law distributions in empirical data. *SIAM review* **51,** 661–703 (2009).

150. Broido, A. D. & Clauset, A. Scale-free networks are rare. *Nature communications* **10,** 1–10 (2019).

151. Pukelsheim, F. The three sigma rule. *The American Statistician* **48,** 88–91 (1994).

152. Saw, J. G., Yang, M. C. & Mo, T. C. Chebyshev inequality with estimated mean and variance. *The American Statistician* **38,** 130–132 (1984).

153. Efron, B. & Tibshirani, R. J. *An introduction to the bootstrap* (CRC press, 1994).

154. Lokhov, A. Y., Mézard, M., Ohta, H. & Zdeborová, L. Inferring the origin of an epidemic with a dynamic message-passing algorithm. *Physical Review E* **90,** 012801 (2014).

155. Lokhov, A. Y., Mézard, M. & Zdeborová, L. Dynamic message-passing equations for models with unidirectional dynamics. *Physical Review E* **91,** 012811 (2015).

156. Magnani, M., Micenkova, B. & Rossi, L. Combinatorial analysis of multiple networks. *arXiv preprint arXiv:1303.4986* (2013).

157. Vickers, M. & Chan, S. Representing classroom social structure. *Victoria Institute of Secondary Education, Melbourne* (1981).

158. Brandes, U. A faster algorithm for betweenness centrality. *Journal of mathematical sociology* **25,** 163–177 (2001).

159. Newman, M. E. A measure of betweenness centrality based on random walks. *Social networks* **27,** 39–54 (2005).

160. Franceschetti, M. *Wave Theory of Information* ISBN: 9781107022317. https://www.cambridge.org/core/product/identifier/9781139136334/type/book (Cambridge University Press, Nov. 2017).

161. Mones, E., Araújo, N. A. M., Vicsek, T. & Herrmann, H. J. Shock waves on complex networks. *Scientific Reports* **4,** 4949. http://www.nature.com/articles/srep04949 (2015).

162. Liao, X. *et al.* Pattern formation in oscillatory complex networks consisting of excitable nodes. *Physical Review E* **83,** 056204. https://link.aps.org/doi/10.1103/PhysRevE.83.056204 (May 2011).

163. Liao, X.-h. *et al.* Oscillation sources and wave propagation paths in complex networks consisting of excitable nodes. *Frontiers of Physics* **6,** 124–132. http://link.springer.com/10.1007/s11467-010-0152-1 (2011).

164. Krackhardt, D. Cognitive social structures. *Social networks* **9,** 109–134 (1987).

165. Chen, B. L., Hall, D. H. & Chklovskii, D. B. Wiring optimization can relate neuronal structure and function. *Proceedings of the National Academy of Sciences* **103,** 4723–4728 (2006).

166. Mäs, M. & Flache, A. Differentiation without Distancing. Explaining Bi-Polarization of Opinions without Negative Influence. *PLOS ONE* **8,** 1–17 (Nov. 2013).

167. Jayles, B. *et al.* How social information can improve estimation accuracy in human groups. *Proceedings of the National Academy of Sciences* **114,** 12620–12625. ISSN: 0027-8424 (2017).

168. Sompolinsky, H., Crisanti, A. & Sommers, H. J. Chaos in Random Neural Networks. *Phys. Rev. Lett.* **61,** 259–262. https://link.aps.org/doi/10.1103/PhysRevLett.61.259 (3 July 1988).

169. Eldar, E., Cohen, J. D. & Niv, Y. The effects of neural gain on attention and learning. *Nature neuroscience* **16,** 1146–1153 (2013).

170. Perra, N., Gonçalves, B., Pastor-Satorras, R. & Vespignani, A. Activity driven modeling of time varying networks. *Scientific reports* **2,** 469 (2012).

171. Starnini, M. & Pastor-Satorras, R. Topological properties of a time-integrated activity-driven network. *Phys. Rev. E* **87,** 062807 (6 June 2013).

172. Moinet, A., Starnini, M. & Pastor-Satorras, R. Burstiness and Aging in Social Temporal Networks. *Phys. Rev. Lett.* **114,** 108701 (10 Mar. 2015).

173. Liu, S., Perra, N., Karsai, M. & Vespignani, A. Controlling Contagion Processes in Activity Driven Networks. *Phys. Rev. Lett.* **112,** 118702 (11 Mar. 2014).

174. Holme, P. & Newman, M. E. J. Nonequilibrium phase transition in the coevolution of networks and opinions. *Phys. Rev. E* **74,** 056108. `https://link.aps.org/doi/10.1103/PhysRevE.74.056108` (5 Nov. 2006).

175. Kimura, D. & Hayakawa, Y. Coevolutionary networks with homophily and heterophily. *Phys. Rev. E* **78,** 016103. `https://link.aps.org/doi/10.1103/PhysRevE.78.016103` (1 July 2008).

176. Kadanoff, L. P. More is the same; phase transitions and mean field theories. *Journal of Statistical Physics* **137,** 777–797 (2009).

177. Huang, K. *Introduction to statistical physics* (CRC press, 2009).

178. Dormand, J. & Prince, P. A family of embedded Runge-Kutta formulae. *Journal of Computational and Applied Mathematics* **6,** 19–26. ISSN: 0377-0427 (1980).

179. Krosnick, J. A. Attitude importance and attitude change. *Journal of Experimental Social Psychology* **24,** 240–255 (1988).

180. Strogatz, S. H. *Nonlinear dynamics and chaos with student solutions manual: With applications to physics, biology, chemistry, and engineering* (CRC press, 2018).

181. Ott, E. *Chaos in dynamical systems* (Cambridge university press, 2002).

182. Chu, M., Chu, M. T., Golub, G. & Golub, G. H. *Inverse eigenvalue problems: theory, algorithms, and applications* (Oxford University Press, 2005).

183. Steidl, G. & Winkler, M. A New Constrained Optimization Model for Solving the Nonsymmetric Stochastic Inverse Eigenvalue Problem. *arXiv preprint arXiv:2004.07330* (2020).

184. Cacace, F., Germani, A. & Manes, C. *Karpelevich Theorem and the positive realization of matrices* in *2019 IEEE 58th Conference on Decision and Control (CDC)* (2019), 6074–6079.

185. Zhao, Z., Jin, X.-Q. & Bai, Z.-J. A geometric nonlinear conjugate gradient method for stochastic inverse eigenvalue problems. *SIAM Journal on Numerical Analysis* **54,** 2015–2035 (2016).

186. Orsi, R. Numerical methods for solving inverse eigenvalue problems for nonnegative matrices. *SIAM Journal on Matrix Analysis and Applications* **28,** 190–212 (2006).

187. Sánchez-García, R. J., Cozzo, E. & Moreno, Y. Dimensionality reduction and spectral properties of multilayer networks. *Physical Review E* **89,** 052815 (2014).

188. Cozzo, E., de Arruda, G. F., Rodrigues, F. A. & Moreno, Y. in *Interconnected Networks* 17–35 (Springer, 2016).

189. Białas, S. & Gurgul, H. On hypothesis about the second eigenvalue of the Leontief matrix. *Economic Systems Research* **10,** 285–290 (1998).

190. Holland, P. W., Laskey, K. B. & Leinhardt, S. Stochastic blockmodels: First steps. *Social Networks* **5,** 109–137. ISSN: 0378-8733. `https://www.sciencedirect.com/science/article/pii/0378873383900217` (1983).

"Lo duca e io per quel cammino ascoso
intrammo a ritornar nel chiaro mondo;
e sanza cura aver d'alcun riposo,
salimmo sù, el primo e io secondo,
tanto ch'i' vidi de le cose belle
che porta 'l ciel, per un pertugio tondo.
E quindi uscimmo a riveder le stelle."

— Dante Alighieri, *Divina Commedia*